Université de Montréal
Faculté des études supérieures

Cette thèse intitulée :

Non-invasive investigation of the response to oxidative stress in living cardiomyocytes by studying mitochondrial NAD(P)H

présentée par :
Swida Aneba

a été évaluée par un jury composé des personnes suivantes :

Dr. Jacques De Champlain, président-rapporteur
Dr. Alzbeta Chorvatova, directeur de recherche
Dr. Blandine Comte, co-directeur
Dr. Christine Des Rosiers, membre du jury

RESUME

La mitochondrie du cardiomyocyte dont la fonction primaire est la production d'ATP, essentielle à la contraction cardiaque, est une source majeure d'espèces réactives de l'oxygène. Dans la chaîne respiratoire, les radicaux libres sont produits par différents sites et peuvent conduire à un stress oxydant lorsque le système de défense antioxydant est défaillant. L'évaluation de l'état rédox mitochondrial est un facteur important dans la détection de changements précoces dans des conditions pathologiques telles que l'ischémie, l'hypertension ou le diabète.

Dans notre étude, nous avons suivi l'autofluorescence (AF) du nicotinamide adénine dinucléotide (phosphate), ou NAD(P)H, un co-facteur donneur d'électrons pour différentes réactions enzymatiques jouant un rôle crucial dans le métabolisme oxydatif cellulaire et une source majeure d'AF des cellules cardiaques suite à une excitation par la lumière UV. Le NAD(P)H a été utilisé ici comme marqueur fluorescent non invasif de la fonction mitochondriale. Nos objectifs étaient de (i) développer une approche de caractérisation de l'empreinte de l'état oxydatif métabolique mitochondrial des cardiomyocytes par la méthode spectrométrique du temps de vie de fluorescence induite par laser (STVF) et (ii) déterminer les changements dynamiques et spectrales de la fluorescence du NAD(P)H *in vitro* et dans des cardiomyocytes isolés de rat lors de modulations métaboliques ou oxydatives. La fluorescence du NAD(P)H a été enregistrée suite à une excitation par une diode à laser UV-pulsé et la détection par STVF avec une mesure simultanée de spectres et de temps de vie de fluorescence. La modulation de l'AF des cardiomyocytes suite à des changement de production et/ou de consommation de NAD(P)H a été étudiée. Nous avons également utilisé cette approche pour investiguer les modifications associées au remodelage oxydatif métabolique lors de la gestation normale et après traitement des animaux avec du canrénoate, un inhibiteur des récepteurs aux minéralocorticoides.

Nos données montrent que la fluorescence du NADPH *in vitro* a un maximum spectral à 450 nm, une décroissance avec au moins deux durées de vie et est sensible aux

changements d'environnement tels que le pH et la viscosité. Nous avons également montré qu'un modèle de décroissance à trois exponentielles est nécessaire pour décrire l'AF du NAD(P)H des cardiomyocytes. Des cellules cardiaques fraîchement isolées ont été traitées avec des agents mimant un stress oxydant : le peroxyde d'hydrogène (H_2O_2) et le 4-hydroxynonénal (HNE). Nos résultats montrent qu'en présence de H_2O_2, et en accord avec sa capacité d'augmenter l'utilisation du NADPH par le système antioxydant du glutathion, les cardiomyocytes présentent une perte de la fluorescence qui est accompagnée par un élargissement spectral vers le rouge. L'analyse des composantes principales faite sur les données révèlent que cet effet résulte d'une diminution des amplitudes des composants résolues, sans modification de leur temps de vie. Parallèlement, le HNE, un produit issu de la peroxydation lipidique connu pour sa capacité de diminuer la production de NADPH par inhibition de l'enzyme mitochondriale l'isocitrate déshydrogénase NADP-dépendante, est également capable de diminuer la fluorescence du NAD(P)H avec un léger élargissement spectral vers le rouge. L'analyse des composantes principales révèle que contrairement aux effets du H_2O_2 sur la fluorescence du NAD(P)H, ceux du HNE s'exercent plutôt sur une diminution des temps de vie, suggérant une conséquence sur l'environnement moléculaire plutôt que sur sa quantité. De plus, en présence d'inhibiteurs de la glutathion réductase (BCNU) ou du complexe I et IV de la chaîne respiratoire, le H_2O_2 et le HNE ont des effets différents sur la fluorescence du NAD(P)H dans les cellules, suggérant des implications différentes sur les voies métaboliques.

Nous avons ensuite choisi la gestation comme exemple pour investiguer la possibilité d'utiliser cette technique dans l'étude du métabolisme oxydatif dans des conditions physiopathologiques. Les caractéristiques de la fluorescence du NAD(P)H ont été étudiées dans les cardiomyocytes vivants, fraîchement isolés de rates gestantes normales ou traitées au canrénoate. Lors de la gestation normale, l'AF du NAD(P)H n'est pas différente de celle mesurée chez les rates nullipares montrant la capacité d'adaptation des cellules cardiaques à cette situation métabolique. Lors d'une gestation en présence de canrénoate, bloquant le récepteur aux minéralocorticoides, les réponses de l'AF du

NAD(P)H aux modulateurs de métabolisme oxydatif varient de celles des conditions normales. L'intensité de la fluorescence qui a tendance à être plus sensible aux changements du ratio lactate/pyruvate et la perte de fluorescence en présence de BCNU, plus prononcée que celle mesurée lors de la gestation normale, suggèrent de mauvaises adaptations cardiaques à cette condition.

La technique STVF est un outil très prometteur pour l'analyse de la fluorescence du NAD(P)H dans les cardiomyocytes vivants. Cette approche devrait nous permettre de mieux comprendre le métabolisme oxydatif des cardiomyocytes et/ou son dysfonctionnement au niveau cellulaire. Elle pourrait également devenir un nouvel outil prometteur pour l'étude des mécanismes cellulaires impliqués dans le développement des maladies cardiaques.

Mots-clés : NAD(P)H, autofluorescence, spectrométrique du temps de vie de fluorescence induite par laser, mitochondrie, cardiomyocyte vivant, état métabolique oxydatif

ABSTRACT

The primary function of cardiac mitochondria is the production of ATP to support the contractions of the heart. This process is considered a major source of reactive oxygen species formation (ROS) in the heart. During ATP generation, free oxygen radicals may arise at different points in the respiratory chain, leading to oxidative stress when the antioxidant system is compromised. Examination of the mitochondrial redox state is therefore crucially important to sensitively detect early signs of mitochondrial dysfunction in pathophysiological conditions, such as ischemia, hypertension, and diabetes. In this study, we monitor cellular autofluorescence (AF) of nicotinamide adenine dinucleotide (phosphate), or NAD(P)H, which plays a crucial role in the management of cellular oxidative metabolism as the principal electron donors for several enzymatic reactions and which is a major source of AF induced in cardiac cells following excitation by UV light. Here, NAD(P)H is studied as a marker for non-invasive fluorescent probing of the mitochondrial function. Our objectives are to (i) develop an approach for fingerprinting of mitochondrial metabolic oxidative state in living cardiac myocytes by spectrally-resolved time-correlated single photon counting (TCSPC) and (ii) report dynamic changes of NAD(P)H fluorescence spectra and decays *in vitro*, and in living rat cardiomyocytes upon metabolic or oxidative modulation. NAD(P)H fluorescence is recorded following excitation by UV-pulsed laser diode and detected by spectrally-resolved TCSPC, allowing simultaneous measurement of the fluorescence spectra and fluorescence lifetimes. Modulation of cardiomyocyte AF following changes in NAD(P)H production and/or consumption is investigated. We also test the eventual application of this approach to examine remodeling of oxidative metabolism in cardiomyocyte during normal pregnancy or after treatment of animals with canrenoate, an inhibitor of mineralocorticoid receptors (MR).

Our preliminary data have shown that NADPH fluorescence *in vitro* with spectral maximum at 450 nm and decay with at least two significant fluorescence lifetimes is

sensitive to changes in the environment, such as pH and viscosity. Also, we have demonstrated that a 3-exponential decay model is necessary to describe NAD(P)H-based cardiomyocyte AF. Freshly-isolated living cardiac cells were treated with oxidative stress mimicking agents: hydrogen peroxide (H_2O_2) or 4-hydroxynonenal (HNE), a by-product of lipid peroxidation. Our results showed that, in agreement with the capacity of H_2O_2 to stimulate the use of NADPH by glutathione system, living cardiac cells showed a loss of NAD(P)H fluorescence in the presence of H_2O_2, which was accompanied by a red spectral broadening. Advanced component analysis performed on gathered data revealed that this effect results from decrease in the amplitudes of the resolved components, without modifications in their lifetimes. In parallel, HNE, a by-product of lipid peroxidation, known for its ability to decrease NADPH production by inhibiting NADP-isocitrate dehydrogenase was also capable of decreasing NAD(P)H fluorescence with a slight red spectral broadening. In contrast to H_2O_2, component analysis revealed that HNE effect on NAD(P)H fluorescence reduction is primarily related to lowering of fluorescence lifetimes, pointing to the effect of HNE on the environment rather than the quantity of NAD(P)H molecules. Furthermore, in the presence of glutathione reductase (GR) inhibitor (BCNU), or of the respiratory chain modulators, H_2O_2 and HNE induced different effects on NAD(P)H-fluorescence in cardiac cells, pointing to implication of separate metabolic pathways.

Next, we have chosen the condition of pregnancy as an example to investigate possible application of the new technique to study cardiomyocyte oxidative metabolic state in pathophysiological situations. We examined characteristics of NAD(P)H fluorescence in living cardiomyocytes isolated from normal pregnant rats and canrenoate-treated ones. In normal pregnancy, NAD(P)H AF response was not different from that of non-pregnant rats, pointing to capacity of adaptation of cardiac cells to this condition. Interestingly, during pregnancy where MR were blocked by canrenoate-treatment, responsiveness of NAD(P)H fluorescence of cardiac cells varied from that in normal conditions. The fluorescence intensity tended to be more sensitive to metabolic substrates lactate/pyruvate than in normal

condition, and in the presence of BCNU the loss of AF was more pronounced compared to normal pregnancy, indicating possible cardiac maladaptions in this condition.

Spectrally-resolved fluorescence lifetime technique provides promising new tool for analysis of NAD(P)H fluorescence in living cardiomyocytes. In the future, this approach will improve our understanding of cardiomyocyte oxidative metabolic state and /or its dysfunction at a cellular level, and could become a promising tool for the study of cellular mechanisms of cardiovascular disease development.

Keywords: NAD(P)H, autofluorescence (AF), spectrally-resolved fluorescence decays, mitochondria, living cardiomyocyte, oxidative metabolic state.

TABLE OF CONTENTS

LIST OF TABLES

LIST OF FIGURES

LIST OF ABBREVIATIONS AND SYMBOLS

AcAc:	Acetoacetate
Acetyl-CoA:	Acetyl-coenzyme A
a_i:	Relative amplitude
α-KGDH:	α-ketoglutarate dehydrogenase
AF:	Autofluorescence
ATP:	Adenosine triphosphate
BCNU:	1,3-bis(2-chloroethyl)-1-nitroso-urea
BHB:	β-hydroxybutyrate
BSA:	Bovine serum albumin
CAT:	Catalase
χ^2:	Chi-square values
DHN:	1,4-dihydroxynonene
DNP:	9,10-dinitrophenol
DPA:	Diphenylanthracene
EGTA:	Ethylene glycol tetraacetic acid
ETC:	Electron transport chain
$FADH_2$:	Reduced flavin adenine dinucleotide
$FMNH_2$:	Reduced Flavin mononucleotide
F6P:	Fructose-6-phosphate
GR:	Glutathione reductase
GPx:	Glutathione peroxidase
G6PDH:	Glucose-6 phosphate dehydrogenase
GSH:	Reduced glutathione

GSSG:	Glutathione disulfide
GTP:	Guanosine trisphosphate
HEPES:	4-(2-hydroxyethyl)-1-piperazineethanesulfonic acid
HNE:	4-hydroxy-2-nonenal
H_2O_2:	Hydrogen peroxide
HO·:	Hydroxyl radical
IRF:	Instrument response function
LPO:	Lipid peroxidation
MDA:	Malondialdehyde
ME:	Malic enzyme
MR:	Mineralcorticoid receptors
NADP-ICDH:	$NADP^+$-isocitrate dehydrogenase
NADKase:	NAD^+ kinase
NADPase:	$NADP^+$ phosphatase
NADP-GDH:	$NADP^+$-glutamate dehydrogenase
NAD(P)H:	Nicotinamide adenine dinucleotide (phosphate)
NP:	Non pregnant
NP_{can}:	Non pregnant treated with canrenoate
ns:	Nano-second
$O_2^{-\cdot}$:	Superoxide anions
P:	Pregnant
P_{can}:	Pregnant treated with canrenoate
PCA:	Principal component analysis
PFK:	Phosphofructokinase
P_i:	Inorganic phosphate
PML:	Photomultiplier
ps:	Pico-second
Prx:	Peroxiredoxin

Q:	Ubiquinone
QH_2:	Ubiquinol
RAAS:	Renin-angiotensin-aldosterone system
ROOH:	Hydroperoxy
ROS:	Reactive oxygen species
S_0:	Ground state of a fluorophore
S_1:	Excited state of a fluorophore
SDHA, B, C or D	Succinate dehydrogenase subunit A, B, C or D
SEM:	Standard error of means
SOD:	Superoxide dismutase
6PGDH:	6-phosphogluconate dehydrogenase
τ:	Fluorescence lifetime
TCA:	Tricarboxylic acid cycle
TCSPC:	Time-correlated single photon counting
TRANES:	Time-resolved Area Normalized Emission Spectra
TRES:	Time-resolved emission spectra
UCPs:	Uncoupling proteins
UV:	Ultraviolet
XO:	Xanthine oxidase

ACKNOWLEDGEMENTS

My M.Sc. thesis has been an inspiring, very challenging, but always interesting and exciting experience. I owe its existence to the help, support, and inspiration of many people. It is pleasure to convey my gratitude to them all in my humble acknowledgement.

First of all, I would like to express my sincere appreciation and gratitude to my supervisor, Dr. Alzbeta Chorvatova, for giving me the opportunity to be one of her research team and for her constant support, patient guidance, and excellent advice through this study. Her truly scientist intuition has made her as a constant oasis of ideas in science, which exceptionally enrich my scientific vision as a student, and a researcher want to be. I am indebted to her more than words can say.

I gratefully acknowledge my co-director Dr. Blandine Comte who was abundantly helpful and offered invaluable assistance, encouragement and guidance. Her involvement with her originality has triggered and nourished my intellectual maturity that I will benefit from, for a long time to come. Dr. Comte, I am thankful in every possible way and hope to keep up our collaboration in the future.

My thanks go in particular to Dr. D. Chorvat Jr. and his colleagues, from International Laser Centre, Bratislava, Slovak Republic, for their crucial contribution to this thesis and providing the component analysis of our experimental data. My special thanks extend to Thierry Ntimbane for his help with HNE measurements in the blood, people in the clinical biomedical lab at Sainte Justine Hospital for analysis of metabolic substrates in the blood, Dr. Christine Des Rosiers for generous gift of AcAc, and A. Mateasik for custom-written procedures for data correction. Acknowledgement extends to V. Bassien-Capsa, F. Elzwiei, Y. Cheng and all other colleagues in Dr. Chorvatova's lab for their friendship, assistance, and sharing experience and knowledge. Also, I would like to thank Dr. R. Couture and Madame J. Payette for their great attitude and for helping me with the

administration work since I started my M.Sc. program. I would like to express my apology if I have missed anyone out, it was done without intentions.

I convey special acknowledgment to the Libyan Ministry of Superior Studies for giving me the financial support, in order to pursue my academic studies in Canada.

I wish to thank my family for their continuous love and encouragement, for always believing in me, and for never failing to provide all the support. I would like to thank in particular, my mother for her prayers and unconditional love, my dear sister, Bouthaina, for continuous communication that made me feel home all times, and my husband whose dedication, love and persistent confidence in me has taken the load off my shoulder. Words fail me to express my appreciation to him for always taking care of me and our kids Sara and Yousef through the duration of my study.

I won't forget my father who deserves special mention. In the first place, he was the person who put the fundament of my learning character, showing me the joy of intellectual pursuit ever since I was a child.

Last but not least, thanks God for giving me the strength and patience I needed to accomplish my goals and never give up.

1. INTRODUCTION

1.1. Oxidative stress and its impact on the heart function

The heart is the major organ in the cardiovascular system which provides the body continuously with blood, delivering the oxygen and essential substrates needed for biological functions, and helping dispose of metabolic wastes. The left ventricle, with thicker walls compared to the right ventricle, serves as the main pumping chamber of the heart forcing blood through the aortic valve into the high resistance systemic circulation, providing oxygen to the entire body. Depending on the workload, the heart can adaptively change its output to ensure adequate energy supply[1]. In order to maintain the proper functioning of the heart it is required to have a sufficient amount of energy to sustain the myocardial contractile activity[2-4]. The heart uses a variety of substrates to meet its energy requirements from the oxidation of fatty acids, glucose, lactate and other oxidizable substrates[4]. There are important mechanisms that exist to supply energy and keep the cellular pool of adenosine triphosphate (ATP). The three main pathways used to generate energy in eukaryotic organisms are glycolysis and the citric acid cycle/oxidative phosphorylation, both components of cellular respiration; and β-oxidation. The majority of ATP production takes place in the mitochondria. The mitochondrion is well known for its ability to produce ATP and regulating cellular metabolism. However, the mitochondrion has many other functions in addition to the production of ATP, such as Ca^{2+} homeostasis[5], signalling and programmed cell death[6].

1.1.1. Energy production as the main function for the mitochondria

A dominant role for mitochondria is the production of ATP, as reflected by the large number of proteins in the inner membrane for this purpose. This is done by oxidizing the

major products of glycolysis, pyruvate, and NADH, which are produced in the cytosol. This process of cellular respiration, also known as aerobic respiration, is dependent on the presence of oxygen. When oxygen is limited, the glycolytic products will be metabolized by anaerobic respiration, a process that is independent of mitochondria[3]. The production of ATP from glucose has an approximately 13-fold higher yield during aerobic respiration compared to anaerobic respiration[7].

In the process of oxidative respiration, each pyruvate molecule formed by glycolysis is actively transported across the inner mitochondrial membrane, and into the matrix where it is oxidized and combined with coenzyme A to form CO_2, acetyl-CoA, and NADH[8]. Fatty acids can also be broken down to acetyl-CoA by β-oxidation. Each round of this cycle reduces the length of the acyl chain by two carbon atoms and produces one NADH and one $FADH_2$ molecule, which are used to generate ATP by oxidative phosphorylation. Because NADH and $FADH_2$ are energy-rich molecules, dozens of ATP molecules can be generated by the β-oxidation of a single long acyl chain[3].

The acetyl-CoA is the primary substrate to enter the citric acid cycle, also known as the tricarboxylic acid (TCA) cycle or Krebs cycle. The enzymes of the TCA cycle are located in the mitochondrial matrix, with the exception of succinate dehydrogenase, which is bound to the inner mitochondrial membrane as part of Complex II. The TCA cycle oxidizes acetyl-CoA to carbon dioxide, and, in the process, produces reduced cofactors (three molecules of NADH and one molecule of $FADH_2$) that are a source of electrons for the electron transport chain (ETC), and a molecule of guanosine triphosphate (GTP) that is readily converted into an ATP molecule[8, 9]. The TCA cycle is regulated mainly by the availability of key substrates, particularly the ratio of NAD^+ to NADH and the concentrations of calcium, inorganic phosphate, ATP, ADP, and AMP. Citrate, the molecule that gives its name to the cycle, is a feedback inhibitor of citrate synthase and also inhibits the phosphofructokinase (PFK), providing a direct link between the regulation of the citric acid cycle and glycolysis[10].

The redox energy from NADH and $FADH_2$ is transferred via dehydrogenation by flavoprotein complexes to oxygen (O_2), which is reduced to water, in several steps via ETC. These energy-rich molecules are produced within the matrix via the citric acid cycle but are also produced in the cytoplasm by glycolysis[8]. Reducing equivalents from the cytoplasm can be imported via the malate-asparate shuttle system of antiporter proteins or feed into the ETC using a glycerol phosphate shuttle[11]. NADH is a substrate or a coenzyme for the enzymatic activity of dehydrogenases that form part of the respiratory chain and reside in the inner membrane of the mitochondria. Flavoprotein complexes in the inner mitochondrial membrane, more precisely Complex I (NADH dehydrogenase, cytochrome c reductase, and cytochrome c oxidase) perform the transfer and the incremental release of energy is used to pump protons (H^+) into the intermembrane space[8]. The enzymes that catalyze these reactions have the remarkable ability to simultaneously create a proton gradient across the membrane, producing a thermodynamically unlikely high-energy state with the potential to do work. This process is well-organized, but a small percentage of electrons may prematurely reduce oxygen, forming reactive oxygen species (ROS) such as superoxide[12]. This can cause oxidative stress in the mitochondria and may contribute to the decline in mitochondrial function.

In mitochondria, four membrane-bound multiprotein complexes have been identified. Each is an extremely complex transmembrane structure that is embedded in the inner membrane. Three of them are proton pumps, namely, NADH dehydrogenase complex, b-c_1 complex and cytochrome oxidase complex. The structures are electrically connected by lipid-soluble electron carriers and water-soluble electron carriers. The four complexes of the ETC are described below.

Complex I (NADH dehydrogenase), also referred to as NADH:ubiquinone oxidoreductase, removes two electrons from NADH and transfers them to a lipid-soluble carrier, ubiquinone (Q). The reduced product, ubiquinol (QH_2) is free to diffuse within the membrane. At the same time, Complex I moves four protons (H^+) across the membrane,

producing a proton gradient. In depth, NADH is oxidized to NAD^+, reducing Flavin mononucleotide to $FMNH_2$ in one two-electron step. The next electron carrier is a Fe-S cluster, which can only accept one electron at a time to reduce the ferric ion into a ferrous ion. $FMNH_2$ can be oxidized in only two one-electron steps, through a semiquinone intermediate. The electron thus moves from the $FMNH_2$ to the Fe-S cluster, then from the Fe-S cluster to the oxidized Q to give the free-radical (semiquinone) form of Q. This happens again to reduce the semiquinone form to the ubiquinol form, QH_2. During this process, four protons are translocated across the inner mitochondrial membrane, from the matrix to the intermembrane space[8]. This creates a proton gradient that will be subsequently used to generate ATP through oxidative phosphorylation. Complex I is one of the main sites at which premature electron leakage to oxygen occurs, thus being one of main sites of production of a harmful free radical called superoxide[12, 13].

Several agents can affect Complex I functioning normally, one of which is rotenone that acts by interfering with the ETC via inhibition of Complex I[14]. Specifically, it restricts the transfer of electrons from iron-sulphur centers in Complex I to ubiquinone. This prevents NADH from being converted into usable cellular energy ATP. It has been suggested that rotenone is capable to induce apoptosis via promoting mitochondrial ROS production[15]. This was confirmed by DNA fragmentation, cytochrome c release, and caspase 3 activity. Also rotenone-induced apoptosis was quantitatively correlated with rotenone-induced mitochondrial ROS generation. This effect of rotenone was inhibited by the use of antioxidants (glutathione, N-acetylcysteine and vitamin C)[15, 16].

Complex II (succinate dehydrogenase) is not a proton pump. It serves to funnel additional electrons into the quinone pool (Q) by removing electrons from succinate and transferring them via FAD to Q[8]. Complex II consists of four protein subunits: subunit A (SDHA), B (SDHB), C (SDHC), and D (SDHD). Other electron donors (e.g., fatty acids

and glycerol 3-phosphate) also funnel electrons into Q (via FAD), again without producing a proton gradient.

Complex III (cytochrome bc_1 complex) removes in a stepwise fashion two electrons from QH_2 and transfers them to two molecules of cytochrome c, a water-soluble electron carrier located within the intermembrane space. Simultaneously, it moves two protons across the membrane, producing a proton gradient. More precisely, in total 4 protons are moved: 2 protons are translocated and 2 protons are released from ubiquinol [8]. When electron transfer is hindered (by high membrane potential, point mutations or respiratory inhibitors such as antimycin A), Complex III may leak electrons to oxygen resulting in the formation of superoxide, a highly-toxic species[14], and other free radicals which are thought to contribute to the pathology of a number of diseases.

Complex IV (cytochrome c oxidase) removes four electrons from four molecules of cytochrome c and transfers them to molecular oxygen (O_2), producing two molecules of water (H_2O) [8]. At the same time, it moves four protons across the membrane, producing a proton gradient. Cyanide acts as an inhibitor, completely blocking electron transport by irreversibly binding to cytochrome c oxidase so as to prevent the binding of O_2[17, 18].

As the proton concentration increases in the intermembrane space, a strong electrochemical gradient is established across the inner membrane. The protons can return to the matrix through the ATP synthase complex, and their potential energy is used to synthesize ATP from ADP and inorganic phosphate (P_i)[8]. Under certain conditions, protons can re-enter the mitochondrial matrix without contributing to ATP synthesis. This process is known as proton leak or mitochondrial uncoupling and is due to the facilitated diffusion of protons into the matrix. The process results in the uncontrolled potential energy of the proton electrochemical gradient being released as heat. In living cells, the drug 2,4-dinitrophenol (DNP) acts as a proton ionophore, an agent that can shuttle hydrogen ions across biological membranes[19]. It uncouples oxidative phosphorylation by carrying protons across the mitochondrial membrane, collapsing the proton motive force that the cell uses to

produce most of its ATP chemical energy, and leading to a rapid consumption of energy without generation of ATP. Cells counteract the lowered yields of ATP by oxidizing more stored reserves such as carbohydrates and fats. However, the importance of uncoupling is not restricted on thermoregulation only, but also can be favourable for the performance of the metabolic and energy-conversion functions of cellular respiration[20]. Furthermore, it is suggested to play a role in the anti-ROS defence system of the cell, such as prevention of oxygen radical formation by mitochondria in the resting state [20].

ATP production in an aerobic eukaryotic cell is tightly regulated by feedback controls, and by the substrate concentration dependence of individual enzymes within the glycolysis and oxidative phosphorylation pathways. Key control points occur in enzymatic reactions that are so energetically favorable that they are effectively irreversible under physiological conditions. In glycolysis, hexokinase is directly inhibited by its product, glucose-6-phosphate[10], and pyruvate kinase is inhibited by ATP itself. The main control point for the glycolytic pathway is PFK which is allosterically inhibited by high concentrations of ATP and activated by high concentrations of AMP[3]. The inhibition of PFK by ATP is unusual, since ATP is also a substrate in the reaction catalyzed by PFK; the biologically active form of the enzyme is a tetramer that exists in two possible conformations, only one of which binds the second substrate fructose-6-phosphate (F6P). The protein has two binding sites for ATP - the active site is accessible in either protein conformation, but ATP binding to the inhibitor site stabilizes the conformation that binds F6P poorly. A number of other small molecules can compensate for the ATP-induced shift in equilibrium conformation and reactivate PFK, including cyclic AMP, ammonium ions, inorganic phosphate, and fructose 1,6 and 2,6 biphosphate[3].

In the process of oxidative phosphorylation, the key control point is the reaction catalyzed by cytochrome c oxidase, which is regulated by the availability of its substrate—the reduced form of cytochrome c. The amount of reduced cytochrome c available is directly related to the amounts of other substrates. Thus, a high ratio of [NADH]/[NAD^+] or

a low ratio of [ADP][P_i]/[ATP] imply a high amount of reduced cytochrome c and a high level of cytochrome c oxidase activity[21, 22]. An additional level of regulation is introduced by the transport rates of ATP and NADH between the mitochondrial matrix and the cytoplasm[22].

1.1.2. The generation of reactive oxygen species in the mitochondria

In number of cells, including cardiac myocytes, oxygen free radicals can be produced by several mechanisms including the enhanced activity of xanthine oxidase (XO), nicotinamide adenine dinucleotide phosphate (NADPH) oxidase, and mitochondrial electron transport chain (Fig. 1). Mitochondria represent 30% of the total volume of cardiomyocytes[4] and provide ~90% of the cellular energy through the oxidative phosphorylation pathway[2]. As it was mentioned previously in (section 1.1.1.), the main function of the mitochondria is to convert the potential energy stored in various substrates, mainly fatty acids and glucose into ATP (but under certain conditions, proteins can also become sources of ATP). The inner membrane of the mitochondria contains 4 complexes of integral membrane flavoproteins, including NADH dehydrogenase (Complex I). Three of those proteins are involved in the respiratory chain activity. The main function of the respiratory chain is to produce ATP by gradually transferring electrons from NADH and $FADH_2$ (originating from the TCA cycle) to O_2. With the addition of protons (H^+), H_2O is generated in Complex IV. Because of an extreme abundance of mitochondria in cardiac myocytes, mitochondrial electron transport chain (ETC) is considered a major subcellular source of reactive oxygen species (ROS) in the heart[14]. It has been found that in rat cardiomyocytes increased contraction frequency results in formation of ROS[23].

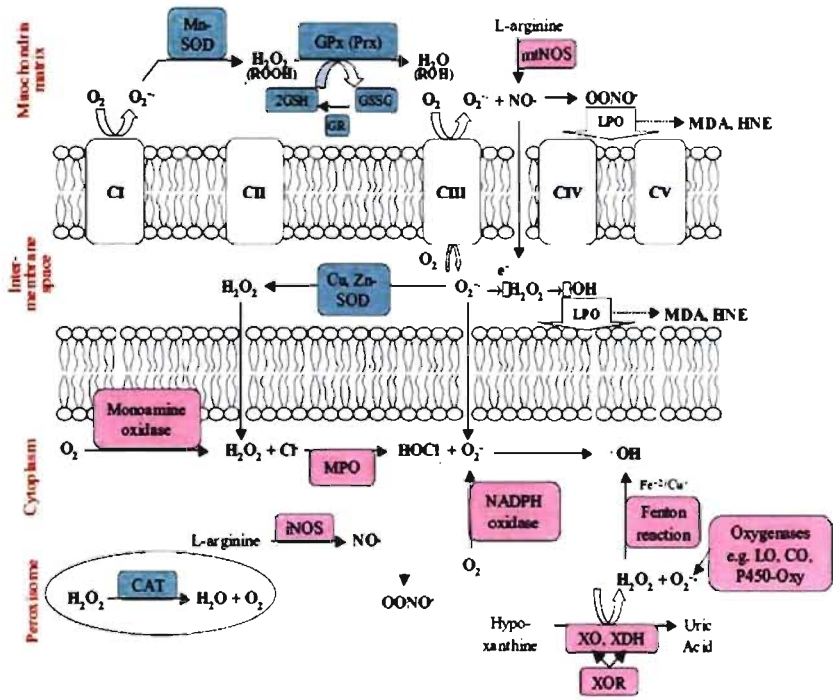

Figure 1: Generation of ROS and their control by antioxidants. Abbreviations: CAT, catalase; CI, CII, CIII, CIV, and CV, respiratory chain complexes I, II, III, IV, and V; CO, cyclooxygenase; CuZnSOD, copper zinc superoxide dismutase; GSH, glutathione; GPx, glutathione peroxidase; GR, glutathione reductase; GST, glutathione S transferase; GSSG, glutathione disulfide; HNE, 4 hydroxynonenal; iNOS, inducible nitric oxide synthase; LO, lipoxygenase; MDA, malondialdehyde; MnSOD, manganese superoxide dismutase; mtNOS, mitochondrial niric oxide synthase; NO, nitric oxide; MPO, myeloperoxidase; P-450-Oxy, cytochrome P450-dependent oxygenases; XO, xanthine oxidase; XDH, xanthine dehydrogenase; XOR, xanthine oxidoreductase; LPO, lipid peroxidation; Prx, peroxiredoxin; ROOH, alkyl hydroxides. (Reproduced from Zacks *et. al.*[24] with permission from the publisher).

ROS are derivatives of molecular oxygen (O_2), e.g. superoxide anions ($O_2\cdot-$), hydroxyl radical ($HO\cdot$), and hydrogen peroxide (H_2O_2). They are unstable and react rapidly with other free radicals and macromolecules in chain reactions to generate increasingly harmful oxidants[25]. The toxic effects of ROS are believed to vary in proportion to the quantity and their oxidant strength e.g. $HO\cdot > > > O_2\cdot > H_2O_2$. While H_2O_2 is not excessively reactive, it is highly diffusible and is a precursor of $HO\cdot$, which is highly reactive at its site of production. H_2O_2 readily crosses membranes and thus, is capable of affecting distant cellular targets in the same cell. The H_2O_2 production is relatively important and leads to a constant cellular concentration between 10^{-9} and 10^{-7} M. The effects of ROS on cell metabolism have been well documented in a variety of species. These include not only roles in programmed cell death and apoptosis and ischaemic injury, specific examples include stroke and heart attack, but also positive effects such as the induction of host defense genes and mobilisation of ion transport systems. This is implicating them more frequently with roles in redox or oxidative signaling [26, 27].

Mitochondria are considered a major source of ROS production in the heart[28]. In mitochondria, the partial reduction of O_2 occurs as a result of leakage of electrons from the ETC, contributing one, two or three electrons to form $O_2^{\cdot-}$, H_2O_2, or $HO\cdot$, respectively. Electron leakage can occur at a number of points in the ETC, producing $O_2^{\cdot-}$[29]. As much as 2–4% of the reducing equivalents escape the respiratory chain, leading to $O_2^{\cdot-}$ formation. ROS production and its effects are controlled by a very sophisticated and complementary cellular antioxidant system. $O_2^{\cdot-}$ can be converted by manganese superoxide dismutase (MnSOD) to H_2O_2 that may then be converted to highly reactive and harmful $HO\cdot$ radicals, the most destructive free radicals, via reaction with Fe^{2+}: Fenton chemistry. For each 2 superoxide radicals encountered by SOD, 1 H_2O_2 is formed. Catalase, which is concentrated in peroxisomes located next to mitochondria but formed in the rough endoplasmic reticulum and located everywhere in the cell, reacts with the H_2O_2 and forms water and oxygen. Glutathione peroxidase reduces H_2O_2 by transferring the energy of the

reactive peroxides to a small sulfur containing peptide called glutathione. The selenium contained in these enzymes acts as the reactive center, carrying reactive electrons from the peroxide to the glutathione. Due to the lower concentration of catalase in the heart, it was suggested that glutathione peroxidase to be more efficient in detoxifying H_2O_2. Peroxiredoxins also degrade H_2O_2, both within the mitochondria, cytosol and nucleus[30].

Generally, the leakage of electrons at Complex I flavoprotein generates $O_2^{\cdot-}$ in mitochondrial matrix while complex III ubisemiquinones ($UQ^{\cdot-}$) generated at Q1 (UQ^{-1}.) and Q*o* (UQ^{-o}.) sites release $O_2^{\cdot-}$ in the matrix and intermembrane space of the mitochondria, respectively[31]. However the main source of ROS production in the respiratory chain remains still controversial.

It was revealed that loss of cytochrome c by mitochondria oxidizing NAD^+-linked substrates causes a remarkable raise of ROS production and respiratory inhibition. This elevated ROS production can resemble to the effect of rotenone as well as other chemical inhibitors of electron flow that act further downstream in the ETC. Due to the fact that this effect of cytochrome c depletion on ROS production and respiration were reversible upon addition of exogenous cytochrome c, it was concluded that a main site of ROS generation in both brain and heart mitochondria is proximal to the rotenone inhibitory site, rather than in Complex III. As a result, it was suggested that the ROS-generating site of Complex I is the Fe-S centre N-1a[16]. Liu *et. al.*[12]showed that ROS generation supported by the Complex II substrate succinate happens at the flavin mononucleotide group (FMN) of Complex I through reversed electron transfer, not at the ubiquinone of Complex III as commonly thought. Indirect indication points out that the unknown ROS-generating site within complex I is also likely to be the FMN group. It is therefore suggested that the major physiologically and pathologically relevant ROS-generating site in mitochondria is limited to the FMN group of complex I[12].

On the other hand, another study showed that restriction of electron transport by the inhibitor rotenone directly before ischemia decreased the production of ROS in cardiac

myocytes and reduced damage to mitochondria. It was found that in mitochondria oxidizing Complex I substrates, rotenone inhibition did not increase H_2O_2, while oxidation of Complex I or II substrates in the presence of antimycin A patently did. Rotenone prevented antimycin A-induced H_2O_2 production in mitochondria with Complex I but not with Complex II substrates[14]. In contrast to intact mitochondria, blockade of Complex I with rotenone markedly amplified H_2O_2 production from submitochondrial particles oxidizing the Complex I substrate NADH. It was concluded that ROS are generated from Complex I by the NADH dehydrogenase located in the matrix side of the inner membrane and are dissipated in mitochondria by matrix antioxidant defense. It was also suggested that in mitochondria, Complex III is the principal site for ROS generation during the oxidation of complex I substrates, and rotenone protects by limiting electron flow into complex III[14].

It increasingly appears that the cardioprotective models of ischemic preconditioning and postconditioning use modulation of mitochondrial oxidative metabolism as a key effector mechanism. The initially unexpected approach to inhibit mitochondrial respiration provides a new cardioprotective paradigm to reduce cellular damage during both ischemia and reperfusion[32].

1.1.3. Antioxidant defence systems against ROS damage

The overall level of cellular ROS is determined by the relative rate of its generation vs. the rate of its reduction by antioxidants or binding to biomolecules (peptides, proteins, DNA). In physiological conditions for instance during exercise, enzymatic antioxidants are expressed in response to ROS production and function as catalysts in reactions that convert specific ROS to different and, presumably, less harmful species such as H_2O_2. The principal enzymatic antioxidants are superoxide dismutase (SOD), catalase (CAT), peroxiredoxin (Prx) and glutathione peroxidase (GPx)[33, 34] (Fig. 1). GPx (isoforms GPx1 – GPx5), using reduced glutathione (GSH), reduces H_2O_2 or ROOH to H_2O or alcohols (ROH),

respectively. GPx1 and GPx3 are the most abundant intracellular isoforms and GPx4 is a mitochondrial isoform.

The role of one of the major non-enzymatic antioxidant GSH, is involved in the maintenance of cellular redox state. GSH cooperates with GPx in the detoxification of H_2O_2 into 2 H_2O (Fig. 1). Glutathione reductase (GR) is a flavoprotein, with nicotinamide adenine dinucleotide phosphate (NADPH) functions to regenerate antioxidant capacity, converting from glutathione disulfide (GSSG) to the sulfhydryl form GSH. For every mole of GSSG one mole of NADPH is required.

$$GSSG + NADPH + H^+ <=> 2\ GSH + NADP^+ \qquad (1)$$

Accumulation of GSSG is toxic to the cell because it may trigger disulfide cross-linkage of protein, enzymes, and DNA. This is why the cellular ratio [GSH]/[GSSG] is highly controlled and related to the maintenance of the redox status. When to high level, GSSG can be exported from the cell.

Possible role for glutathione was suggested in the determination of functional damage induced by myocardial ischemia and reperfusion. In isolated and perfused rabbit heart, ischemia evoked a rapid decline of contractility was associated with a reduction of the content of tissue GSH with no significant changes in GSSG. Reperfusion induced a small recovery of heart contractility, a substantial release of total glutathione and a further decrease in the content of tissue GSH with a significant increase of tissue GSSG. Ischemia and reperfusion had no effect on glutathione reductase and glutathione peroxidase activities[35].

The activity of GR can be selectively inhibited by 1,3-bis(2-chloroethyl)-1-nitroso-urea (BCNU); a chemotherapeutic drug that may mediate some toxic effects. It was reported that its inhibitory effect on GR was reversible but the GR activity remained below control. Although thiol containing agents such as reduced glutathione can be modulated by

BCNU, it can protect cells against BCNU and a change in glutathione concentrations could alter its effectiveness. BCNU also lowered creatine kinase, malate dehydrogenase, and lactate dehydrogenase activities. The inhibition of GR *in vitro* occurred only after biochemical reduction of the enzyme with NADPH. The oxidation state of GR may determine its sensitivity to BCNU in the human erythrocyte. However, a specific effect or an unusually high sensitivity of BCNU on GR could not be demonstrated[36].

In rat heart mitochondria, BCNU was shown to enhance H_2O_2 formation. However, in submitochondrial particles, H_2O_2 formation and oxygen uptake were not affected in the presence of BCNU, indicating that this substance do not modify respiration. Mitochondria were also able to rapidly metabolize added H_2O_2 in a process partially prevented by BCNU. Moreover, BCNU caused the release of cytochrome c that occurs also in the absence of mitochondrial swelling. Therefore BCNU is capable of shifting mitochondrial thiol-linked redox balance towards a more oxidized condition and causing depletion of GSH and result in oxidative stress[37, 38].

As a result of above, the imbalance between free radical production (for example, the peroxidation of lipids) and antioxidant protection is defined as oxidative stress. When ROS are produced in excess or for sustained periods, or when the antioxidant system is compromised, cells are unable to efficiently scavenge free radicals, leading to ROS accumulation. ROS can rapidly oxidize proteins, lipids and DNA[39, 40], thereby resulting in dysfunction of physiological processes and cellular damage leading to cell/tissue death. Oxidative stress triggers the mitochondrial death pathway thereby causing a variety of human diseases. It plays a central role in the pathogenesis of a number of cardiovascular diseases, such as ischemic heart disease, heart failure, and atherosclerosis. It has been shown that oxygen free radicals cause contractile failure and structural damage in the myocardium.

Results of a variety of studies in mammalian systems have shown that oxidative stress can be reliably measured by oxidative-damage biomarkers, such as lipid peroxides[41], protein carbonyls[42], and oxidative DNA modifications[43].

1.1.4. Lipid peroxidation and the production of 4-hydroxy-2-nonenal

Lipid peroxidation (LPO) is the major biochemical consequence of oxidative deterioration of polyunsaturated lipids in cell membranes and causes damage to membrane integrity and loss of membrane protein function[44]. Peroxidation is in general initiated by oxidative attack-mediated removal of an H· atom. This results in carbon centered radical, that following exposure to O_2 gives a peroxyl radical. Peroxyl radicals can combine with each other, attack membrane proteins, or remove H· from adjacent fatty acids side chains in a membrane thereby propagating a chain reaction of LPO. The ETC and membrane phospholipids such as those in the mitochondrial membrane are particularly susceptible to LPO (Fig. 1). The oxidative degradation of lipids most often affects polyunsaturated fatty acids, because they contain multiple double bonds in between which lie methylene-CH_2-groups that possess especially reactive hydrogens, and also because of their abundance.

As with any radical reaction, the reaction consists of three major steps: initiation, propagation and termination. Initiation is the step whereby a fatty acid radical is produced. The initiators in living cells are most notably ROS, such as $OH^{\cdot}$, which combines with a hydrogen atom to make water and a fatty acid radical. The fatty acid radical is not a very stable molecule, so it reacts readily with molecular oxygen, thereby creating a peroxyl-fatty acid radical. This too is an unstable species that reacts with another fatty acid producing a different fatty acid radical and H_2O_2 or cyclic peroxide if it had reacted with itself. This cycle continues as the new fatty acid radical reacts in the same way. When a radical reacts, it always produces another radical, which is why the process is called a "chain reaction mechanism." The radical reaction stops when two radicals react and produce a non-radical

species. This happens only when the concentration of radical species is high enough for there to be a high probability of two radicals actually colliding. Living organisms have generated different molecules that speed up termination by catching free radicals and therefore protect the cell membrane. One important such lipophilic antioxidant is α-tocopherol, also known as vitamin E.

Among a wide range of aldehydic compounds, 4-hydroxy-2-nonenal (4-HNE or HNE) and malondialdehyde (MDA)[45] are the most common reactive products of the peroxidation of membrane phospholipids[46] (Fig. 1). These aldehydic products are relatively stable compounds compared to ROS, and are able to diffuse and attack targets in the near vicinity as well as those distant from their site of origin. HNE is the primary α,β-unsaturated hydroxyalkenal which is formed in cells by LPO process. It is generated in the peroxidation of lipids containing polyunsaturated omega-6 acyl groups, such as arachidonic or linoleic groups, and of the corresponding fatty acids. HNE has 3 reactive groups: an aldehyde, a double-bond at carbon 2, and a hydroxy group at carbon 4. It is found throughout animal tissues, in micromolar range and in higher quantities during oxidative stress due to the increase in the LPO chain reaction, due to the increase in stress events. Several researchers hypothesize that HNE plays a key role in cell signal transduction, in a variety of pathways from cell cycle events to cellular adhesion. Constitutive levels of HNE may be needed for normal cell functions - lowering of this constitutive HNE level in cells promotes proliferative machinery while an increase in this level promotes apoptotic signaling[47, 48]. On the other hand, in cardiomyocytes, HNE has been shown to be capable of affecting NADPH production, at least partially, by inactivating mitochondrial $NADP^+$-isocitrate dehydrogenase (NADP-ICDH) activity, an important enzyme that controls redox and energy status[49-51]. In isolated cardiac mitochondria, HNE inhibits α-KGDH and reduces NADH production initiated by addition of α-ketoglutarate[52].

1.2. The role of NADPH during oxidative stress

NADPH, the reduced form of $NADP^+$, is similar to the coenzyme abbreviated NADH. It consists of two nucleotides joined through their phosphate groups: with one nucleotide containing nicotinamide, and the other containing an adenosine ring with two phosphate groups (Fig. 2). In rat liver, the total amount of NAD^+ and NADH is approximately 1 μmole per gram of wet weight, about 10 times the concentration of $NADP^+$ and NADPH in the same cells[53]. The $NADP^+$/NADPH ratio is normally about 0.005, around 200 times lower than the NAD^+/NADH ratio which ranges from 3-10 depending on the (patho)physiological condition [54, 55], so NADPH is the dominant form of this coenzyme[56]. The $NADP^+$/NADPH ratio is kept very low because NADPH is needed to drive redox reactions as a strong reducing agent. So these different ratios are keys to the different metabolic roles of NADH and NADPH.

The fate of all aerobic organisms is dependent on the varying intracellular concentrations of NADH and NADPH. The former is the primary ingredient that fuels ATP production via oxidative phosphorylation, while the latter helps sustain the reductive environment necessary for this process and other cellular activities. Some NAD^+ can be converted into $NADP^+$ by NAD^+ kinase (NADKase), which phosphorylates NAD^+[57, 58]. However, the oxidative branch of the pentose phosphate pathway is the major source of NADPH in cells. NADPH can also be produced by several enzymes such as malic enzyme and glutamate dehydrogenase, but also by the activity of $NADP^+$-ICDH in the cytosol as well as the mitochondrion, and uses $NADP^+$ as a cofactor instead of NAD^+. Cardiac mitochondria are equipped with both NAD^+- and $NADP^+$-dependent ICDH. However, the role of the $NADP^+$-ICDH is still not perfectly understood[59].

NADPH is used in anabolic reactions, such as lipid and nucleic acid synthesis, cholesterol synthesis and fatty acid chain elongation, which require NADPH as a reducing agent. In addition, NADPH provides the reducing equivalents for biosynthetic reactions and

for oxidation-reduction involved in protection against the toxicity of ROS. It has been demonstrated that a metabolic network enhancing NADPH production and limiting NADH synthesis is a consequence of an oxidative injury. The activity and expression of glucose-6-phosphate dehydrogenase, malic enzyme, and $NADP^+$-isocitrate dehydrogenase, the major generators of NADPH, were clearly modefied during oxidative challenge. Furthermore, numerous tricarboxylic acid cycle enzymes that provide intracellular NADH were significantly downregulated[58]. It was found that NADKase and $NADP^+$ phosphatase (NADPase), enzymes known to regulate the levels of NAD^+ and $NADP^+$, were capable of modulating these metabolic pathways even further. In oxidative stress condition, the NADKase was upregulated, whereas the phosphatase activity was markedly increased in control cells. Thus, NADKase and NADPase play a crucial role in controlling the cross talk between metabolic networks that produce NADH and NADPH and are integral components of the mechanism involved in preventing oxidative stress[58].

All organisms that use oxygen as the terminal e^- acceptor have evolved complex molecular strategies that allow them to fight the inherent dangers associated with living in an aerobic environment. Catalase, superoxide dismutase (SOD), and GPx are some of the enzymes that help decrease oxidative tension during aerobic respiration[60]. However, the effectiveness of these proteins as the scavengers of ROS depends on the availability of NADPH. Production of NADPH required for the regeneration of glutathione in the mitochondria is critical for scavenging mitochondrial ROS through glutathione reductase and peroxidase systems. This nucleotide supplies the reductive power necessary to suppress the oxidative potential of ROS. Hence, the production of this reducing agent is an essential part of the oxidative energy-generating machinery of all aerobic organisms. Production of ATP via oxidative phosphorylation cannot proceed effectively in the absence of a continual supply of NADPH[61]. The role of mitochondrial NADP-ICDH in controlling the mitochondrial redox balance and subsequent cellular defense against oxidative injury was

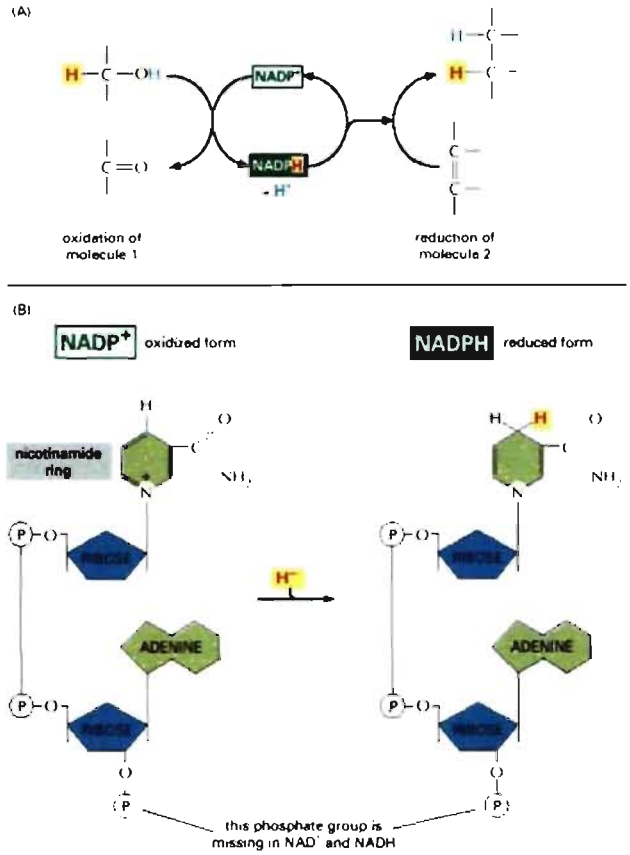

Figure 2: NADPH, an important carrier of electrons. (A) NADPH is produced in reactions of the general type shown on the left, in which two hydrogen atoms are removed from a substrate. The oxidized form of the carrier molecule, $NADP^+$, receives one hydrogen atom plus an electron (a hydride ion), and the proton (H^+) from the other H atom is released into solution. Because NADPH holds its hydride ion in a high-energy linkage, the added hydride ion can easily be transferred to other molecules, as shown on the right. (B) The structure of $NADP^+$ and NADPH. The part of the $NADP^+$ molecule known as the nicotinamide ring accepts two electrons together with a proton (the equivalent of a hydride ion, H^-), forming NADPH. The molecules NAD^+ and NADH are identical in structure to $NADP^+$ and NADPH, respectively, except that the indicated phosphate group is absent from both. (From Alberts *et. al.* 1994)[8].

demonstrated, as a major NADPH producer in the mitochondria[61, 62]. Glucose-6 phosphate dehydrogenase (G6PDH), NADP-ICDH, malic enzyme (ME), 6-phosphogluconate dehydrogenase (6PGDH), and $NADP^+$-glutamate dehydrogenase (NADP-GDH) are some of the important enzymes that enable aerobic cells to fulfill their requirement for NADPH. NADH, which is generated essentially during the catabolism of acetyl-coenzyme A via the TCA cycle, is considered as a powerful proxidant as its downstream metabolism mediated by complexes I, III, and IV produces the majority of the ROS generated in aerobic organisms[63]. Hence, a fine balance has to be maintained between these two nicotinamide nucleotides if a cell is to function in an efficient manner. Thus, a normal functioning cell has to have adequate levels of NADPH and ATP and a small amount of NADH. On the other hand, a high concentration of NADH coupled with a low concentration of NADPH provokes an oxidative milieu, a condition that may lead to cellular dysfunction and diseases[63].

1.3. Oxidative stress during normal and pathological pregnancy

Pregnancy induces significant adaptations in the cardiovascular system, associated with hemodynamic and endocrine changes that contribute to maternal volume expansion and are necessary for fetal homeostasis, development and well-being[64]. Systemic arterial vasodilatation represents one of the first detectable changes in hemodynamics that initiates a cascade of compensations in the circulation and volume homeostasis that also affect the heart: cardiac output rises in response to increase in the heart rate and achieves the greatest value in the final stages of delivery, placing an enhanced volume load on the heart. Blood volume expansion leads to adaptations of the myocardium that affects mainly left ventricle, more susceptible to increased load. In contrast to pathological conditions, these alterations are associated with physiological reduction of blood pressure (BP) and are reversible. The natural volume overload in pregnancy is frequently associated with increase in left ventricular size and mass, leading to left ventricular hypertrophy[65-67]. In Sprague-Dawley

rats, an adaptive hypertrophic remodelling of the left ventricular in normal pregnancy has been demonstrated[68]. Structural changes within the heart reflect the volume loading of pregnancy. Despite the fact that clear resemblance has been demonstrated between cardiovascular changes associated with pregnancy vs. training and/or exercise[69], mechanisms behind those changes are still not fully understood.

Pregnancy is well known to be associated with significant changes in carbohydrate metabolism[70], resulting from the primary dependence of the fetus on maternal glucose for its fuel requirement. Glucose homeostasis is affected due to increased glucose uptake of fetus, drained by the fetoplacental unit. This leads in a more rapid conversion from predominantly carbohydrate to predominantly fat utilization because of earlier depletion of liver glycogen stores, associated with increased lactate and pyruvate levels. Such metabolic changes are also likely to affect heart function. In the heart, there is a crucial crosstalk between protein function and metabolism. The maintenance of energy homeostasis is highly dependant on a continuous supply of oxygen, ADP, inorganic phosphate and reducing equivalents. The heart is able to use a wide range of substrates for energy production, including fatty acids, glucose, lactate, pyruvate and ketone bodies. Acute changes in the relative concentration of energy substrates can induce important modifications in metabolic fluxes[71]. Several cardiovascular diseases have been associated with metabolic switches in the fuel partitioning for energy production[72]. These switches occur in response to various stimuli such as hormones, changes in substrate availability, oxygen supply and/or workload and can therefore also play an important role in pregnancy.

Cardiovascular adaptations during pregnancy are also linked to hormonal changes. Plasma volume increases in response to estrogen, primarily by its stimulation of the renin-angiotensin-aldosterone system (RAAS), leading to sodium ion and water retention[73]. Recent studies indicate that aldosterone stimulates production of ROS[74, 75] by activation of NADPH oxidase in blood vessels[76]. It is to be expected that the effect of hormones that stimulate ROS formation, such as aldosterone, to be depending on the pre-existing redox

status of the cells. Thus in situations with increased levels of oxidative stress, a further stimulation of ROS formation by aldosterone is more likely to lead to pathological damage[77]. At low oxidative stress, aldosterone promotes NO production while in situations with increased oxidative stress (such as heart failure) the further production of superoxide initiated by aldosterone is likely to have unfavorable effects on vascular function. Inhibition of MR was therefore proposed to be beneficial for cardiovascular function[77]. In pregnancy, it has been found that concentrations of lipid peroxides in the placenta are higher than in blood, and increased levels of lipid peroxides has also been reported in blood in pregnant women when compared to non-pregnant[78]. During pregnancy, elevated levels are seen in the second trimester and these diminish later in gestation, decreasing further after delivery[78]. LPO levels in placental tissue follow a different pattern than in blood over period of gestation[79]. Both peroxidation and antioxidant reactions are enhanced during pregnancy. During uncomplicated gestation, ROS levels are elevated[80]; however, they are counterbalanced by an increased activity of antioxidants[81]. Maternal levels of vitamin E and lipid peroxides are both increased in pregnancy compared with non-pregnancy. Increased lipid peroxides during pregnancy may be related to increase in spontaneous auto-oxidation of serum lipids. Placenta lipid peroxides apparently contribute to maternal circulating levels because plasma lipid peroxide levels decrease abruptly after delivery[81]. It has been shown that normal pregnancy is associated with the formation of susceptible oxidizable particles and an increase in oxidative damage[82]. In the third trimester of normal pregnant women, a significant increase in the levels of circulating MDA, a marker of LPO, was observed as compared to non pregnant controls[83]. However, this observation was accompanied by a decreasing trend for some non-enzymatic antioxidants like reduced glutathione, vitamin E, C and A. These findings were augmented in the case of pathological pregnancy such as pregnancy induced hypertension or diabetic pregnancy[83, 84].

1.4. NAD(P)H fluorescence as a tool to investigate mitochondrial oxidative metabolism

NADH and NADPH, collectively referred to as NAD(P)H, are endogenous fluorophores which become fluorescent when excited by UV light. Both of them are of sufficient concentration in cells to yield a detectable fluorescence signal[85, 86] and they belong to the principal endogenous indicators of cellular energetic metabolism[87, 88]. Modifications of the amount and distribution of these intrinsic fluorophores or chemical-physical properties of their microenvironment can be due to changes occurring in the cell and tissue state during physiological and/or pathological processes. Therefore, analytical techniques based on autofluorescence monitoring can be used in order to obtain information about physiological state of cells and tissues[89, 90].

Fluorescence is the property of some atoms and molecules to absorb light at a particular wavelength and to subsequently emit light of longer wavelength after a brief interval[91]. The fluorescence process is governed by three important events, all of which occur on timescales that are separated by several orders of magnitude. First, excitation of a molecule by an incoming photon happens in femtoseconds, while subsequent fast vibrational relaxation of the electron in excited states to the lowest excited energy level (S_1) is much slower and can be measured in picoseconds. The final event - fluorescence, returning the molecule to its ground state (S_0), occurs usually at the relatively longer time range of several nanoseconds[91]. A photon emitted during fluorescence has energy that corresponds to the energy difference between S_1 and S_0 state. A characteristic time when molecule remains in S_1 prior to returning to S_0 is called the fluorescence lifetime. The fluorescence lifetime is the characteristic time that a molecule remains in S_1 prior to returning to S_0 and is an indicator of the time available for information to be gathered from the emission profile. The decay of fluorescence intensity as a function of time in a uniform population of molecules excited with a brief pulse of light is described by an exponential function:

$$I_{(t)} = I_0 \bullet e^{(-t/\tau)} \qquad (2a)$$

where $I_{(t)}$ is the fluorescence intensity measured at time t, I_0 is the intensity observed immediately after excitation, and τ is the fluorescence lifetime. Formally, the fluorescence lifetime is defined as the time in which the fluorescence of a molecule decays to 1/e of the initial intensity[87]. In the absence of any other deactivation processes, the radiative lifetime τ_0 is the reciprocal of the rate constant k_F for transfer from S_1 to S_0 state. However, in real system other rates of excited state decay can exist, such as quenching, energy transfer, internal conversion or inter-system crossing. If the rate of any such non-radiative pathway changes, this will be reflected in the change of the observed excited state lifetime τ. If we sum all non-radiative rates of excited state decay together into the term k_{NR}, we can define fluorescence lifetime as

$$\tau = 1 / (k_{NR} + k_F) \qquad (2b)$$

This quantity is the reciprocal of the rate constant for fluorescence decay from S_1 to S_0.

Since the ratio between the concentrations of free and protein-bound NAD(P)H can give an indication about the metabolic activity of cells, the development of autofluorescence techniques which accurately measure the modifications to this ratio is particularly significant. Furthermore, it has been demonstrated that protein-NAD(P)H complexes are characterized by different fluorescence lifetimes and these are not uniformly distributed all over the cell, but are concentrated in certain cellular regions. Changes in fluorescence lifetimes can indicate either modification in protein-NAD(P)H complexes or different bond strengths between NAD(P)H and the protein in these complexes[92]. Moreover, autofluorescence analysis can be performed in living cells or tissues in real time because it does not require any treatment of fixing or staining of the specimens. In the past

few years spectroscopic and imaging techniques have been developed for many different applications both in basic research and diagnostics[89, 90].

There are no known photophysical means of discriminating NADH and NADPH[93]. It is therefore necessary to consider the relative contributions of these two reduced pyridine nucleotides to the measured intracellular fluorescence. Previous biochemical studies have determined that the blue fluorescence observed in the heart originates predominantly from NAD(P)H in the mitochondria, but with a negligible contribution of cytoplasm[94-96]. The concentrations of pyridine nucleotides have been measured by high performance liquid chromatography in mouse hippocampus. It was found that the total concentration of NADH and NAD^+ is greater than that of NADPH and $NADP^+$ by a factor of ~10. The concentration of the reduced fluorescent species NADH was found to be ~5 times greater than that of the fluorescent NADPH. In isolated heart mitochondria, NADH has as much as a fourfold greater fluorescence yield than NADPH, at least 80% of the AF can essentially be considered to be from NADH alone[95, 97-101]. Furthermore, the enhancement of mitochondrial NADH quantum yield due to environmental effects has been estimated to be a factor of 1.25–2.5 greater than that of NADPH. Overall, the given evidence implies that while the contribution of NADH is prevailing in the intrinsic cell fluorescence, the NADPH represents smaller but non-negligible fraction of the UV-excited autofluorescence. Like NADH, the ratio between the fluorescent NADPH and its non-fluorescent oxidized form $NADP^+$ is dependent upon the relative rates of NADPH source/consumption reactions. However, NADH and NADPH are distinct in their biochemical roles: NADH being largely restricted to energy metabolism and NADPH largely to reductive biosynthesis. It has been reported that the chemical kinetics of NADH and NADPH differ in certain reactions. However, tissue analyses of pyridine nucleotide content in heart and liver have confirmed that the fluorescence changes during the normoxic-anoxic transition are dominated by changes in NADH with only a minor (~10%) contribution from NADPH.

The observed blue autofluorescence is dependent on the mitochondrial redox state, on the conformation of the fluorescing molecule, and on its environment[85]. Fluorescence intensity is proportional to the concentration of mitochondrial NAD(P)H; an increase in the fluorescence intensity indicates a more reduced state of NAD(P)H and of the rest of the mitochondrial ETC. Fluorescence lifetime is insensitive to the concentration changes because it is specific for different molecular conformations, thus reflecting possible interactions of the fluorescing molecule with its surroundings. Any change in molecular conformation, binding to surrounding molecules and/or chemical compartments therefore results in modification of the relative amplitudes and/or lifetime of the fluorescing molecule. NAD(P)H binding to protein cofactors resulting in enhancement of fluorescence decay time and/or altering the wavelength of maximal emission[85, 102]. The pronounced dependence of NAD(P)H fluorescence on microenvironment leads to a multi-exponential fluorescence decay kinetics in most solvents, due to the effect of dynamic quenching related to the formation of non-fluorescent transient species from the first excited state[103, 104]. In addition, NAD(P)H forms complexes with several enzymes, which makes the interpretation of the NAD(P)H signals from intact tissues particularly difficult in living cells. Thus any change in molecular conformation, binding to surrounding molecules and/or chemical compartments results in modification of the relative amplitudes and/or lifetime of the fluorescing molecule.

1.5. Objectives of present study

NADPH, as an endogenous fluorophore, has an important role as a cofactor for several enzymatic reactions including those of the defense mechanism pathways against oxidative stress, such as GR. We propose a hypothesis that NADPH, modulated by changes in oxidative metabolic state, can be used as a non-invasive sensor of oxidative stress in living cardiac cells. We aimed to investigate changes in the oxidative redox state of the cardiac cells in response to oxidative stressors. To study NAD(P)H fluorescence, we have

adopted spectrally-resolved fluorescence lifetime detection to identify its parameters, namely changes in the amplitudes and also in fluorescence decay lifetimes of the molecule *in vitro* and in living cardiomyocytes in the aim to better understand its participation in the cellular metabolic activity in response to oxidative stress. To accomplish our goal, our partial objectives were to:

1. test the sensitivity of NADPH fluorescence *in vitro* in intracellular media-mimicking solutions to changes in the NADPH concentration, pH, or viscosity. Fluorescence spectra, as well as fluorescence lifetimes will be investigated. Modulation of NADPH fluorescence *in vitro* by GR will be also studied to analyze whether NADPH binding to its enzymes affects its fluorescence kinetics.

2. study the effect of oxidative stressors on NAD(P)H fluorescence in single living rat cardiomyocytes to determine its sensitivity to oxidative changes in the cell environment. Oxidative stress-mimicking agents: the non-specific hydrogen peroxide (H_2O_2) and the by-product of lipid peroxidation, HNE, will be used in the presence or absence of the modulators of GR, 1,3-bis (2-chloroethyl)-1-nitrosurea (BCNU), or of respiratory chain, 2,4-dinitrophenol (DNP) (uncoupler of ATP synthesis), and rotenone and cyanide (inhibitors of the Complex I and IV of the respiratory chain respectively).

3. explore the potential application of the tested method to study changes in metabolic oxidative status under pathophysiological conditions. Pregnancy is well known to provoke significant metabolic adaptations in the cardiovascular system, namely metabolic switch from the use of glucose to the use of lactate and pyruvate. NAD(P)H fluorescence of left ventricular cardiomyocytes will be examined in normal pregnancy rat model. Oxidative changes will be induced by inhibition of mineralcorticoid receptors (MR) by its antagonist potassium canrenoate, and verified by blood measurements of HNE-protein adducts. NAD(P)H fluorescence will be analyzed in the absence and in the presence of oxidative stressors H_2O_2 and HNE.

2. MATERIAL AND METHODS

2.1. Material

2.1.1. Animal models

In this study female Sprague-Dawley rats (13-14 week old, Charles River, Canada) were used. All procedures were performed in accordance with the Canadian Council on Animal Care (CCAC) guidelines and were evaluated by the local committee, "Comité Institutionnel des Bonnes Pratiques sur les Animaux en Recherche" (CIBPAR), accredited by the CCAC. One group of non pregnant (NP) rats was used as control for rats in normal pregnancy (P). Other groups of non pregnant and pregnant rats were treated with a mineralcorticoids receptors (MR) antagonist, potassium canrenoate also called canrenoic acid potassium salt (20 mg/kg/day) in tap water *ad libitum* referred to (NP_{can}) and (P_{can}) respectively. Rats were treated for seven days (last days in the case of pregnancy), and were sacrificed by decapitation (21^{st} day in the case of pregnancy, i.e. one day prior to parturition).

2.1.2. Isolation of left ventricular cardiomyocytes

2.1.2.1. The heart isolation system

Left ventricular myocytes were isolated following retrograde perfusion of the heart with proteolytic enzymes[105, 106]. The system of perfusion comprises a Langendorff system connected to a pump to control the flow of perfused solutions as shown in (Fig. 3). All the bottles including the perfusion column have a double wall, and the space between both walls is filled with water heated to 36±1 °C using a circulatory bath so that the solutions are

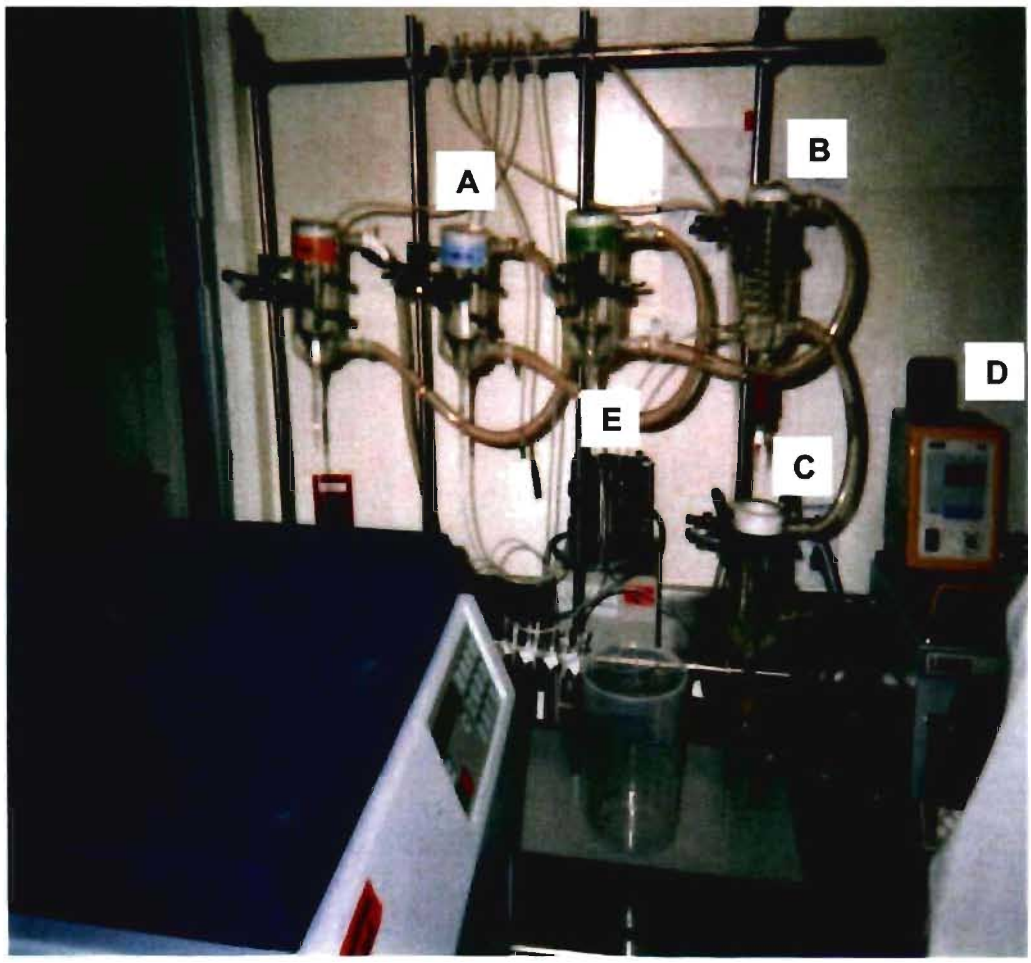

Figure 3: System of perfusion of the heart. A: columns of perfused solutions. B: column of Langendorff. C: place of attachment of the heart. D: water bath adjusted to 36±1 °C. E: Electric pump to control the flow of perfused solutions.

maintained at this temperature when perfused. Three bottles contain the isolation solutions for perfusion, and the fourth one is put under the perfusion column to keep the heart warm, and to collect the enzyme solution for recirculation. The perfusion column is connected to a needle on which the heart is attached during all isolation. All solutions are oxygenated with air. To avoid any bacterial growth, the system is washed with deionized water three times before and after use, and the residual water is removed from the tubes.

2.1.2.2. Perfusion of the heart

The animals were euthanized in the morning by decapitation. The heart was rapidly removed, leaving sufficiently long aorta for attachment of the heart on the column, and then cleaned by the Tyrode solution to clear the heart from the excess of the blood. The heart is attached on the column with a clip, and tied securely with silk thread (about 0.22 mm in diameter) to ensure that the heart remains well fixed during the experiment. The heart should be contracting at this moment. By bringing up the bottle located under the perfusion column, the heart will be warmed up in a space of which the temperature is 36±1 °C. The perfusion starts with tyrode solution containing $CaCl_2$ 0.75 mM, to maintain the functioning heart and allow the contractions to eliminate the remaining blood. When the solution coming out from the heart is clear, without blood, isolation begins. To stop the contractions, the heart is perfused with Tyrode solution with the addition of EGTA 0.1mM, a chelating agent that is a suppressor of Ca^{2+} ions. This solution is perfused for 5 minutes after the contractions stop completely. Finally the heart is perfused with Tyrode solution containing 0.05 mM of $CaCl_2$ and the two proteolytic enzymes: collagenase type II (300-350 U/mg) and the protease type XIV (4.9 U/mg). Once the enzymes reach the heart, the heart is perfused for about 7-10 minutes depending on its size. It is preferred to touch the heart tissue several times to feel whether it is soft or not. The collected enzyme is then supplemented with 5 ml of BSA 10 %[105, 106].

2.1.2.3. Isolation of living cardiac cells

The heart is cut crosswise so the atriums are avoided and placed in a glass Petri dish. The right ventricle is excised, and the left ventricle, which represents the rest of the heart, is then cut in pieces which are placed in 5 ml of enzyme solution introduced with the addition of BSA to a final concentration of 1 %. The solution is oxygenated by a provision of air. After circular and manual agitation of 5 min in a bath at 36±1 °C, the cells are filtered through the nylon of pores of 250μm, and the rest of the tissue replaced under the agitation in the same conditions. The filtrate containing myocytes is supplemented until 10 ml with Tyrode solution containing $CaCl_2$ 750 μM to dilute the enzyme solution and stop its action, then centrifuge (at 100 x g for 2 min). The supernatant is discarded and 5ml of 750 μM $CaCl_2$ is added to the pellet. The last steps are repeated 3 or 4 times by using the cells in the water bath depending on the quality. Cells are washed twice with 750 μM Ca^{2+} solution before storing in the refrigerator to remove the remaining enzyme which could harm the cells. Then cells are put into refrigerator in labelled Petri dishes until use. Only cells that showed clearly defined striations and edges were used in up to 10 hrs following isolation[105, 106].

2.1.3. Solutions

2.1.3.1. Solutions for study of free NADPH fluorescence in vitro

Basic intracellular solution contained (in mM): NaCl, 10; KCl, 140; $MgCl_2$, 1; 4-(2-hydroxyethyl)-1-piperazineethanesulfonic acid (HEPES), 10; adjusted to pH 5.4, 7.4 or 9.8 with KOH. Solution was prepared using deionized water and kept frozen at -20 °C until use. NADPH fluorescence *in vitro* was measured in this solution at concentrations from 1 to 20 μM. This solution was also used for the production of NADPH by $NADP^+$-ICDH (3.9 U/ml) from isocitrate (89 mM) and $NADP^+$ (0.5 mM) with or without GSSG (50 nM) and

GR (0.5 U/ml). To perform the viscosity experiments, different amounts of glycerol were added vs. purified water.

2.1.3.2. Solutions for study of cardiomyocyte autofluorescence

(1) The isolation solution: contained (in mM): NaCl, 130; KCl, 5.4; $CaCl_2$, 0.75; $MgCl_2$ 1.5; NaH_2PO_4, 0.4; creatine, 10; taurine, 20; glucose, 10; Hepes, 10; pH 7.3 with NaOH. $CaCl_2$, 0.75 and ethylene glycol tetraacetic acid (EGTA), 0.1.

(2) Basic external solution: contained (in mM): NaCl, 140; KCl, 5.4; $CaCl_2$, 2; $MgCl_2$ 1; glucose, 10; HEPES, 10; pH 7.35 with NaOH. This solution was used to study the NAD(P)H fluorescence in cells. All solutions were prepared with deionized water and stored at 4 °C prior to use.

2.1.4. Reagents

Cells were treated (in basic external solution for 30 min at 35 °C before recording) with neutral solutions of different agents such as 1,3-bis(2-chloroethyl)-1-nitroso-urea (BCNU, 100 μM); and/or hydrogen pyroxide (H_2O_2, 1 μM); or 4-hydroxy-2-nonenal (HNE, 25 or 50 μM). Rotenone (1 μM), Na-cyanide (4 M) and 9,10-dinitrophenol (DNP, 50 μM)) were added for 5 min at 24 °C prior to cell incubation; The Na-3-β-hydroxybutyrate (BHB, 3 mM) and Na-pyruvate (100 μM) were prepared freshly, while Na-acetoacetate (AcAc, 150 μM or 1.5 mM) was added from 250 mM stock solution. Lactate (1 mM) was added to the basic external solution from the 100 mM stock-solution, where pH was carefully adjusted to 7.20 with HCl. All chemicals were from Sigma-Aldrich (Canada), except cyanide which was from Fisher (Canada).

2.2. Methods

2.2.1. Analyses of the blood

Blood was collected from the body immediately after decapitation in the animal house. The samples from whole blood for substrates and lipids were processed immediately and determined by standard enzymatic methods[107] by the clinical biomedical lab at Saint Justine Hospital. For pyruvate measurement, blood sample was treated with 5% trichloroacetic acid and immediately vortexed for 2 min. Each sample was then centrifuged for 4 min at 10,000 x g, the supernatant collected and rapidly frozen at -20 °C. Pyruvate was subsequently determined by standard enzymatic dosage.

The blood samples for LPO markers were analyzed by Thierry Ntimbane (lab Dr. Comte). Quantification of HNE bound to proteins in whole blood samples (400 µl, EDTA tubes) was performed upon the method described by Asselin *et al*[108] as follows: after addition of 200 µl of NaB^2H_4 (1 M) reducing HNE to its corresponding alcohol chemically stable [^{2}H]DHN, proteins were precipitated with saturated sulfosalicylic acid (200 µl). The protein pellet was extracted twice with mixed methanol:chloroform (3 ml; 2:1, vol:vol), rinsed thrice with water (1 ml) before resuspension in guanidine buffer (0.5 ml; pH 7.2) and addition of internal standard [$^2H_{11}$]1,4-dihydroxynonene (DHN; 0.1 nmol). After treatment with Raney Nickel, extraction and evaporation, the residue was treated with N-methyl-N-(*t*-butyldimethylsilyl)-trifluoroacetamide (75 µl), heated (90 °C, 3 h) and left overnight (70 °C) for derivatization.

Two µl aliquots were injected into a Hewlett Packard 6890 Series GC System version A.02.14 (Hewlett Packard, Paolo Alto, CA, USA) equipped with HP-5 capillary column (50 m x 0.2 mm x 0.33 µm) coupled to a Mass Spectrometer (Agilent Technologies Mass Selective Detector 5973 Network) operated in ammonia positive chemical ionization mode. Two ion sets were measured: *m/z* 389, 390 and 400, corresponding to the molecular ion and 257, 258 and 268, resulting from fragmentation, for the analyses of DHN,

[^{2}H]DHN and internal standard [$^2H_{11}$]DHN respectively. The MS source and quadrupole were set at 180°C-126°C and 300°C-176°C for the 2 ion sets respectively. The chromatograph temperature program was: 170 °C for 1 min, increased by 10 °C/min up to 210 °C, increased by 5 °C/min up to 280 °C and by 20 °C/min up to 320 °C for 10 min. Levels of HNE-proteins were calculated over a minimum of duplicate injections.

2.2.2. Spectrally-Resolved Time-Correlated Single Photon Counting (TCSPC)

In our study, we have used a combination of fluorescence microscopy and spectrally-resolved time-correlated single photon counting (TCSPC) (Fig. 4). Samples were mounted on an inverted microscope (Axiovert 200M, Zeiss, Canada) (Fig. 4B). Picosecond diode laser with emission line at 375 nm (BDL-375, Becker&Hickl, Boston Electronics, U.S.A) (Fig. 4A) was used as an excitation source for NAD(P)H (output power ~1 mW, repetition rate 20 MHz, pulse widths typically < 100 ps). The laser beams were combined by dichroic filters and reflected to the sample through epifluorescence path of Axiovert 200 inverted microscope to create slightly defocused elliptical spot (20 x 10 μm). The size of the spot was chosen in regard to the average width (20-30 μm) of one cardiac myocyte[68]. Emitted NAD(P)H autofluorescence was spectrally separated from excitation light using standard dichroic filter cubes (395 nm dichroic and 397 nm long-pass filter for excitation at 375 nm) in the microscope filter turret. A polarizer in a "magic-angle" orientation was fitted in front of the detection system at the microscope output port to avoid distortions of decay kinetics due to depolarization effects in the microscope optics.

The spectral decomposition of fluorescence was obtained using a 16-channel photomultiplier array (PML-16, Becker-Hickl, Boston Electronics, U.S.A)(Fig. 4D), running in the photon-counting regime and feeding the time-correlated single photon counting interface card SPC 830 using SPCM software (both Becker-Hickl, Boston Electronics, U.S.A), attached to the imaging spectrograph (Solar 100, Proscan, Germany) (Fig. 4C). Fluorescence decays were measured for 30 s with 25 ns TAC time-base sampled

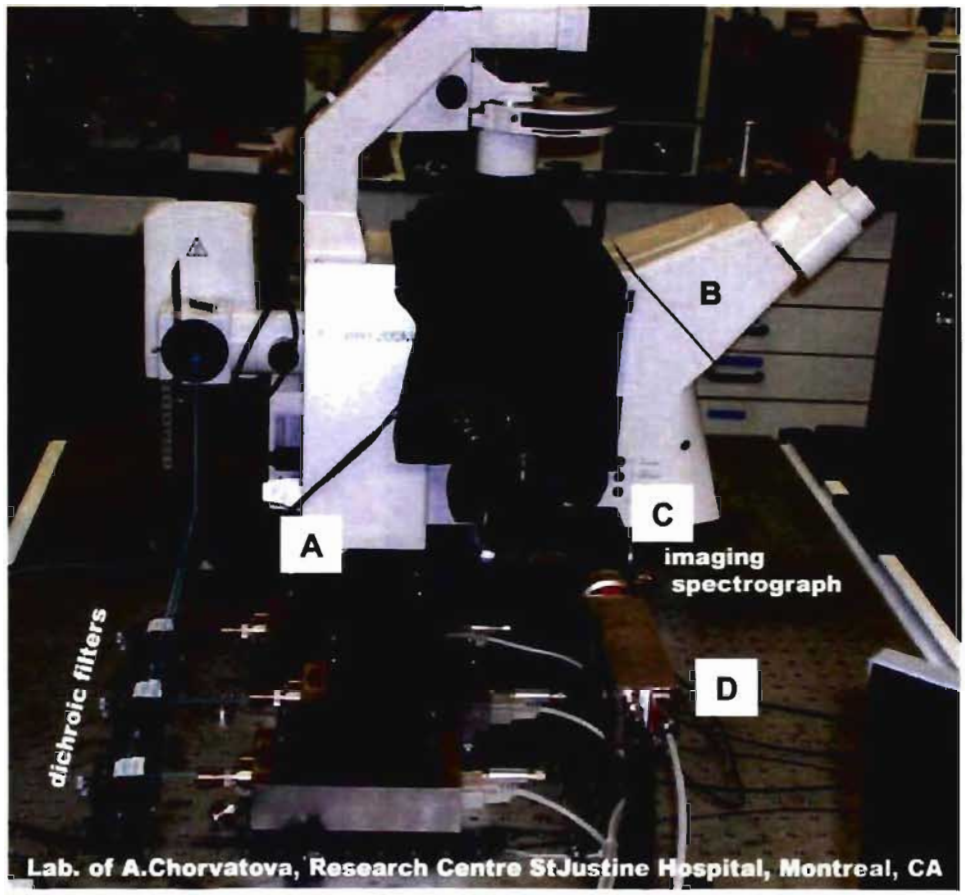

Figure 4: The spectrally-resolved time-correlated single photon counting (TCSPC) instrumentation. A: Picosecond laser diode with emission of 375 nm, B: Axiovert 200M inverted fluorescence microscope, C: imaging spectrograph, D: 16-channel photomultiplier.

by 1024 points, leading to the temporal resolution of 24.4 ps/channel. Decay kinetics were measured for 30 s, with the number of counts at each channel reaching maximum intensity of about 500-5000 counts and the typical background noise of 10-100 counts per channel, present mostly due to ambient light. We have opted for a 20 MHz repetition rate in order to ensure a sufficient time-window (50 ns) for observed fluorescence kinetics. Cells and *in vitro* samples were mounted on an inverted microscope (Axiovert 200M, Zeiss, Canada) and studied in 4-well chambers with UV-proof coverslip-based slides (LabTech, Canada).

In living left ventricular cardiac myocytes bathed in basic external solutions, NAD(P)H autofluorescence was recorded simultaneously at all 16 channels. Steady-state emission spectra of the cardiomyocyte autofluorescence were determined from the total photon counts on each spectral channel.

The half-width of instrument response function (IRF) of our setup was 0.2-0.25 ns, according to the measurement of the Raman scattering peak of water[109]. The spectrometer was calibrated using the emission maxima of known reference dyes (such as DPA) and the water Raman peak[109]; the spectral range of our system was estimated to ~390-680 nm with 16 equidistantly-spaced spectral intervals 18 nm-wide[109].

2.2.3. Analysis of NAD(P)H fluorescence

Steady-state autofluorescence was evaluated as total photon counts for each spectral channel. Each lifetime component was assessed by examining its fluorescent lifetime (τ_i) and relative amplitude (a_i). In our experiments we typically collected a photon-counting histogram of spectrally resolved autofluorescence decay $P(\lambda_j, t_k)$. The histogram was measured simultaneously on 16 spectral channels denoted as λ_j, and on 1024 temporal channels denoted t_k, equidistantly spaced by 24.4 ps. The steady-state autofluorescence spectra $S(\lambda_j)$ were calculated as a total photon count for each spectral channel:

$$S(\lambda_j) = \sum_{k=1}^{1024} P(\lambda_j, t_k) \qquad (3)$$

The fluorescence decay kinetics were analyzed using a sum of three exponential terms, according to the model $I(\lambda_j, t)$ with the functional form:

$$I(\lambda_j, t) = I_{baseline} + \sum_{i=1}^{3} a_{i,j} \times \exp(-(t - t_0)/\tau_{i,j}) \qquad (4)$$

Where (t_0) is the variable zero-time shift, $I_{baseline}$ fits the background intensity, and the amplitude (a_i) represent the fractional population of the molecules associated with each decay component *i*. Sum of these fractional populations for each selected wavelength equals to one hundred percent:

$$\sum_{i=1}^{3} a_{i,j} = 100 \qquad (5)$$

In the fitting procedure (nonlinear least-squares minimization routine implemented in SPCImage by Becker&Hickl), the parameters of the model function $I(\lambda_j, t)$ were iteratively changed, while being convolved with the instrument response function to best fit the measured photon histogram $P(\lambda_j, t_k)$. Thus, each lifetime component *i* was assessed by examining its estimated fluorescent lifetime $\tau_{i,j}$ and relative amplitude $a_{i,j}$, both being dependent on the emission wavelength λ_j. For simplicity, we provide the results either in the form where these parameters are plotted against wavelength coordinate, or we specify the particular emission wavelength used, omitting the second index (j).

Once the fitting parameters have been obtained, the following derived quantities were calculated:

1) the average fluorescence lifetime $<\tau>$;

$$\langle \tau \rangle = \sum_{i=1}^{3} (a_i \times \tau_i) \Big/ \sum_{i=1}^{3} a_i = \sum_{i=1}^{3} (a_i \times \tau_i)/100 \qquad (6)$$

2) the relative intensity of each species $a_i\tau_i$;

3) the relative fraction r_i of the fluorescence generated by each species *i*, with respect to the total fluorescence;

$$r_i = (a_i \times \tau_i) \Big/ \sum_{i=1}^{3} (a_i \times \tau_i) \qquad (7)$$

The time-resolved emission spectra (TRES)[109] were constructed by summing the photons registered over a chosen time interval δt after a temporal delay Δt with respect to the channel k_{max}, where the maximal number of photon counts was detected (P_{max}, i.e. the peak of the excitation impulse):

$$TRES(\lambda_j) = \sum_{k=(k_{max}+\Delta t)}^{(k_{max}+\Delta t+\delta t)} P(\lambda_j, t_k) \qquad (8)$$

where k_{max} corresponds to channel with maximal detected photon counts, i.e. the peak of the excitation impulse, λ_j to emission wavelength, $P(\lambda_j, t_k)$ to the photon-counting histogram of spectrally-resolved AF decay. We have used the TRES interval width δt of 1ns (in regard to the instrument response width) leading to the time interval expressed in channel numbers as $k \in (\Delta t, \Delta t + \delta t)$, where 1 channel ~ 24 ps.

2.2.4. Data Analysis

Data were analyzed using SPCImage software (Becker&Hickl, Boston Electronics, U.S.A), Origin 7.0 (OriginLab, USA) and custom-written procedures for data correction and analysis written in C++ with the help of NAG numerical libraries and visualization system Iris Explorer (NAG, Oxford). Steady-state emission spectra measured simultaneously at 16 acquisition channels were determined as the total photon counts on each spectral channel. Three-exponential decay model was used to analyze measured fluorescence lifetime kinetics. Home-made database was used for appropriate data management. Data are shown as mean ± standard error (SEM). In all presented data, comparison between means was made at spectral maximum of 450 nm, using one-way analysis of variance (ANOVA), followed by Tukey post-test, except for the measurements of the lipid peroxidation markers in the blood, which comparison between the means was done by unpaired *t*-test. In all presented data $P<0.05$ was considered as significantly different; however, $P<0.005$ was considered as significantly different in the comparison of measurement of lipid peroxidation markers between NP and NP_{can}. All data are presented as mean ± SEM of *n* experiments or cell analyses performed.

3. RESULTS

3.1. Study of NADPH fluorescence in vitro

Part of this study has been published in Aneba S., Cheng Y., Mateasik A., Comte B., Chorvat D. Jr, Chorvatova A., 2007: Probing of Cardiomyocyte Metabolism by Spectrally Resolved Lifetime Detection of NAD(P)H Fluorescence. ***The Computers in Cardiology.*** 39:349-352., see attached Appendix I.

3.1.1. Concentration-dependence of NADPH fluorescence

It is well known that fluorescence of NADH and/or NADPH is linearly dependent on its concentration[99]. To confirm this relationship in our experimental conditions, we characterized changes in the kinetics of intrinsic NADPH fluorescence with rising concentration. Fluorescence spectra and fluorescence lifetimes of NADPH were studied *in vitro* in intracellular media-mimicking solutions (pH 7.25). Steady-state emission spectra measured simultaneously at 16 acquisition channels were determined as the total photon counts on each spectral channel. To test the dose dependence of spectral and lifetime properties of the NADPH fluorescence *in vitro*, concentrations ranging from 1 to 20 μM of NADPH in intracellular media-mimicking solutions were used. These experiments were performed to understand changes of NADPH kinetics due to alteration in NADPH/$NADP^+$ ratio associated with pathophysiological conditions. Our results showed that NADPH had fluorescence with spectral maximum at 450 nm (Fig. 5A). The spectral intensity of NADPH was linearly dependent on their concentration at the maximum emission wavelength of 450 nm, as illustrated at (Fig. 5C). Normalized spectra for NADPH concentrations from 1 to 20 μM overlaid perfectly (Fig. 5B), confirming the same molecular origin.

A 3-exponential model was used to analyse fluorescence lifetimes of NADPH fluorescence and their relative amplitudes, giving the best fit with chi-square values (χ^2)

were <1.2. However, at the maximum wavelength of 450 nm we have resolved only two significant fluorescence lifetime pools (Table 1). Our data indicate that fluorescence decay kinetics were not dependent on NADPH concentration in the studied range (Fig. 5D). These findings suggest that there is a correlation between free NADPH fluorescence intensity and changes in its concentration, but not their fluorescence decays.

3.1.2. pH-sensitivity of NADPH fluorescence

Several pathological conditions, namely ischemia are associated with metabolic alkalosis or acidosis. To understand effects of changing of the pH on NADPH fluorescence kinetics, we therefore investigated the fluorescence of NADPH (10 μM), measured in basic intracellular solution adjusted with 1.0 M NaOH to different pH (5.4, 7.25, 9.8). These values were chosen as close to cytoplasmic pH (7.25), and mitochondrial pH (5.4). We also tested highly alkalized solution of pH 9.8. Our results showed that when compared to pH 7.25 there was a loss of NADPH fluorescence intensity in the presence of pH 5.4, while NADPH fluorescence recorded in the presence of pH 9.8 was not significantly affected (Fig. 6A). Normalized spectra revealed that pH modification caused no significant difference on the spectral shape of NADPH fluorescence (Fig. 6B). Also, the fluorescence decays were not significantly affected by changing pH (Fig. 6C). These data indicate that acidic environment can have some effect on the NADPH fluorescence intensity.

3.1.3. Viscosity-dependence of NADPH fluorescence

The fluorescence decays are known to be sensitive to molecular environment, namely its viscosity[103]. We therefore investigated changes of fluorescence decay kinetics of NADPH (50 μM) in solutions with different degrees of viscosity ranging from 0-100%. This was achieved by addition of glycerol (0%, 25%, 50%, 75%, and 100%) *vs.* purified H_2O. Our findings showed that NADPH fluorescence intensity is indeed dependent on the viscosity of the solution (Fig. 7A). The total photon counts, measured at maximum λ_{em} (450

nm) revealed rise of the peak of NADPH fluorescence intensity with the viscosity (Fig. 7C). We also noted a slight 10 nm blue spectral shift when NADPH fluorescence was recorded in more viscous environment (Fig. 7B). Furthermore, we have found that NADPH fluorescence lifetime depend on the viscosity as well, as illustrated at λ_{em} 450 nm (Fig. 7D) with clear prolongation of the fluorescence lifetimes in highly viscous environment. We propose that this result can be related to the change in the molecular mobility and/or modification in the conformation of NADPH molecules in more viscous medium. In agreement with previously observed findings for NADH[103], gathered results point to the sensitivity of the kinetics of NADPH fluorescence decays to the modification in the molecular environment.

3.1.4. NADPH fluorescence produced by isocitrate dehydrogenase and its modulation by glutathione reductase

$NADP^+$-ICDH has been shown to play an important role in increasing NADPH pool in heart mitochondria, especially during oxidative stress[61, 62, 110]. We therefore utilized the activity of $NADP^+$-ICDH to produce NADPH *in vitro*, and study its spectral and lifetime properties. Our data revealed that NADPH produced *in vitro* from $NADP^+$-ICDH had comparable spectral and lifetime characteristics as NADPH in intracellular media-mimicking solution, although some differences were noted for the 2nd and 3rd lifetime pools and their relative amplitudes (Table 1). We advance that these can be due to the fact that when NADPH was produced *in vitro* the samples were not measured in intracellular media only. As expected, our observations indicated that ICDH-produced NADPH fluorescence has comparable characteristics to that of free NADPH (data not illustrated).

Furthermore, we investigated whether binding of NADPH to GR have repercussions on its spectral and lifetime fluorescence properties. NADPH is a cofactor that is essential for glutathione system, one of the defence mechanisms against oxidative stress. NADPH is used by GR to convert GSSG into GSH, which is needed to detoxify H_2O_2 and change it

into water[35]. We have found that the addition of GR in the presence of GSSG lowered (at concentration 0.5 U/ml) or nearly completely abolished (at 1 U/ml) NADPH fluorescence produced by $NADP^+$-ICDH (Fig. 8A). This observation is in agreement with dehydrogenation of NADPH by GR. Normalized and blank-corrected spectra showed no difference of NADPH spectral properties in the presence or in the absence of GR with GSSG (Fig. 8B). Our data revealed no modifications of NADPH lifetime kinetic properties by GR (Fig. 8C) (Table 2). These results show that the loss in fluorescence intensity is correlated with the use of NADPH by GR, converting it to the oxidized form $NADP^+$.

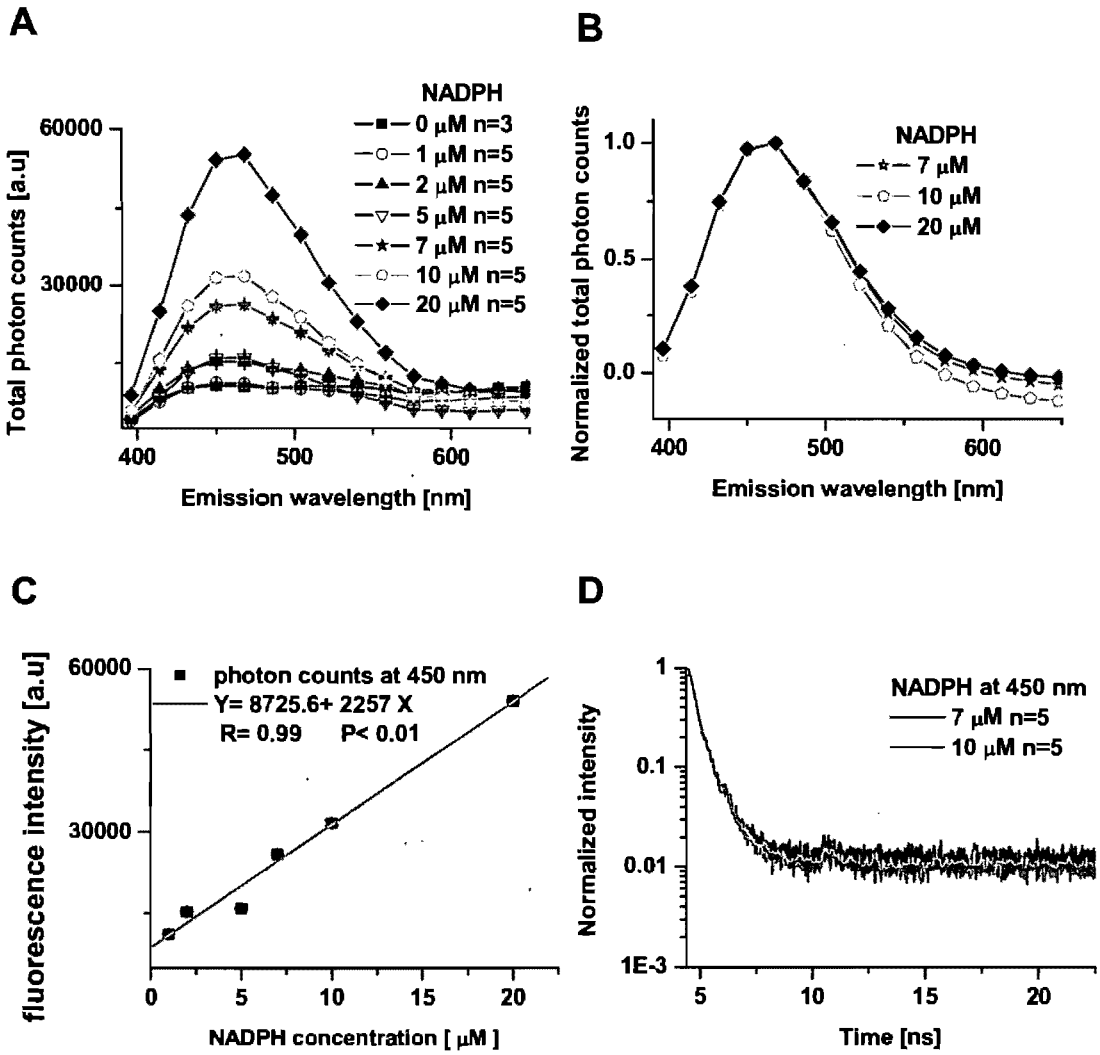

Figure 5: Concentration-dependence of NADPH fluorescence *in vitro*. Emission spectra and lifetime properties of NADPH fluorescence recorded in intracellular media-mimicking solutions (pH 7.25). A: Number of photon counts of NADPH fluorescence spectra at concentrations ranging from 1 to 20 µM. B: Normalized, background-corrected spectra of NADPH fluorescence for NADPH concentrations between 5 to 20 µM. C: Linear relationship between the number of photon counts and NADPH concentration at maximum fluorescence intensity (λ_{em} = 450 nm). D: Normalized fluorescence decays of NADPH concentrations of 7 and 10 µM (at λ_{em} = 450nm).

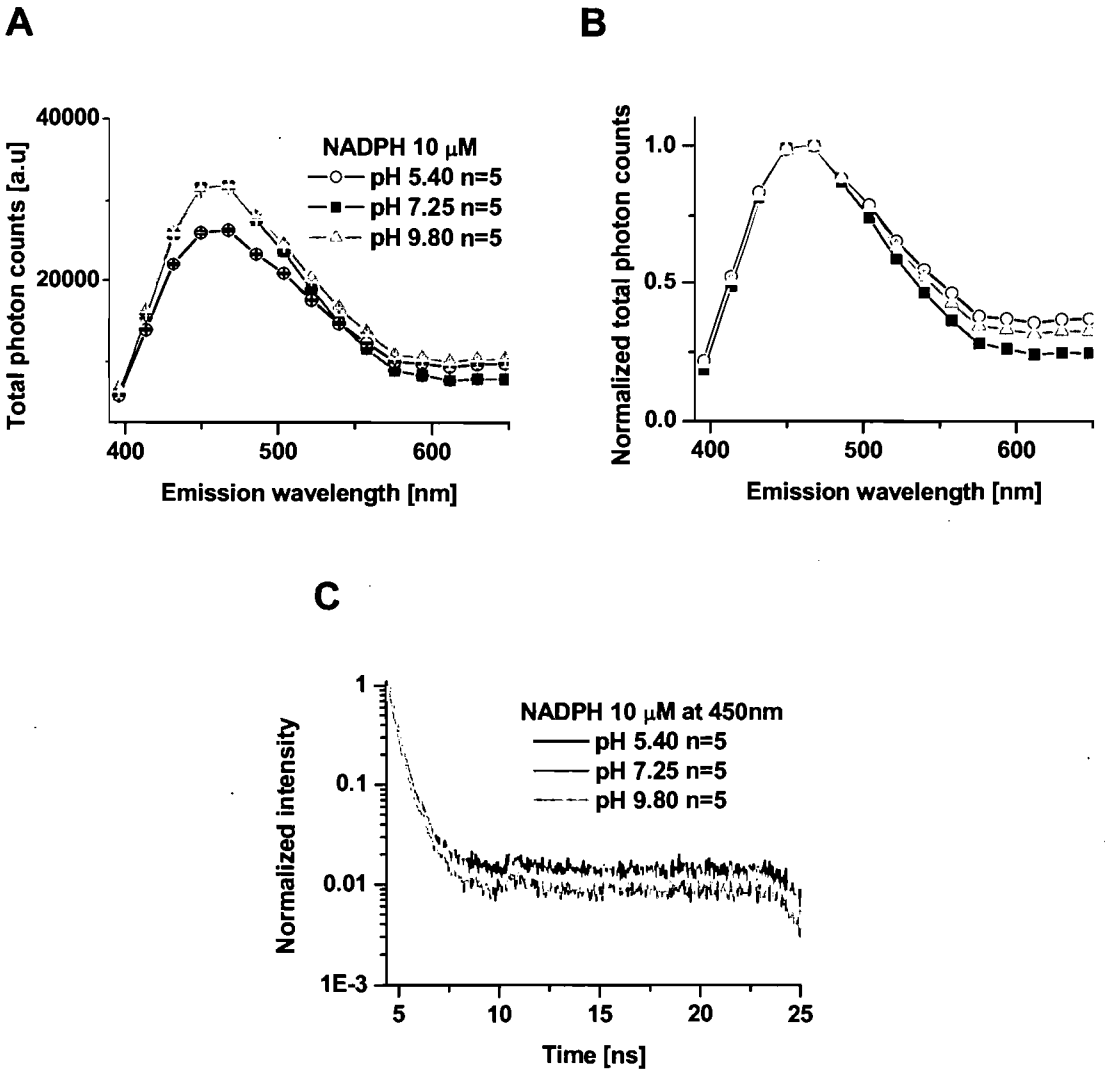

Figure 6: pH-dependence of NADPH fluorescence *in vitro*. Emission spectra and fluorescence decay characteristics of NADPH (10 μM) recorded in intracellular solution with modified pH (5.40, 7.25, or 9.80). A: number of photon counts of NADPH fluorescence spectra. B: Normalized spectra of NADPH fluorescence. C: Fluorescence decays of NADPH (at λ_{em} =450nm).

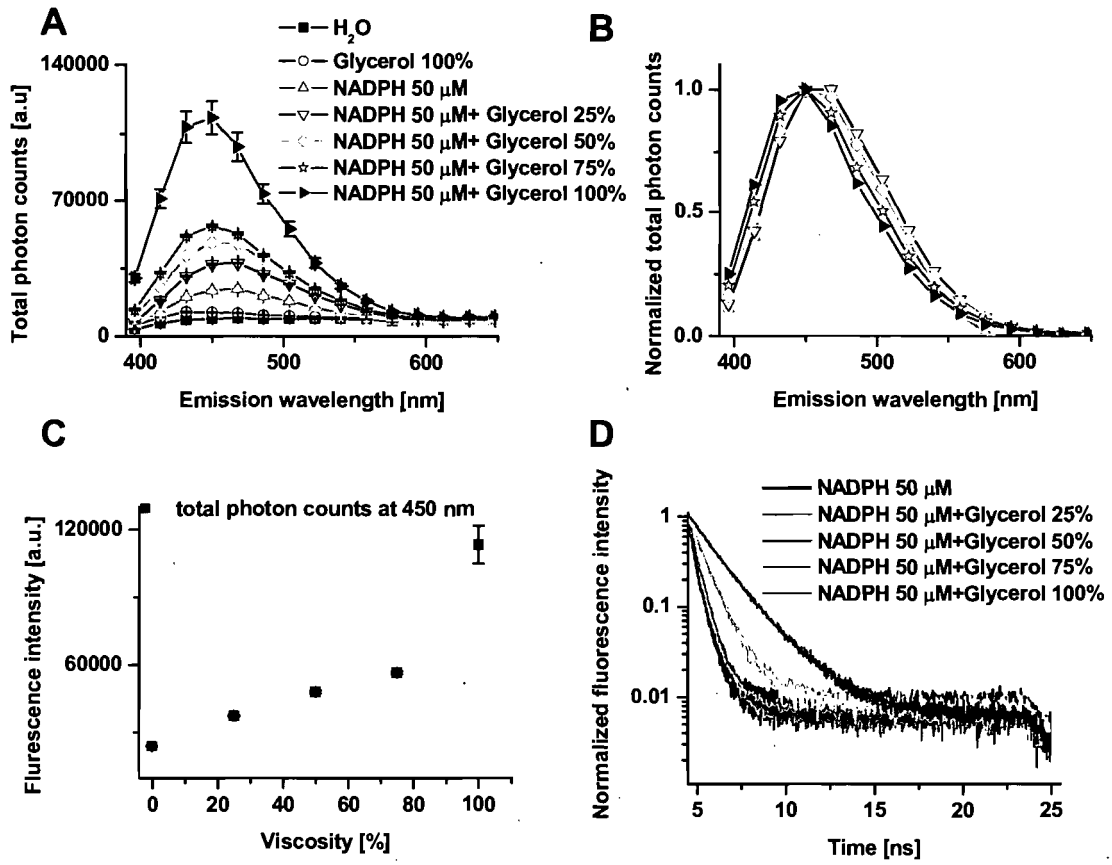

Figure 7: Viscosity-dependence of NADPH fluorescence *in vitro*. Emission spectra and fluorescence decays of NADPH (50 µM) recorded in intracellular media-mimicking solution with the addition of glycerol (0%, 25%, 50%, 75% and 100%) vs. H_2O. A: Fluorescence spectra of NADPH with added amounts of glycerol. B: Normalized fluorescence spectra of NADPH with glycerol. C: Total photon counts of NADPH fluorescence at (λ_{em} 450 nm) in intracellular media with different viscosity. D: Normalized fluorescence decays of NADPH fluorescence at (λ_{em} = 450 nm).

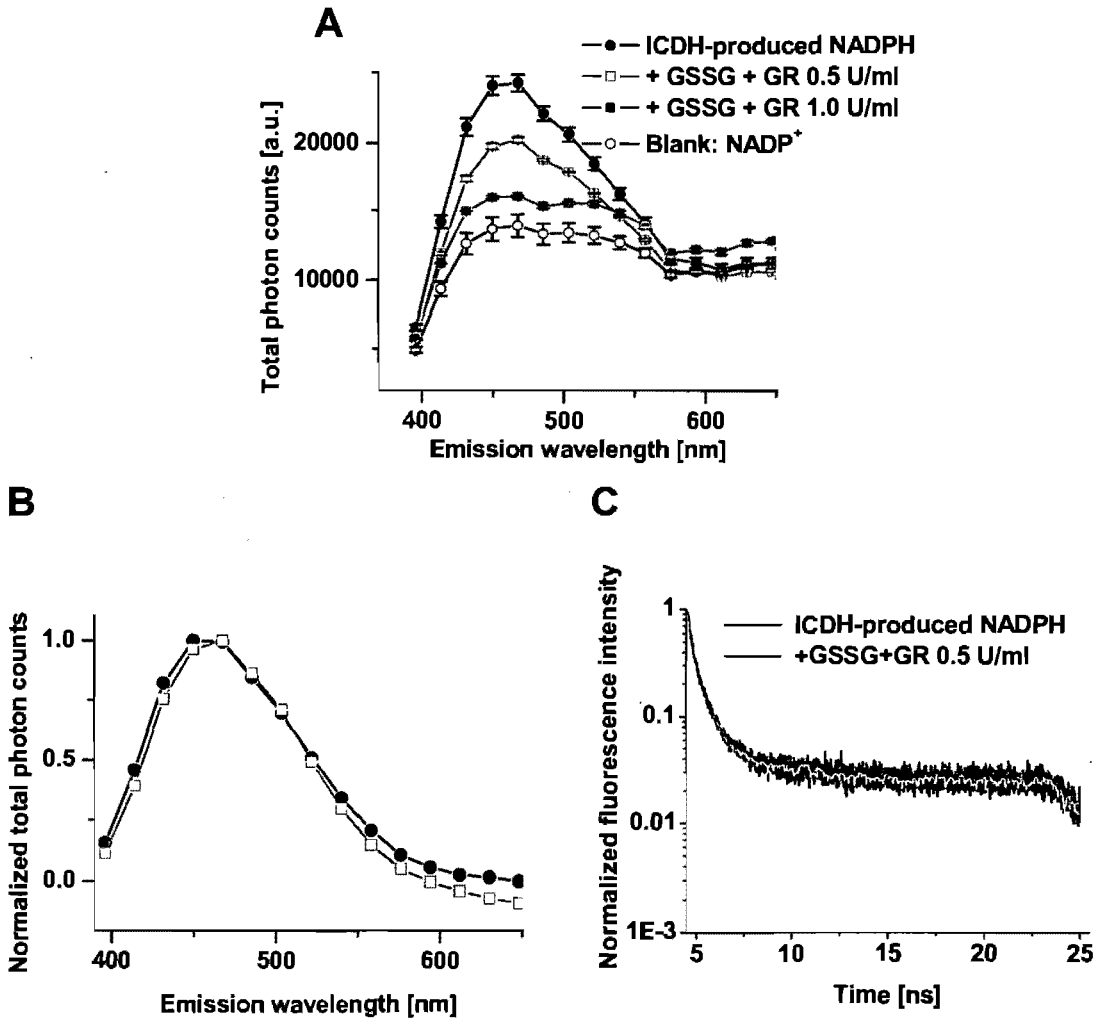

Figure 8: $NADP^+$-ICDH produced NADPH fluorescence and its modulation by GR *in vitro*. $NADP^+$-ICDH produced NADPH fluorescence in the absence or presence of GR (0.5 or 1.0 U/ ml) in intracellular solution. A: steady state spectra. B: normalized emission spectra. C: Normalized fluorescence decays (at λ_{em} = 450nm).

parameters	Total photon counts [a.u.]	a_1	τ_1 [ps]	a_2	τ_2 [ps]	a_3	τ_3 [ps]
NADPH 7 μM n=5	25890±190	74.4±3.67	313.3±10.5	21.7±3.93	781.3±43.6	0.32±0.04	27950±2050
NADPH 10 μM n=5	31576±426	74.5±1.33	310.0±4.6	25.2±1.34	781.4±20.6	0.30±0.04	22470±4020
NADPH 20 μM n=5	54068±251	74.6±2.42	310.6±9.7	25.3±2.93	753.7±29.5	0.14±0.02	25940±2500
ICDH-Produced NADPH (0.5 mM)n=10	24104±647	75.6±1.67	310.6±9.8	23.1±1.61	997.9±33.3	1.32±0.11	16100±1410
ICDH-Produced NADPH (0.5mM) +GR 0.5 U/ml n=5	19767±210	73.9±5.72	308.2±18.9	24.6±5.53	981.8±93.4	1.60±0.24	16400±2100

Table 1: Fluorescence parameters of NADPH in intracellular media-mimicking solutions ($\lambda_{ex}/\lambda_{em}$ = 375 nm/450 nm). Total photon counts, fluorescence lifetimes (τ1 to τ3) and their relative amplitudes (a1 to a3) of free NADPH, or ICDH- produced NADPH in the absence and in the presence of GR 0.5U/mL. Data are shown as mean ± S.E.M.

3.2. Study of NAD(P)H fluorescence in living cardiac myocytes

To investigate the endogenous fluorescence of NAD(P)H in living left ventricular cardiac myocytes, spectrally and time-resolved AF decays were recorded in cells bathed in basic external solutions. Laser beam at 375 nm was used as an excitation source. Normalized steady-state emission spectra of the cardiomyocyte AF had spectral maximum at 450 nm (Fig. 9Bb) and were similar to those of NADPH *in vitro*. However, NAD(P)H fluorescence of cardiomyocytes had three significant lifetime pools (Table 2).

3.2.1. Respiratory chain modulation

3.2.1.1. NAD(P)H fluorescence in response to inhibitors of the respiratory chain

We tested whether modulation of the respiratory chain activity is capable of affecting fluorescence spectral and/or lifetime characteristics of cardiomyocyte AF. Treatment with rotenone (1 μM) and Na-cyanide (4 mM), the inhibitors of the Complex I[111, 112] and Complex IV[113] of the respiratory chain respectively induced a significant increase in cardiomyocyte NAD(P)H fluorescence (Fig. 9Ba). This observation is in agreement with the rise in mitochondrial NADH content due to accumulation NADH following limitation of the respiratory chain to dehydrogenation. Normalized AF spectra in control conditions and in the presence of rotenone and cyanide were identical (Fig. 9Bb), suggesting same molecular contributors: NAD(P)H molecules. Also, no membrane damage was observed in the presence of the inhibitors as evidenced by transmission images (Fig. 9Ab). In addition, inhibitors of the respiratory chain induced no effect on the lifetimes and their relative amplitudes when compared to control cells (Table 2).

3.2.1.2. Cardiomyocyte autofluorescence and uncoupling of ATP synthesis

To enhance NADH dehydrogenation to NAD^+ by complex I of the respiratory chain, we applied DNP, an uncoupling agent for ATP synthesis leading to a rapid energy consumption[114, 115]. As expected, use of DNP resulted in a significant decrease in cardiomyocyte AF (Fig. 9Ba), in accordance with a markedly enhanced NADH dehydrogenation rate. Interestingly, after normalization, spectral broadening towards red spectral region of about 20 nm was found in the presence of the uncoupler (Fig. 9Bb). However, DNP did not modify the cell shape as shown in Fig. 9Ac.

3.2.2. Redox state changes

3.2.2.1. Cytoplasmic NAD(P)H changes

The concentration ratio of lactate/pyruvate in plasma was showed to be between 10 and 20 in non-pregnant rats[68] (see also Table 3). We have therefore used a similar concentration ratio to test the effect on NAD(P)H AF in cardiomyocytes. Because intracellular lactate and pyruvate concentration are very rapidly in equilibrium through the action of the cytosolic lactate dehydrogenase, adding fixed ratio of these substrates allow to clamp the NAD/NADH ratio to a fixed value and induce cytosolic NAD(P)H redox changes. To analyse the contribution of cytosolic NAD(P)H, lactate (1 mM) was added in the presence of pyruvate (100 µM). These substrates did not significantly affect the total photon count spectra of cardiomyocyte AF (Fig. 10Ba and Bb), indicating that recorded AF signal is mainly resulting from mitochondrial NAD(P)H.

3.2.2.2. Mitochondrial NADH production

To stimulate mitochondrial NADH production in cardiomyocytes, we have administered BHB (3 mM) in basic extracellular solution in the presence of different concentrations of AcAc: low 150 μM (ratio 20:1) to favor NADH production and high 1.5 mM (ratio 2:1), closer to physiological conditions[116]. In fact, similar to the lactate/pyruvate ratio in the cytosol, mitochondrial BHB and AcAc concentrations are very rapidly in equilibrium through the action of the BHB dehydrogenase, reflecting the mitochondrial NAD/NADH ratio. The BHB/AcAc ratio of 20:1 induced no significant change in cardiomyocyte AF when compared to control conditions (Fig. 10Ca and Cb). However, decreasing the ratio to 2:1 led to loss in the cell AF (Fig. 10Ca), in agreement with expected lower NADH production, but without modification of the spectral shape (Fig. 10Cb). These results suggest that our cells are at the level of high gradient for the NADH production. If the cardiomyocyte AF is simply set by mitochondrial NADH production, our cells are in condition favourable to NADH production.

3.2.3. Inhibition of glutathione system

The reduced form of NADPH is crucial as an electron donor, used by GR to maintain sufficient amount of GSH. To modulate the consumption of NADPH, BCNU (100 μM) was used to inhibit GR. In the presence of the inhibitor, we observed no significant changes in the cardiomyocyte AF although some decreasing tendency could be noted (Fig. 11Ba). We also found no modification of the spectral shape as observed from the normalized spectra (Fig. 11Bb). Besides, the cell shape was not affected by the presence of BCNU (Fig. 11A).

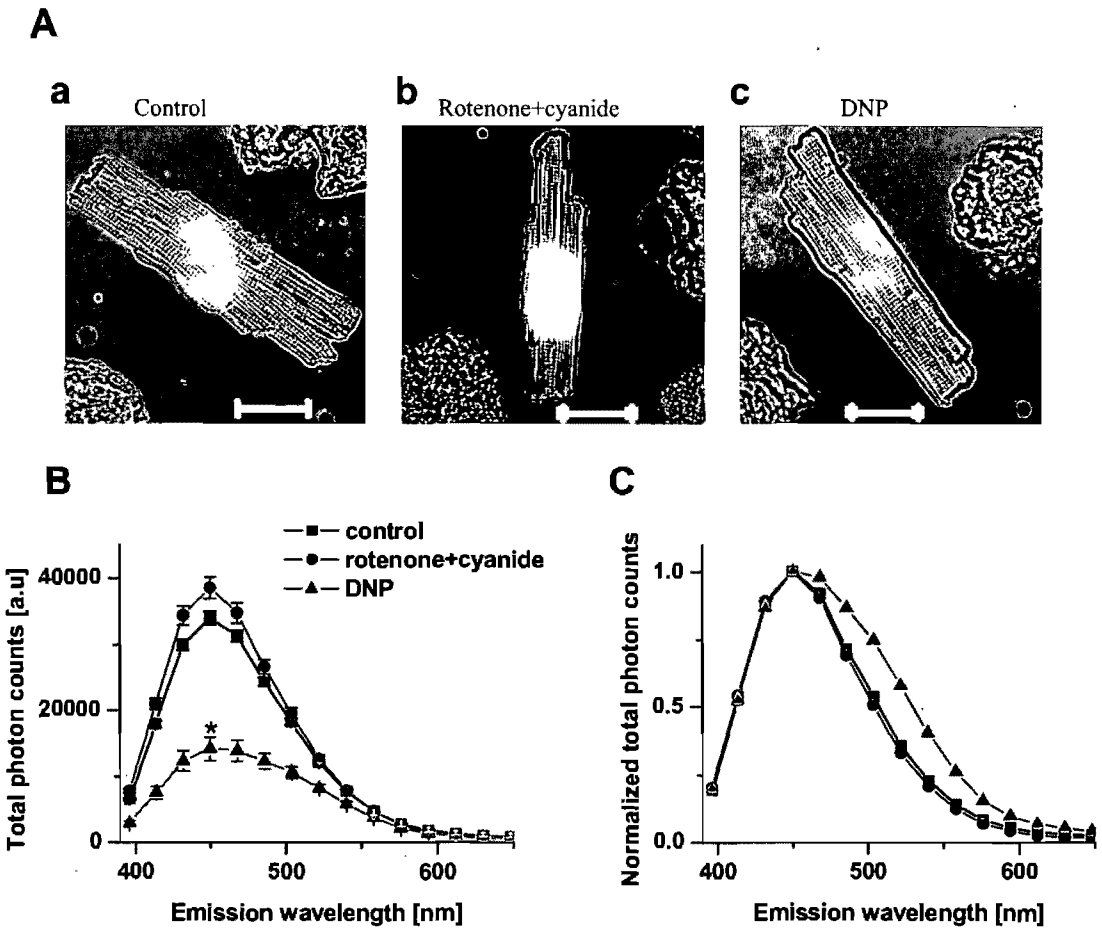

Figure 9: Response of NAD(P)H fluorescence to respiratory chain modulation in living cardiomyocytes. A: transmission images of living cardiac cells, scale = 33μm (number of cells/ number of animals); a: control (91/18), b: treated with rotenone and cyanide (1 μM and 4 mM respectively, 30/6), c: treated with DNP (50 μM, 15/3). B: Steady state and C: normalized NAD(P)H fluorescence spectra in cardiomyocytes in the absence and/or the presence of the modulators. *$p < 0.05$ vs. control.

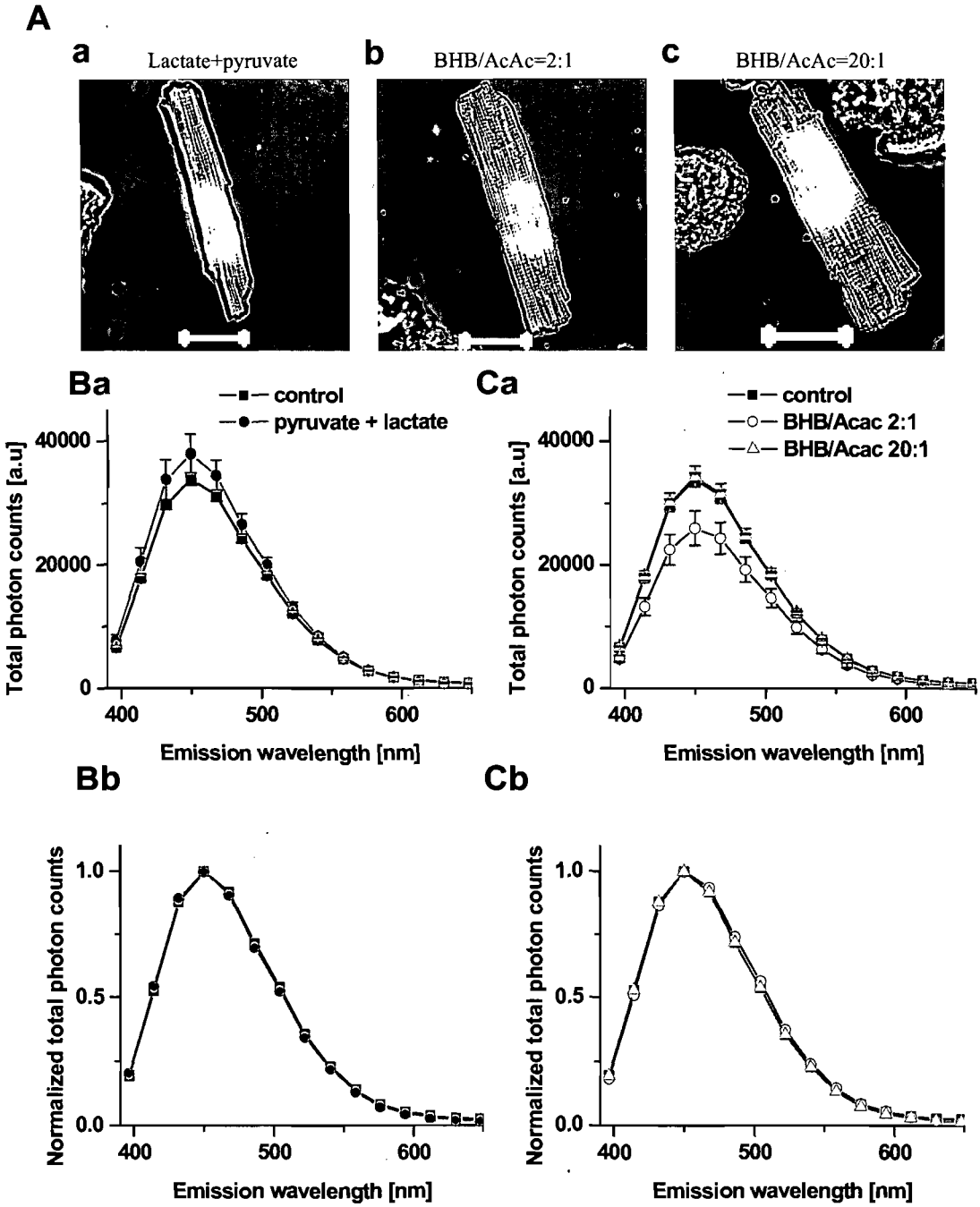

Figure 10: Investigation of NAD(P)H-based cardiomyocyte AF response to change in NADH production. A: transmission images of living cardiac cells (number of cells/ number of animals) scale = 33 μm; a: supplemented with pyruvate (100 μM) and lactate (1 mM) (15/3), b: or treated with BHB (3 mM) in the presence of c: AcAc (1.5 mM, ratio 2:1) (16/3) or d: AcAc (150 μM, ratio 20:1) (15/3). Steady state and normalized NAD(P)H fluorescence spectra in the absence or presence of (Ba and Bb): lactate and pyruvate, (Ca and Cb): varied BHB/AcAc ratio.

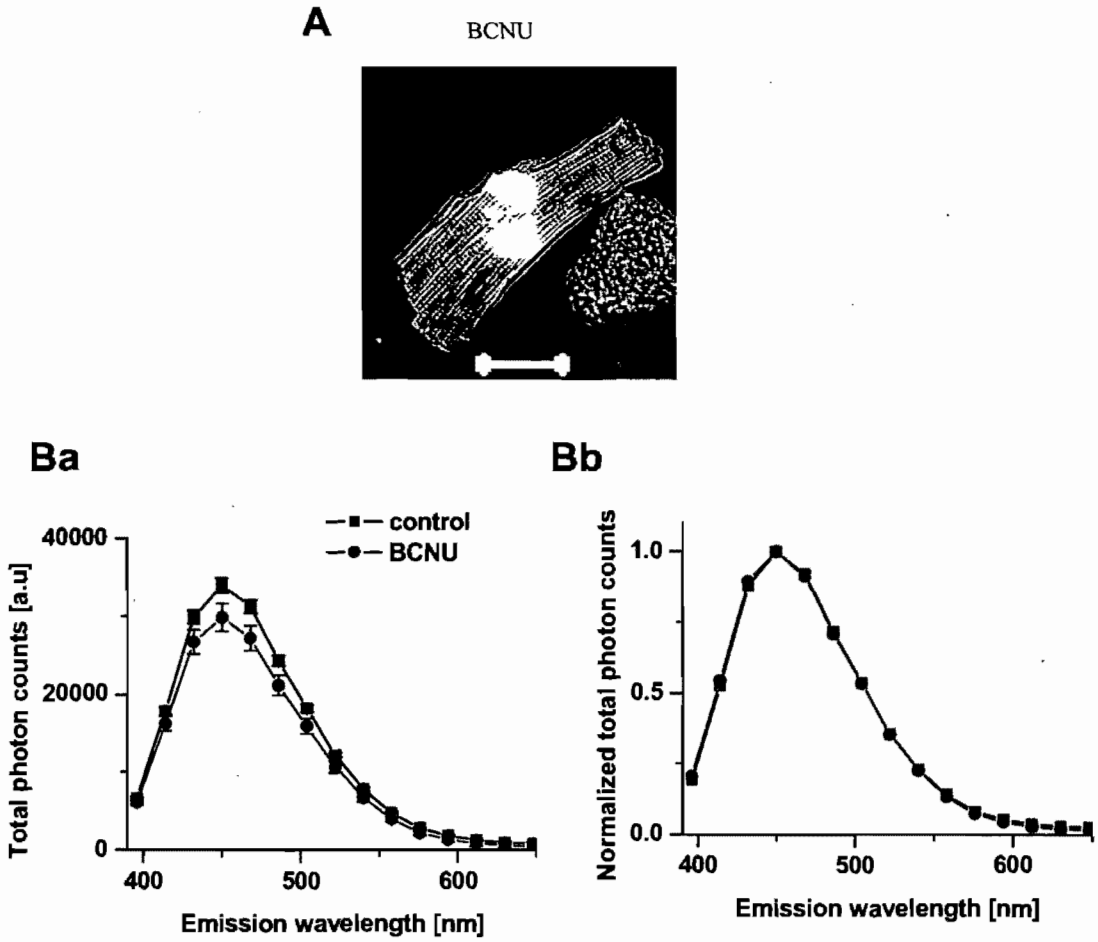

Figure 11: Response of NAD(P)H fluorescence in living cardiomyocytes to glutathione reductase inhibition. A: Transmission image of a living cardiac cell (number of cells/ number of animals) scale = 33µm, treated with BCNU (100 µM, 32/6). Ba: Steady state and Bb: Normalized NAD(P)H fluorescence spectra in the absence or presence of BCNU.

	Total photon counts [a.u.]	a_1	τ_1 [ps]		a_2	τ_2 [ps]		a_3	τ_3 [ps]		
		$a_1\tau_1$ [a.u.] |*10^3|		r_1	$a_2\tau_2$ [a.u.] |*10^3|		r_2	$a_3\tau_3$ [a.u.] |*10^3|		r_3	$<\tau>$ [ns]
Control 35 C (42/8)	**40740±1470**	**62.8±1.3**	**524.4±18.2**		**33.2±1.2**	**1550±36.6**		**4.1±0.3**	**7805±295**			
		33.5±1.7		0.3±0.0	50.2±1.3		0.4±0.0	30.7±1.8		0.3±0.0	1.1±0.0
H_2O_2 (28/3)	**18150±460***	**53.8±1. 8**	**286.5±15.9***		**41.9±1.2**	**1494±82.6**		**5.3±0.3**	**11278±792**			
		15.5±1.1*		0.1±0.0*	62.4±3.6		0.5±0.0	57.0±3.9		0.4±0.0*	1.4±0.1
HNE (10/3)	**23580±1070***	**59.41±2.9**	**693.9±44.4***		**36.4±2.88**	**2026±80.8**		**4.2±0.5**	**14730±2000***			
		41.7±3.8		0.3±0.0	71.5±4.4		0.4±0.0	48.5±3.0		0.3±0.0	1.6±0.1
BCNU (17/3)	**41320±2590**	**64.5±2.0**	**508.5±15.4**		**31.9±1.76**	**4105±2530**		**3.6±0.3**	**8013±785**			
		33.1±1.7		0.3±0.0	107.6±57.5		0.5±0.0	26.6±2.5		0.2±0.0	1.7±0.6
BCNU+ H_2O_2 (12/2)	**23250±1530***	**52.5±3.2**	**358.7±26.5***		**42±2.7**	**1670±1.0**		**5.5±0.6**	**11280±1740**			
		18.9±2.1*		0.1±0.0*	68.5±2.6		0.5±0.0	57.2±7.8		0.4±0.0*	1.5±0.1
BCNU+HNE (13/2)	**17050±749***	**49.7±5.9***	**758.3±57.4***		**42±6.1**	**2165±114**		**8.3±1.0*+**	**21300±2200*+**			
		39.5±6.4		0.2±0.0*+	89.0±12.9		0.3±0.0*+	168.7±25.2*+		0.5±0.0*+	3.0±0.3*+
Rotenone+cyanide (20/4)	**49280±1950***	**61.0±1.9**	**536.8±17.8**		**35.5±1.7**	**1484±87.4**		**3.8±0.3**	**7427±402**			
		33.1±1.8		0.3±0.0	50.7±2.9		0.5±0.0	26.9±1.1		0.3±0.0	1.1±0.0
Rotenone+cyanide +H_2O_2 (10/2)	**19640±1690***	**51.7±3.7**	**516.9±50.2&**		**43.3±3.2**	**1863±126**		**5.0±0.7**	**16400±2500***			
		27.6±4.2		0.2±0.0*	78.8±6.5		0.4±0.0	75.0±11.8*		0.4±0.0*	1.8±0.2
Rotenone+cyanide +HNE (5/1)	**54210±1660* +**	**64.5±3.0**	**477.9±23.2+**		**31.8±2.7**	**1530±86.9**		**2.8±0.3**	**7037±326**			
		31.1±2.9		0.3±0.0	47.7±1.5		0.3±0.0*	27.0±11.8		0.3±0.0	1.1±0.0

Table 2: Fluorescence parameters of NAD(P)H cardiomyocyte AF ($\lambda_{ex}/\lambda_{em}$ = 375 nm/450 nm). Total photon counts, fluorescence lifetimes (τ1 to τ3) and their relative amplitudes (a1 to a3) of single cardiomyocytes in control conditions and in the presence of: 1 μM H_2O_2 or HNE 25 μM, and/or BCNU 100 μM, 1 μM rotenone and 4 mM cyanide. In grey, calculated relative intensities and relative fractions for each component, as well as average lifetime. Data are shown as mean ± S.E.M (number of cells/number of animals); *$p<0.05$ vs. control, $^{+}p<0.05$ vs. HNE, $^{\&}p<0.05$ vs. H_2O_2.

3.3. Cardiomyocyte autofluorescence sensitivity to oxidative stress

3.3.1. Study of hydrogen peroxide effect

3.3.1.1. Cardiomyocyte autofluorescence in response to hydrogen peroxide

To test cardiomyocyte AF sensitivity, we first used conditions where oxidative stress was mimicked by H_2O_2, a well known oxidative stressor[117]. The addition of H_2O_2 (1 μM) significantly lowered the cardiomyocyte AF of NAD(P)H excited at 375 nm (Fig. 12Ba, Table 2.). Also, H_2O_2 induced membrane damage, as evidenced by a change in the cell membrane shape shown by transmission images (Fig. 12Aa). Normalized spectra revealed that H_2O_2 induced red spectral broadening of about 20 nm of the NAD(P)H fluorescence (Fig. 12Bb) and reduced first lifetime pool (Table 2.). Higher concentrations of H_2O_2 (100 μM) caused severe membrane damage and lead to cellular death of most cells (data not shown). These results are in agreement with H_2O_2-induced lowering of NAD(P)H levels due to stimulation of GR, following increased GSSG inside cardiomyocytes.

3.3.1.2. Response to hydrogen peroxide following respiratory chain inhibition

To test whether cardiomyocyte response to H_2O_2 (1 μM) could be affected by the presence of the respiratory chain inhibitors, rotenone (1 μM) and cyanide (4 mM), inhibitors of the Complex I and IV of the respiratory chain respectively[111, 113], were added. As reported previously (Section 3.2.1.1.), these inhibitors were capable of inducing a rise in NAD(P)H fluorescence due to accumulation of NADH. Interestingly, these inhibitors had no effect on the reduction of NAD(P)H fluorescence caused by H_2O_2 (Fig. 12Ba, Table 2.), but resulted in further red spectral broadening induced by the addition of H_2O_2 (Fig. 12Bb). These observations suggest that H_2O_2 effect is independent on the respiratory chain.

3.3.1.3. Effect of hydrogen peroxide after glutathione reductase inhibition

To investigate the stimulation of glutathione cycle by the presence of H_2O_2 (1 μM), cells were pretreated with BCNU (100 μM), the inhibitor of GR[37, 38]. Our data showed that pretreatment with BCNU prevented some of the loss of cardiomyocyte AF that was reduced by H_2O_2 (Fig. 13Ba), in agreement with an accumulation of NADPH. Besides, the spectral shape was less affected in the presence of the inhibitor (Fig. 13Bb). The effect of H_2O_2 can therefore be attributed, at least partially, to the use of NADPH by GR.

3.3.2. Cardiomyocyte autofluorescence responsiveness to lipid peroxidation: investigation of 4-hydroxy-2-nonenal effects

3.3.2.1. Concentration dependence of 4-hydroxy-2-nonenal effects

Lipid peroxidation can be initiated by free radical attack and result in production of toxic molecules such as HNE[46], which are capable of modifying proteins. It has been found that HNE can inactivate $NADP^+$-ICDH[50, 51] that has an important role during oxidative stress by producing NADPH. Oxidative stress induced by HNE (25 μM) provoked a decrease in cardiomyocyte NAD(P)H fluorescence (Fig. 14Ba, Table 2.). It also induced a slight red spectral broadening of about 10 nm (Fig. 14Bb), and increase of the lifetime of the first lifetime pool (Table 2.). We also noted some deterioration of the cell membrane shape (Fig. 14Aa). This effect was augmented when HNE (50 μM) was used (Fig. 14Ab, Ba and Bb), suggesting its effect is a concentration-dependent. Damage of cells caused by HNE was irreversible.

3.3.2.2. Effect of 4-hydroxy-2-nonenal after modulation of the respiratory chain

We have tested whether mediators of the respiratory chain modulate the effects of HNE. Interestingly, in cells pretreated with rotenone (1 μM) and cyanide (4 mM), HNE (25 μM) failed to lower cardiomyocyte AF excited at 375 nm (Fig. 15Ba,

Table 2). The inhibitors of the respiratory chain prevented HNE-induced loss of cardiomyocyte AF as well as the spectral broadening induced by HNE (Fig. 15Bb). On the other hand, the uncoupler of ATP synthesis, DNP (50 μM), was able to further decrease the fluorescence (Fig. 15Ba) and enlarge spectral broadening in the presence of HNE (Fig. 15Bb). HNE effect was comparable to the one induced by DNP alone (Fig. 9). These results suggest that oxidative phosphorylation modulates HNE action.

3.3.2.3. The effect of 4-hydroxy-2-nonenal after glutathione reductase inhibition

To investigate implication of GR in the HNE action, we have analyzed the effects of HNE on cardiomyocyte AF in the presence of GR inhibitor BCNU. We hypothesized that inhibition of GR could prevent loss of cell AF in the presence of HNE. Surprisingly, in cells pre-treated with BCNU (100 μM), HNE (25 μM) induced further lowering of the cell autofluorescence (Fig. 16Ba, Table 2.) accompanied by even broader red spectral broadening (Fig. 16Bb). This effect was even greater when concentration of HNE was raised to 50 μM (Fig. 16Ca and Cb).

3.3.2.4. Effect of 4-hydroxy-2-nonenal after modification of mitochondrial NADH production

To test whether setting the gradient for NADH production affect the HNE-induced decrease of cell AF, we analyzed effect of HNE in cells pre-treated with different BHB/AcAc gradients, as described in section 3.2.2.2. Cells supplemented with BHB/AcAc = 20:1 prevented some loss of the cardiomyocyte AF that was quenched by HNE (25 μM) (Fig. 17Ba) and the spectral shape was recovered completely (Fig. 17Bb). On the other hand, when the ratio was decreased: BHB/AcAc = 2:1, it did not cause any significant change to the effect of HNE (Fig. 17Ba and Bb).

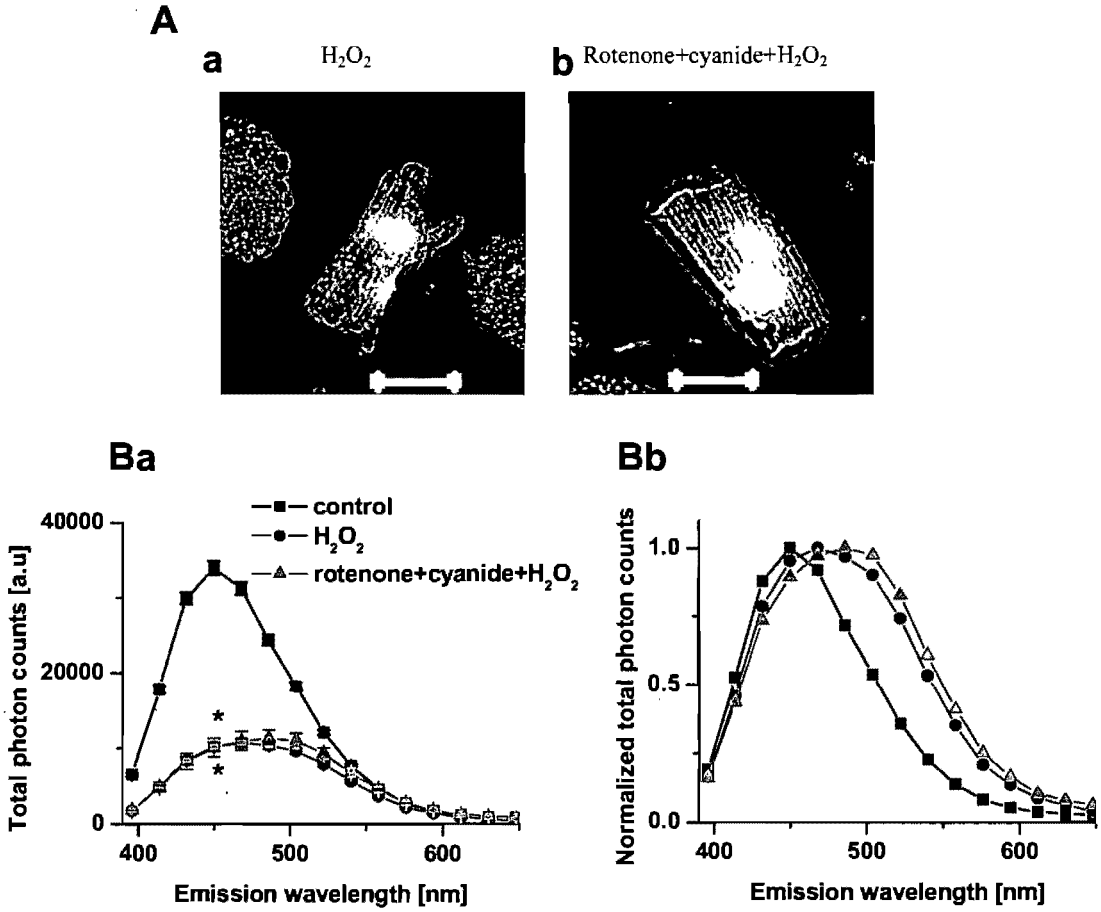

Figure 12: Response to oxidative stress challenge by H_2O_2 following inhibition of respiratory chain. A: transmission images of living cardiac cells (number of cells/ number of animals) scale = 33 μm; a: treated with H_2O_2 alone (1 μM, 28/5), or b: H_2O_2 in the presence of rotenone and cyanide (1 μM and 4 mM respectively, 15/3). Ba: steady state and Bb: normalized NAD(P)H fluorescence spectra in the absence or presence of H_2O_2 alone or after application of rotenone and cyanide. *$p< 0.05$ vs. control.

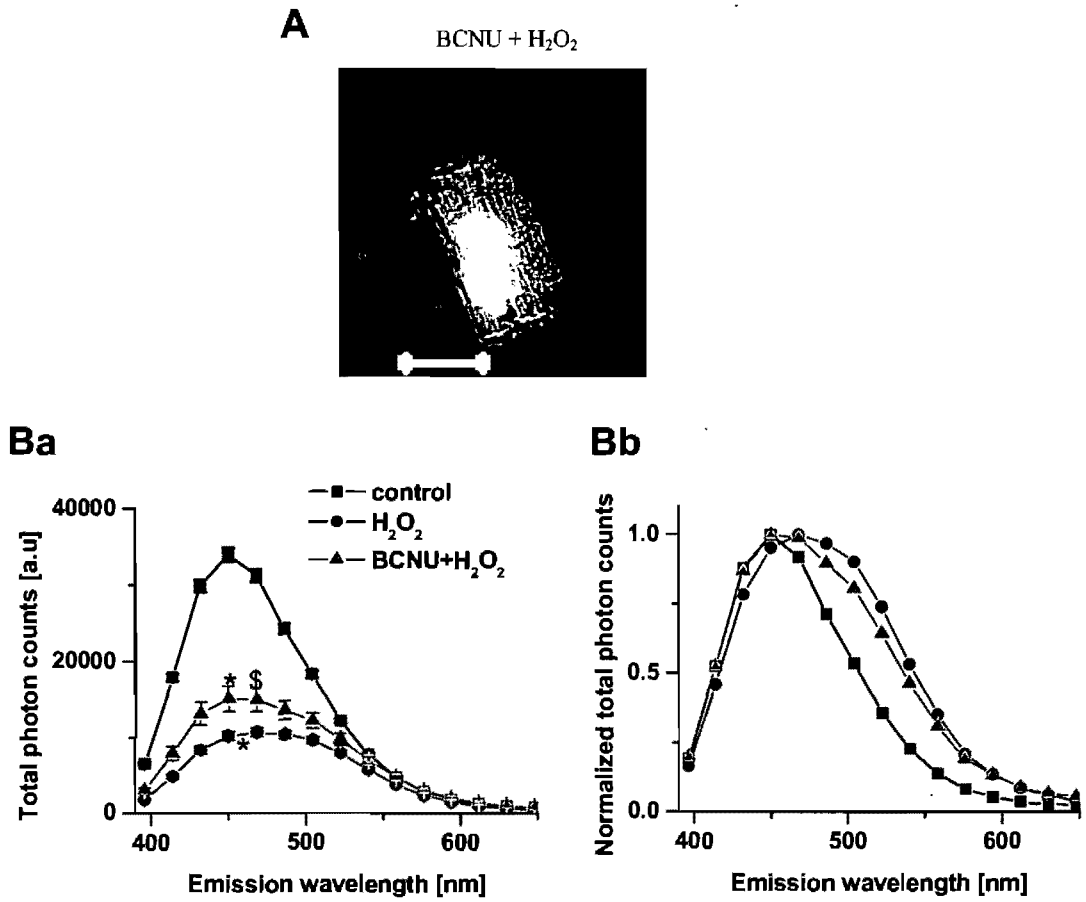

Figure 13: Response to oxidative stress by H_2O_2 in the absence or presence of glutathione cycle inhibition. A: Transmission images of living cardiac cell (number of cells/ number of animals) scale = 33 μm, treated with H_2O_2 in the presence of BCNU (100 μM, 17/3). Ba: Steady state and Bb: normalized NAD(P)H fluorescence spectra in the absence or presence of H_2O_2 alone or after treatment with BCNU. *p< 0.05 vs. control; $ p< 0.05 vs. H_2O_2. (at λ_{em} = 450nm).

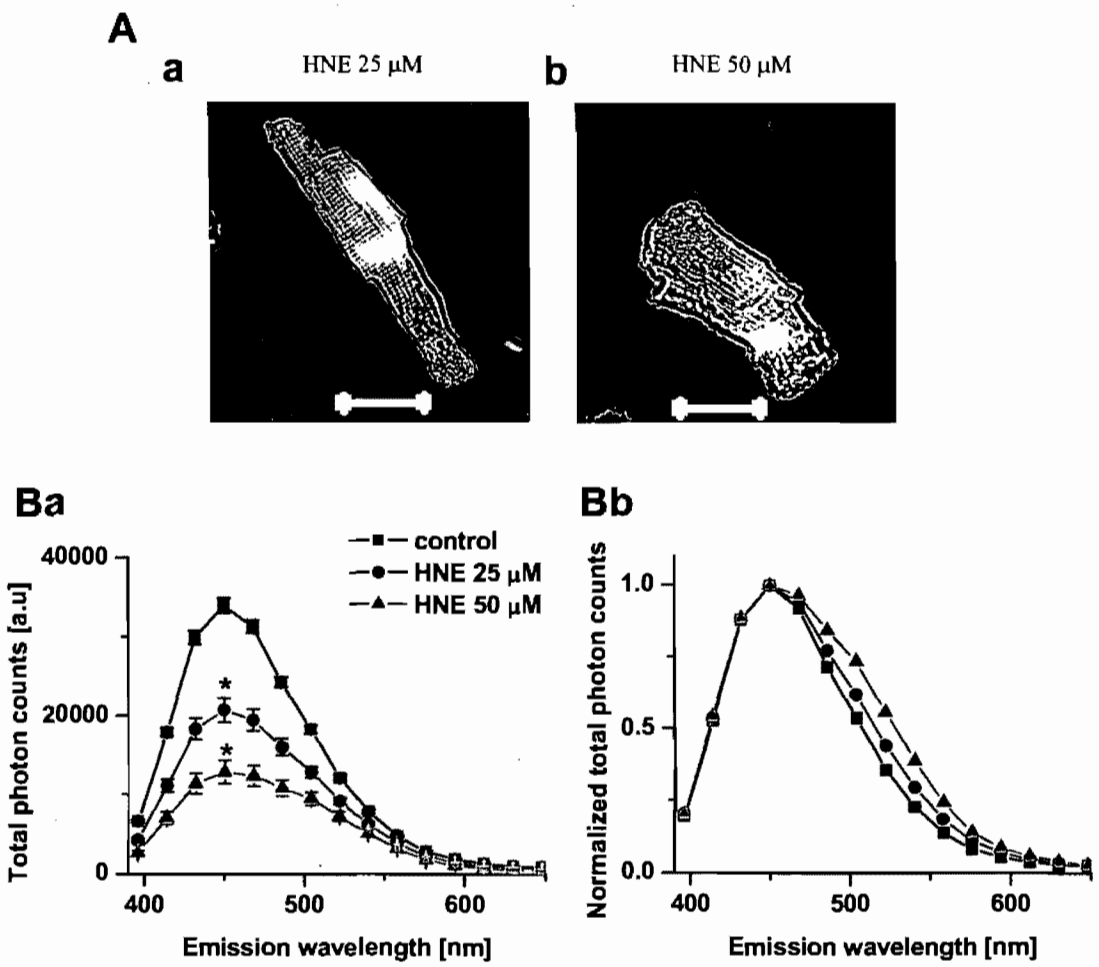

Figure 14: Cardiomyocyte autofluorescence response to concentration-dependence of 4-hydroxynonenal. A: transmission images of living cardiac cells (number of cells/ number of animals) scale = 33 µm, treated with HNE a: (25 µM, 65/13) or b: (50 µM, 24/4). Ba: steady state and Bb: normalized NAD(P)H fluorescence spectra in the absence or presence of different concentration of HNE. *$p < 0.05$ vs. control.

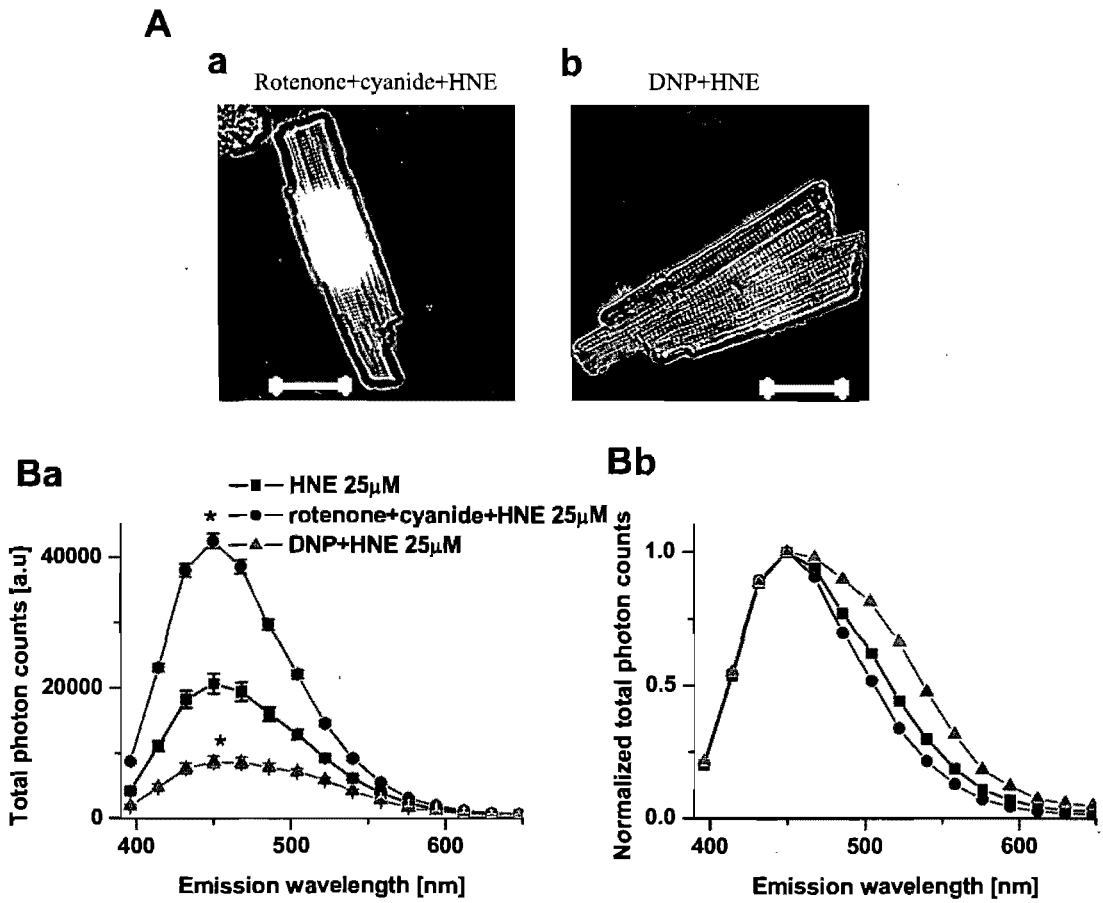

Figure 15: Effect of 4-hydroxynonenal following modulation of the respiratory chain. A: transmission images of living cardiac cells (number of cells/ number of animals) scale = 33μm, treated with HNE (25 μM), a: after treatment with rotenone and cyanide (1 μM and 4 mM respectively, 25/5), or b: DNP (50 μM, 15/3). Ba and: steady state and Bb: normalized NAD(P)H fluorescence spectra in cardiac cells treated with HNE in the absence or presence of rotenone and cyanide or DNP. *p< 0.05 vs. control.

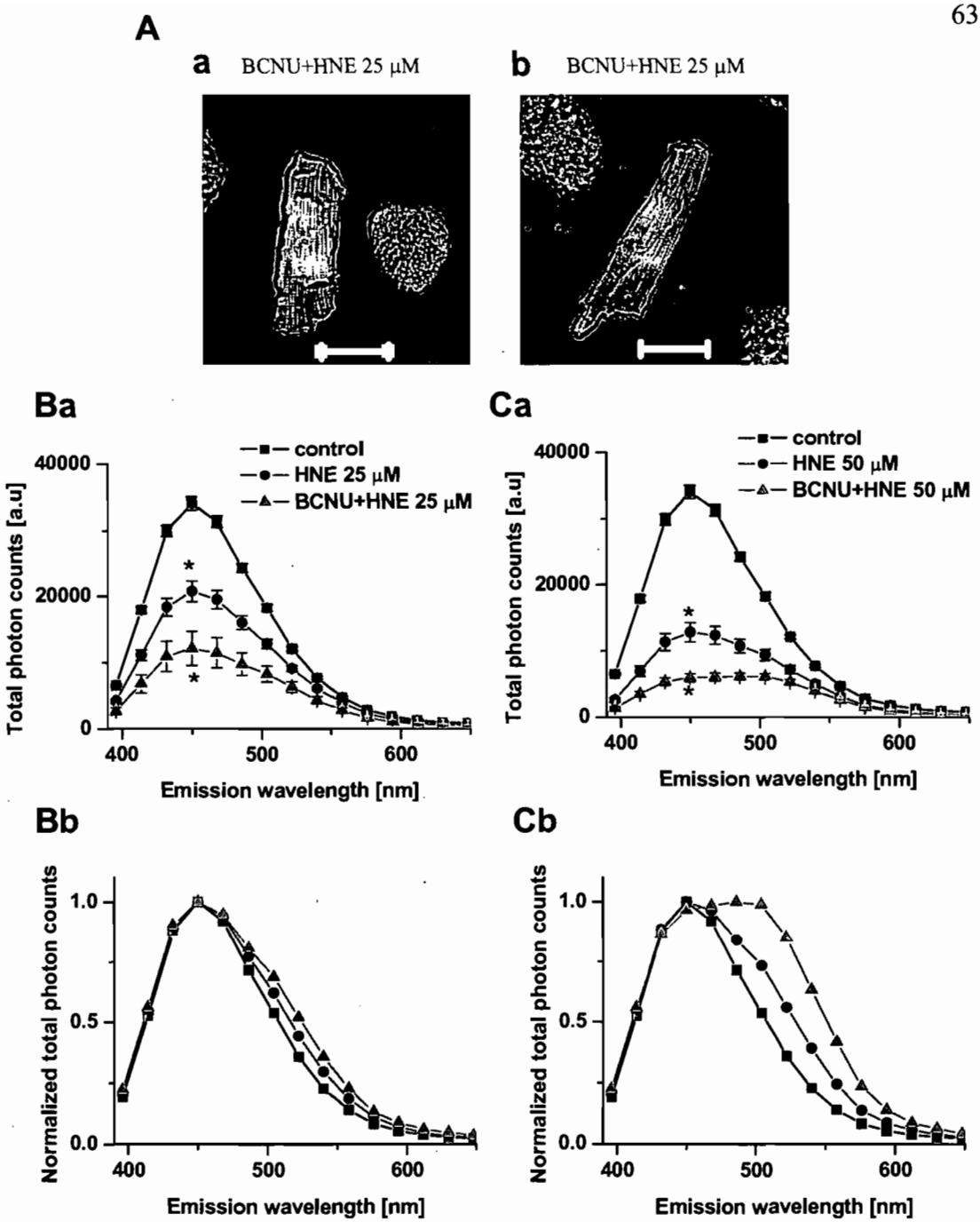

Figure 16: Effect of HNE in the presence of the inhibitor of GR. A: transmission images of living cardiomyocytes (number of cells/ number of animals) scale = 33 µm, a: pre-treated with BCNU (100 µM) and then treated with HNE (25 µM) (15/3), or b: HNE (50 µM) (18/3). (Ba and Bb) and/or (Ca and Cb): steady state and normalized NAD(P)H fluorescence spectra in cardiac cells treated with HNE 25 µM or 50 µM in the absence or presence of BCNU. *p< 0.05 vs. control.

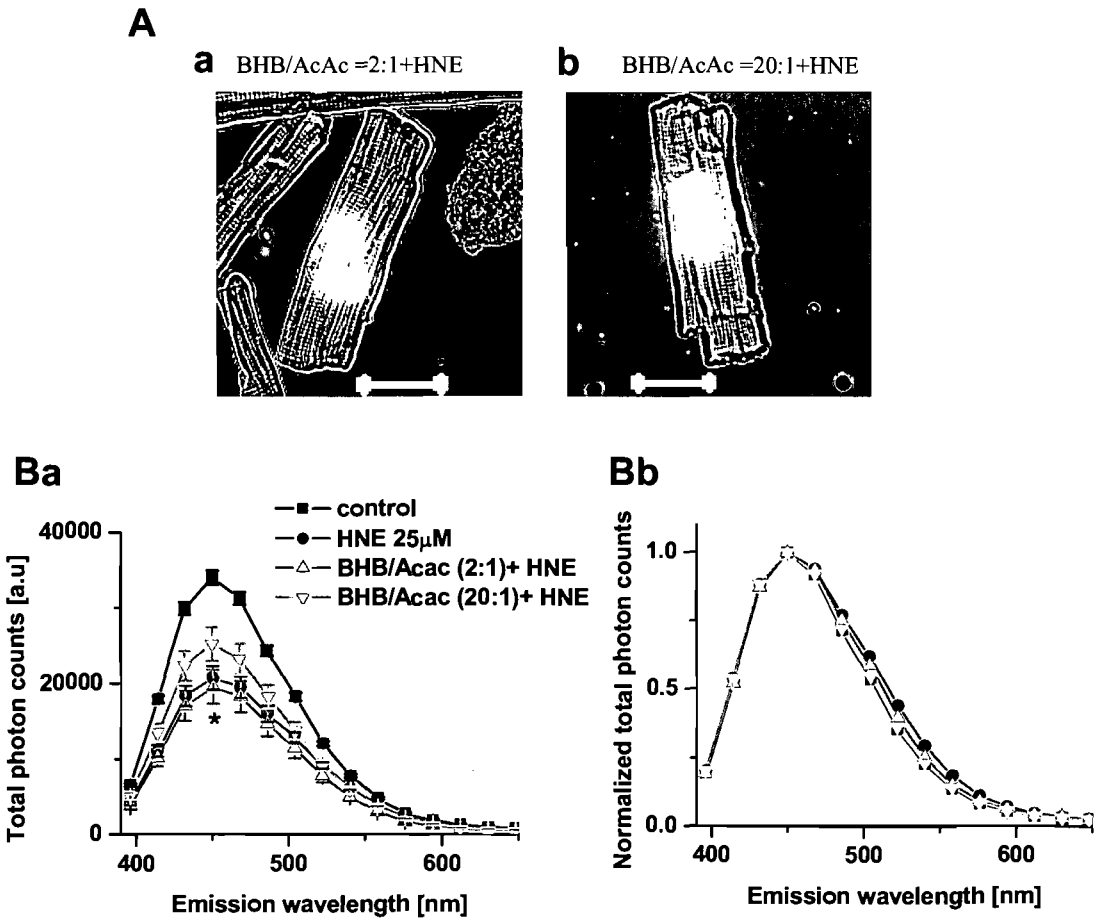

Figure 17: Effect of HNE following modulation of NADH production. A: transmission images of living cardiomyocytes (number of cells/ number of animals) scale = 33 μm; a: control (91/18), b: HNE alone (25 μM, 65/13), c: pre-treated with BHB/AcAc 2:1 (16/3), or d: pre-treated with BHB/AcAc 20:1 (16/3). Ba: steady state and Bb: normalized NAD(P)H fluorescence spectra in cardiac cells treated with HNE 25μmol/L in the absence or presence of different BHB/AcAc gradient. *$p < 0.05$ vs. control.

3.4. Analysis of components of cardiomyocyte autofluorescence

To improve our understanding of observed complex cell responses to oxidative stressors, we aimed to efficiently resolve distinct components of NAD(P)H AF in isolated cardiac myocytes. In the lab, new routines were developed for an extended analysis of the multispectral time-resolved data, as described by Chorvat and Chorvatova 2006[109].

3.4.1. Time Resolved Emission Spectra

First, we have used the gathered 3-dimensional spectral and time-dependent recordings (Fig. 18A) to construct Time-Resolved Emission Spectra (TRES) of cardiomyocyte AF (Fig. 18C), applying approach described in the Method (Section 2.2.2.). TRES were constructed by summing the photons registered over a chosen time interval[109]. TRES plot allows to complement the exponential decay analysis and to further explore time-resolved spectral changes of the UV-excited fluorescence in cardiac cells.

3.4.2. Time-Resolved, Area Normalized, Emission Spectroscopy

Second, to identify the number of components in complex cell sample, we have opted for a Time-Resolved, Area Normalized Emission Spectroscopy (TRANES), applied on NAD(P)H AF in cardiac cells (Fig. 18D). The TRANES allows analyzing the time-resolved decay data without a-prior knowledge of the excited-state kinetics of the sample and thus permits to quantitatively compare AF changes in the recorded experimental conditions. Therefore, it gives us quantitative information about the number and the localization of independent spectral components present in the recorded UV-stimulated autofluorescence. In our case, TRANES spectra revealed presence of at least 3 different components, based on the presence of two iso-emissive points (each indicating at least two different components, as described in Chorvat and Chorvatova 2006[109]).

3.4.3. Principal component analysis and linear unmixing

Third, to determine the spectral characteristics of individual components identified in complex cellular environment, in addition to previous approach, we have then applied the singular value decomposition technique followed by Principal Component Analysis (PCA)[118]. To achieve this task, we have used cell responsiveness to modulators of oxidative metabolism and redox state, as described in Sections 3.2. and 3.3. We have confirmed presence of at least three significant spectral components with spectral maximum of 450, 470 and 510 nm (Fig. 19A). The fluorescence decays of individual components were then reconstructed by analyzing TRES of each resolved component with specific spectral characteristics. Using monoexponential fit of these data, in control conditions, we have identified fluorescence lifetimes of 1.59 ± 0.20 ns (Fig. 19B), 1.0 ± 0.4 ns (Fig. 19C), and 1.26 ± 0.11 ns (Fig. 19D) for the component 1, 2 and 3 respectively. Finally, to separate the individual components and identify changes in the amplitudes and fluorescence decays of the resolved spectral components in single cells under different metabolic oxidative conditions, linear unmixing approach was used[109, 118].

3.4.4. Component analysis of gathered data

Study of changes of components resolved by spectral unmixing with specific characteristics by individual modulators led to several findings. We have observed that the inhibition of the respiratory chain by rotenone (1 μM) and cyanide (4 mM) increased the amplitude of the 1^{st} component, with similar tendency of the 2^{nd} component. On the contrary, fluorescence lifetime of the 2^{nd} component was shortened, while that of the 1^{st} component remained unchanged in the presence of the inhibitors (Fig. 20). Modifications of the third component were difficult to analyze due to its very small amplitude under most of the studied conditions. For this reason, we have therefore decided that further study is necessary to precisely comprehend the

origins and the behavior of this component and we limited our analysis to characterization of cellular changes in only the component 1 and 2.

Analysis of the individual components 1 and 2 revealed that modulation of cytosolic NAD(P)H redox states by lactate (1 mM) in the presence of pyruvate (100 μM) induced the most noticeable effect on the amplitudes of the 1st and 2nd component, and on the fluorescence lifetime of the 2nd component (Fig. 20), similarly to the effect of inhibitors of the respiratory chain. Modulation of the consumption of NADPH by GR inhibition using BCNU (100 μM) affected the 2nd component only by increasing its amplitude and reducing its fluorescence lifetime.

H_2O_2 (1 mM) and HNE (25 μM) had differential effect on the amplitudes and the fluorescence lifetimes of the two resolved components. H_2O_2 mainly decreased amplitudes of the 1st and 2nd component, but no effect on their fluorescence lifetimes was observed. In contrast, HNE shortened the fluorescence lifetimes of the 1st and 2nd component, while their amplitudes remained unaffected (Fig. 20). This result point to differential mechanisms underlying decrease in the total photon counts, observed previously in sections 3.3.1.1 and 3.3.2.1.

Furthermore, following inhibition of the respiratory chain by rotenone in the presence of cyanide, analysis of total photon counts (Section 3.3.1.2.) revealed no change in the amplitude of the H_2O_2 effect. Component analysis confirmed this observation, as we found no change in the amplitudes, or fluorescence lifetime of the 1st and 2nd component in the two conditions (Fig. 20). This result is therefore pointing to the capacity of H_2O_2 to act despite inhibition of respiratory chain. Interestingly, rotenone and cyanide prevented the decrease in the fluorescence lifetime of the 1st but not the 2nd fluorescence component induced by HNE, action accompanied by increased fluorescence amplitudes of both components.

Total photon counts pointed to partial recovery of the H_2O_2 effect in the presence of GR inhibitor BCNU (Section 3.3.1.3.). Component analysis brought better understanding why this effect seems only partial (Fig. 20). Indeed, this analysis

confirmed some recovery of the H_2O_2–induced decrease in the fluorescence amplitudes of both components, but it also revealed that the capacity of BCNU to reduce fluorescence lifetime of the 2nd component, which can explain the lack of apparent recovery of the overall photon counts. In the case of HNE, inhibition of the GR pathway by BCNU was capable to prevent the decrease of the fluorescence lifetime of 1st component by HNE, but was without effect on the 2nd one. Surprisingly, we also observed a decrease in the amplitude of the 1st component by HNE in the presence of BCNU when compared to HNE or BCNU alone. HNE did not prevent the rise in the fluorescence amplitudes with higher gradient for NADH production, set by BHB and AcAc (Fig. 20). HNE, in the presence of BHB/AcAc (2:1), decreased the amplitudes of the 1st and 2nd component and the fluorescence lifetime of the 2nd one. Modifying the BHB/AcAc ratio to (20:1) resulted in an increase of the amplitude of the 2nd component.

As presented in section 3.3.2.2., we also observed significantly smaller total photon counts when HNE was applied in the presence of DNP. Component analysis revealed that in this condition the amplitudes of the two components are significantly reduced, while HNE effect on fluorescence lifetimes is, at least partially, lost.

Gathered results on the effect of oxidative stressors on NAD(P)H fluorescence in single living rat cardiomyocytes showed that our technique has sufficient sensitivity to study the oxidative metabolic changes in living cell environment, thus providing a highly-sensitive tool for optical fingerprinting of the metabolic state directly in these cells.

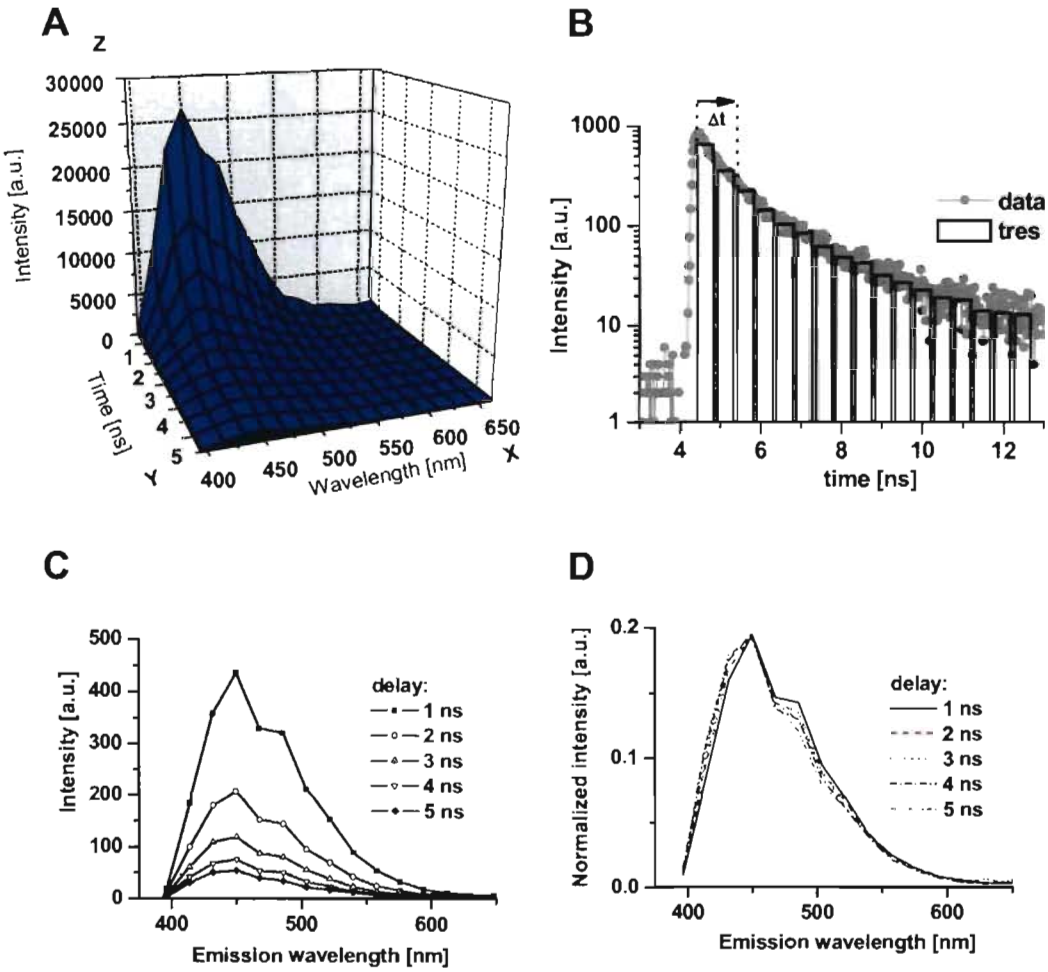

Figure 18: Analysis of NAD(P)H fluorescence in living cardiac cells. A: 3-dimensional original recording of spectrally and time-resolved fluorescence decay. B: principle of the construction of time-resolved emission spectra (TRES) from representative original recording of cardiomyocyte NAD(P)H fluorescence. C: Example of TRES of cardiomyocyte AF resolved with 1 ns resolution in control conditions. D: Time-resolved, area-normalized emission spectra (TRANES) of NADPH-based cardiomyocyte AF.

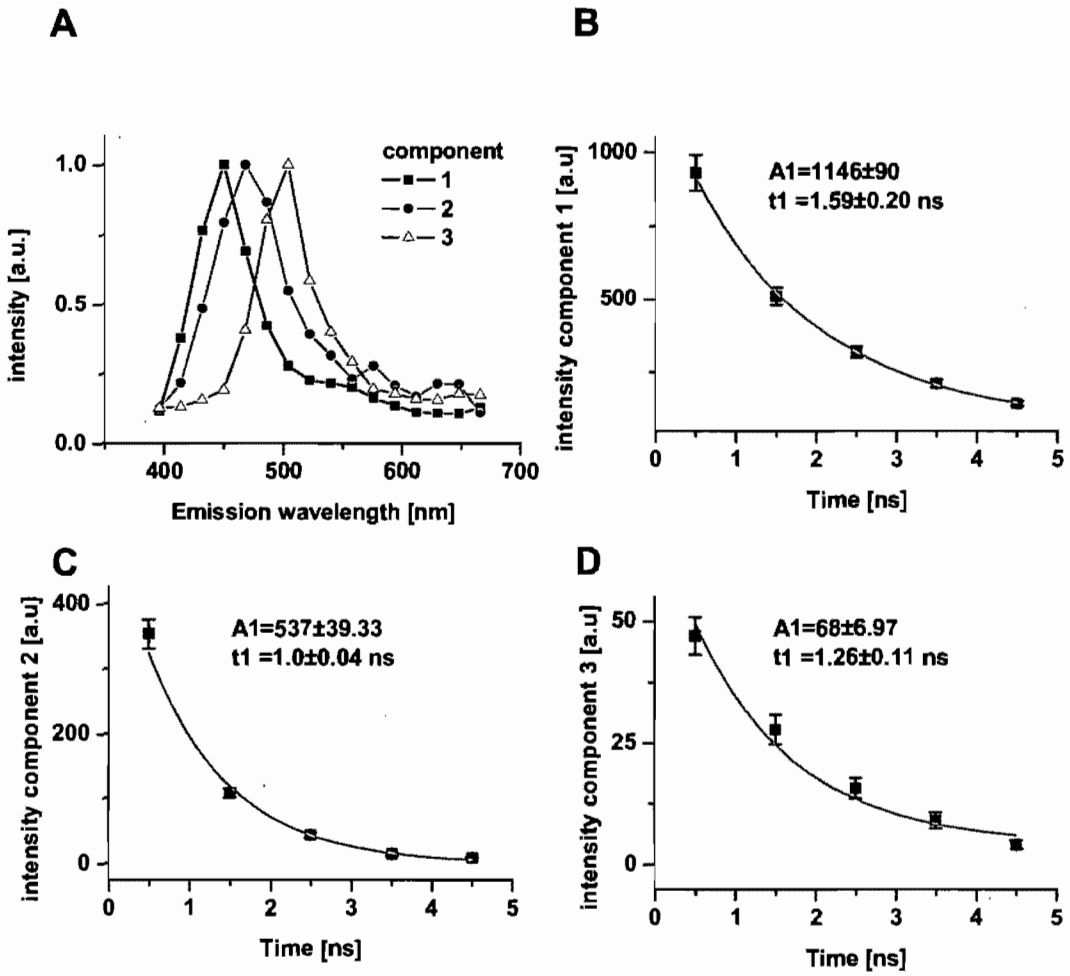

Figure 19: Separation of spectral components of NAD(P)H fluorescence in living cardiac cells. A: Reference spectra of individual NAD(P)H fluorescence components, computed by principal component analysis (PCA). (B, C and D): Monoexponential fit for the component 1, 2 and 3 respectively; A1 and t1 correspond to amplitude and lifetime of each component, respectively.

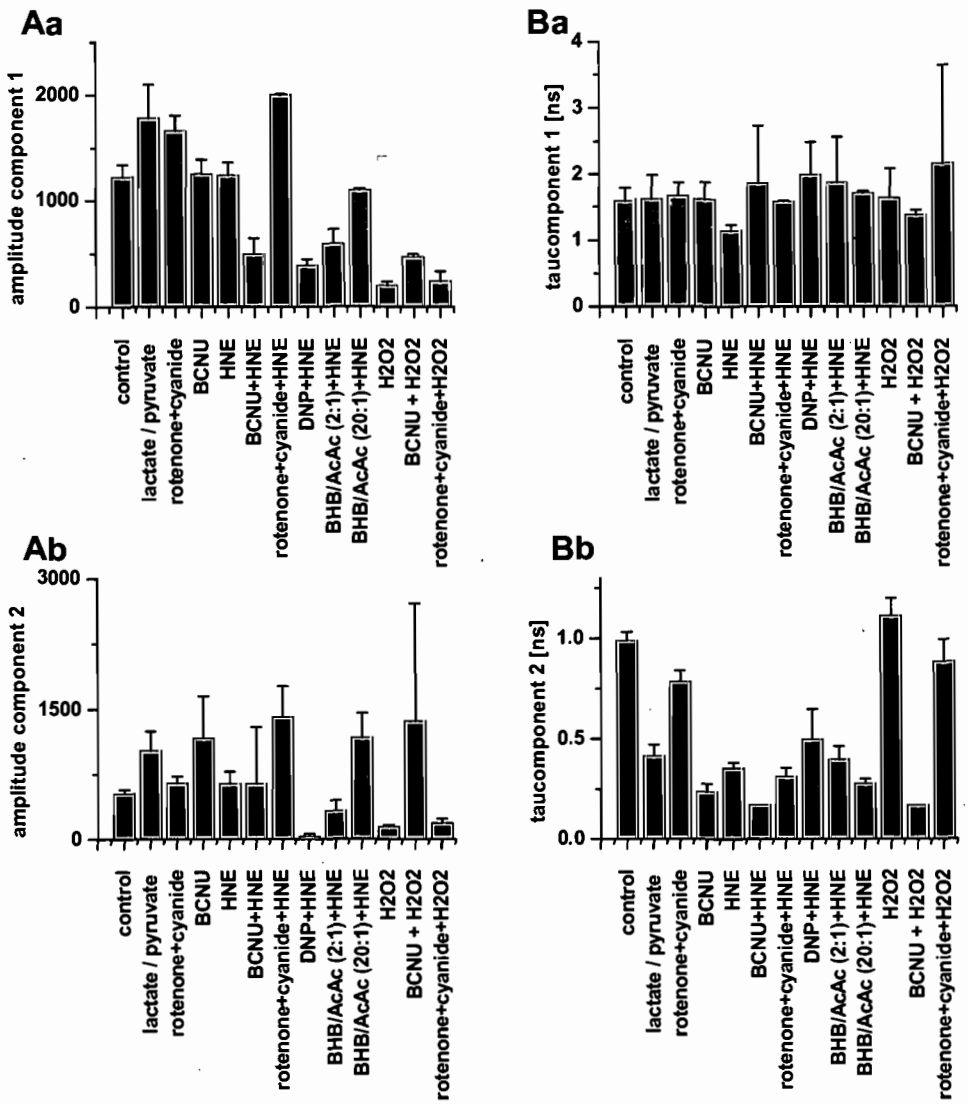

Figure 20: Sensitivity of principal components of NAD(P)H fluorescence to different modulators in living cardiac cells. Component analyses of NAD(P)H fluorescence in control cells; following modulation of: lactate (1 mM) and pyruvate (100 mM); rotenone (1 μM) and cyanide (4 mM); BCNU (100 μM) ; HNE (25 μM) alone, or in the presence of BCNU, rotenone and cyanide, DNP (50 μM), BHB/AcAc (2:1), or BHB/AcAc (20:1); H_2O_2 (1 μM) alone, or after the addition of BCNU, or rotenone and cyanide. (Aa and Ab): Amplitudes of the component 1 and 2 respectively. (Ba and Bb): Lifetimes of the component 1 and 2 respectively. Data are presented as mean ± SEM.

3.5. Application: investigation of responses to oxidative stress in pregnancy

3.5.1. Response to oxidative stress in normally pregnant rats

To study the condition of normal pregnancy, we have chosen to use the rat model due to close resemblances of pregnancies in rats[119, 120] and in humans[121] in multiple indicators, including hemodynamic, hormonal, lipidic as well as cardiovascular ones.

3.5.1.1. Blood analysis in normal pregnancy

Pregnancy was proposed to be a state where oxidative metabolic status is changing, as demonstrated by modification in the blood substrates and lipid content[68], as well as markers of LPO[122]. Therefore, we analyzed the blood concentration of these markers in the studied experimental conditions (Fig. 21). Our lab previously has demonstrated that significant physiological changes occur during pregnancy, necessary to ensure the availability of adequate amount of nutrients for the developing fetus, mainly dependent on glucose[68]. These include modifications in triglycerides, but also in carbohydrate metabolism, including blood levels of lactate, pyruvate, and glucose. In P, compared to NP, we confirmed a significant increase in the levels of lactate about two folds, leading to a significant change in the lactate/pyruvate ratio (Table 3), indicating an important modification of the redox status. Also, the level of triglycerides was significantly increased more than two folds in this condition, as reported in normal pregnant women in the third trimester[123]. Glucose levels were significantly decreased in P in accordance with this substrate being utilized by the fetus (Table 3). We also examined possible changes in the oxidative stress markers. Interestingly, in contrast to previously observed changes in MDA[83], analysis of blood concentration of HNE-protein adducts in our P rats showed no significant difference compared to NP (Fig. 21).

3.5.1.2. Investigation of sensitivity to oxidative stress in normal pregnancy

NAD(P)H fluorescence, determined as the total photon counts, of cardiomyocytes from P rats was not significantly different from the ones isolated from NP (Fig. 22Ba and Bb). We then investigate responses to oxidative stressors H_2O_2 and HNE. NAD(P)H fluorescence in cardiac cells isolated from P rats and treated with H_2O_2 (1 μM), measured as total photon counts, was significantly decreased (Fig. 22Ba). The effect was comparable to that recorded in NP rats, although normalized spectra revealed less spectral broadening (Fig. 22Bb). Interestingly, the cells from P rats treated with H_2O_2 (Fig. 22Ab) presented less membrane damage in comparison to those treated with the oxidative stressor in NP rats (Fig. 12Aa). Treatment with HNE (25 μM) induced a loss of NAD(P)H fluorescence intensity of cardiomyocytes from P rats (Fig. 23Ba), without modifying the cell shape (Fig. 23A). This response was identical to that observed in the NP group, measured as total photons counts (Fig. 23Ba), or normalized spectra (Fig. 23Bb). BCNU (100 μM), which had no effect on NAD(P)H fluorescence in P rats (Fig. 24Ba) caused, in the presence of HNE (25 μM), further significant decrease in NAD(P)H fluorescence (Fig. 24Ba). This effect, accompanied by red spectral broadening of normalized spectra (Fig. 24Bb), was more pronounced than in NP rats.

In pregnancy, we confirmed (Table 3) previously observed results of the rise in the levels of lactate leading to a significant alteration in the lactate/pyruvate ratio[68]. We therefore tested cardiomyocyte AF response to addition of lactate (1 mM) in the presence of pyruvate (100 μM) and observed a tendency of NAD(P)H fluorescence to increase in cardiomyocytes obtained from P rats (Fig. 25Ba). Normalized spectra showed no difference in comparison to the control cells (Fig. 25Bb). Overall, our results point to the capacity of cells from P rats to adapt to this condition by showing no significant differences in the cell responsiveness to oxidative stressors.

3.5.2. Mineralcorticoid receptor blockage by canrenoate in non pregnant rats

3.5.2.1. Blood analysis in non pregnant rats treated with canrenoate

We noted a significant decrease in the blood lactate concentration in NP_{can} rats, with a similar tendency for pyruvate, causing no significant change in the lactate/pyruvate ratio (Table 3). Neither glucose nor triglycerides levels were significantly different. In addition, in the blood of NP_{can} rats, we observed a significant rise in the levels of HNE-protein adducts when compared to non-treated NP rats (Fig. 21). These results suggest that modulation of MR receptors affect oxidative metabolic state of cardiac cells by acting on both oxidative and metabolic status.

3.5.2.2. Responsiveness to oxidative stressors in canrenoate-treated non pregnant rats

We wanted to test whether observed changes in oxidative and metabolic state induced by inhibition of MR receptors by canrenoate has also repercussions on cardiomyocyte sensitivity to oxidative stressors. In control conditions (external solutions only containing glucose as substrate), our data revealed no significant difference in NAD(P)H fluorescence, measured as total photons counts (Fig. 26Ba), or normalized AF (Fig. 26Bb), between NP_{can} and NP rats (Fig. 9Ba and Bb). Also, we noted no change in the quality of the cell shape, as evidenced by the transmission image (Fig. 26Aa). We then investigated the response of cardiomyocyte AF to H_2O_2 (1 μM). In cardiomyocytes isolated from NP_{can} rats, H_2O_2 provoked cell membrane damage (Fig. 26Ab), and decrease in NAD(P)H fluorescence (Fig. 26Ba), comparably to non-treated ones. Nevertheless, we noted more important red spectral broadening in canrenoate-treated rats in comparison to non-treated ones (Fig. 26Bb).

Application of HNE (25 μM) to NP_{can} rats did not induce visible effects on the shape of the cell membrane (Fig. 27Aa), comparably to findings in NP at this

concentration. Cells from both groups responded identically to treatment with HNE, when measured as total photon counts (Fig. 27Ba) or as normalized NAD(P)H fluorescence (Fig. 27Bb). Also, BCNU – alone or in the presence of HNE (Fig. 27Ba) - induced same effects in NP_{can} vs. NP conditions. Finally, the addition of lactate (1 mM) in the presence of pyruvate (100 μM) did not significantly affect NAD(P)H fluorescence in cardiomyocytes obtained from NP_{can} rats (Fig. 28Ba). Normalized spectra showed no difference in comparison to the control (Fig. 28Bb). These results indicate that cardiomyocytes from NP rats can adapt to oxidative and metabolic changes induced by inhibition of MR receptors by canrenoate.

3.5.3. Mineralocorticoid receptor blockage by canrenoate in pregnant rats

3.5.3.1 Oxidative stress and substrate availability in canrenoate-treated pregnant rats

HNE-protein adduct concentration increased significantly in the blood of P_{can} rats (Fig. 21), while it remained unchanged in comparison to P ones. On the other hand, this level of oxidative stress marker, significantly increased with the canrenoate treatment in NP rats, failed to rise in P_{can}. Furthermore, blood lactate levels were significantly decreased in P_{can} rats when compared to P ones (Table 3). This effect did not prevent the lactate concentration to rise significantly *vs.* NP_{can}, as expected for pregnancy condition. However, pyruvate concentration, as well lactate/pyruvate ratio, were maintained in P_{can}, as no significant differences were observed when compared to P. Likewise, glucose or triglyceride levels were not significantly affected by the treatment with canrenoate when compared to non-treated pregnant rats. As a result, all the measured substrate levels were significantly increased in P_{can} when compared to NP_{can}. These results demonstrate that inhibition of MRs induce important metabolic and oxidative changes in pregnancy.

3.5.3.2 Investigation of sensitivity to oxidative stress in canrenoate-treated pregnant rats

After identification of metabolic and oxidative changes in the blood following canrenoate-treatment in pregnancy, we aimed to test the responsiveness of cardiomyocytes to oxidative stressors in this condition. NAD(P)H fluorescence intensity, evaluated as total photon counts, tended to be higher in P_{can} than in P (Fig. 29Ba), with no modification in the spectral shape (Fig. 29Bb). H_2O_2 (1 μM) significantly lowered NAD(P)H AF intensity of P_{can} but it was less effective in comparison to P (Fig. 29Ba) while causing comparable cell membrane damage as in P (Fig. 29Ab). H_2O_2 also resulted in similar spectral broadening P_{can} when compared to P (Fig. 29Bb). Cardiomyocytes from P_{can}, treated with HNE (25 μM) responded similarly as in P condition (Fig. 30Ba). Normalized spectra showed a slight broadening of the spectral shape, identical in both conditions (Fig. 29Bb). Interestingly, BCNU (100 μM) caused significant loss of AF intensity of cardiac cells from P_{can} (Fig. 31Ba) without affecting spectral shape (Fig. 31Bb). This effect was in contrast to what observed in P where no change in the spectral intensity by BCNU was noted (Fig. 24Ba). In the presence of HNE (25 μM), in P_{can} rats, BCNU was able to nearly completely extenuate AF intensity (Fig. 31Ba) to the same extent as in P (Fig. 24Ba), accompanied by red spectral broadening (Fig. 31Bb). We observed no significant change in the AF intensity or spectral shape in P_{can} rats after application of lactate (1 mM) in the presence of pyruvate (100 μM) (Fig. 32Ba and Bb). These results suggest that while NP rats were also able to adapt to MR inhibition by canrenoate, in P rats some maladaptive components were identified and need to be further studied in the future. Gathered data also demonstrate that the technique developed has the sensitivity to explore potential changes in metabolic oxidative changes under pathophysiological conditions.

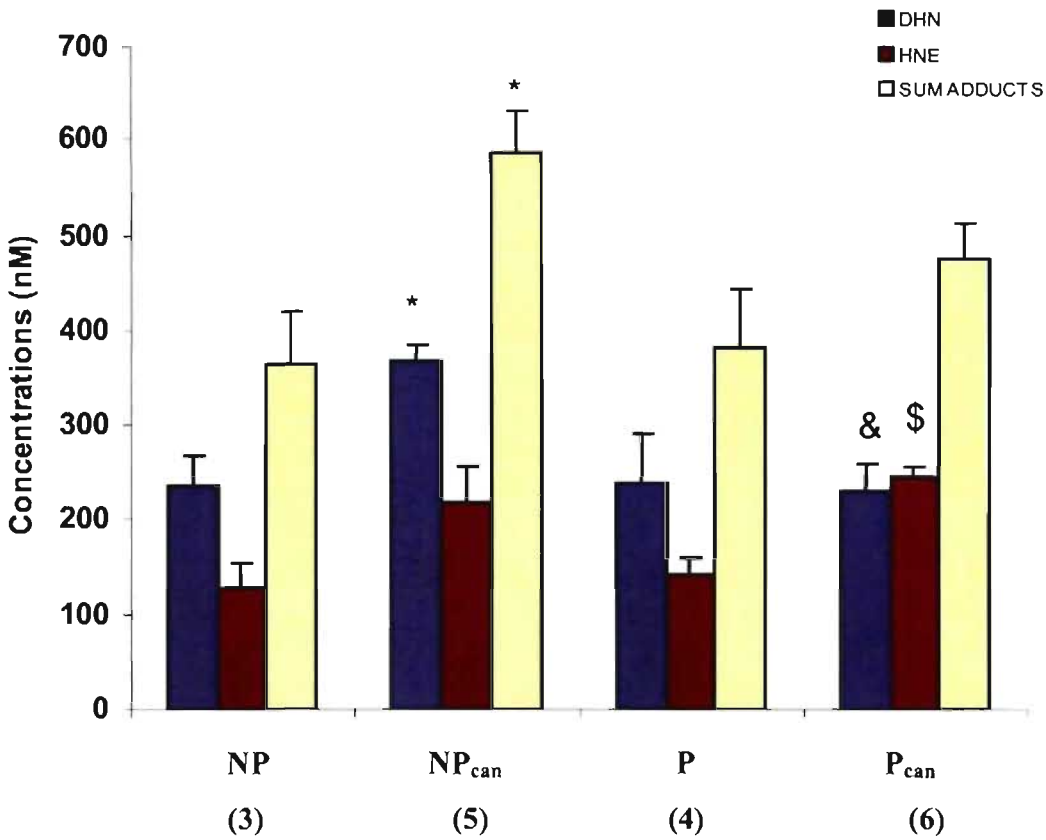

Figure 21: Measurement of lipid peroxidation markers in the blood. Protein-bound with HNE and/or its corresponding alcohol 1,4-dihydroxynonene (DHN), Data are presented as mean ± S.E.M. * $p< 0.005$ vs. NP; & $p<0,05$ vs. NP_{can}; $ $p< 0.05$ vs. P. (number of animals).

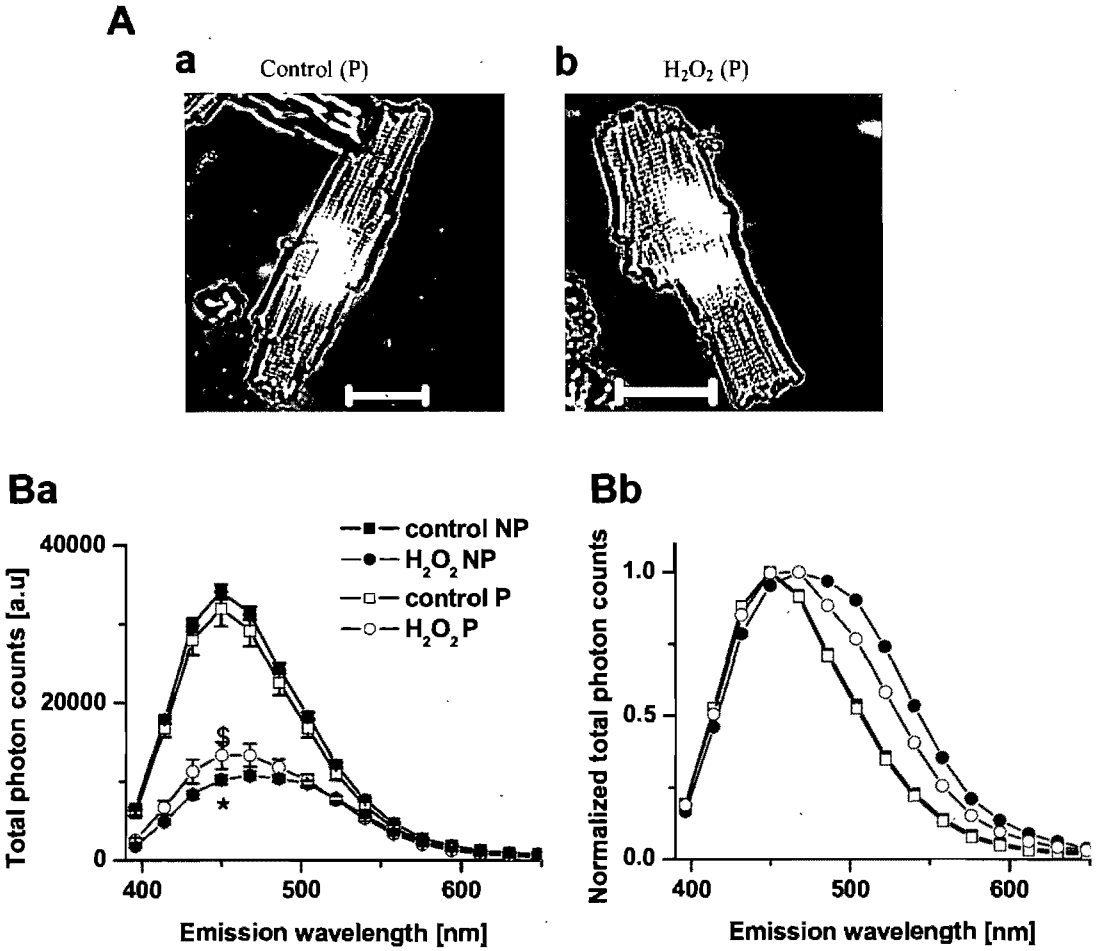

Figure 22: Comparison of response to oxidative stress induced by H_2O_2 in P vs. NP. A: transmission images of living cardiac cells (number of cells/ number of animals) obtained from P rats; a: control (26/5), b: treated with H_2O_2 (1 μM, 15/3) scale = 33 μm. Ba: steady state and Bb: normalized NAD(P)H fluorescence spectra in NP or P in the absence or presence of H_2O_2. *$p< 0.05$ vs. NP control; \$ $p< 0.05$ vs. P control.

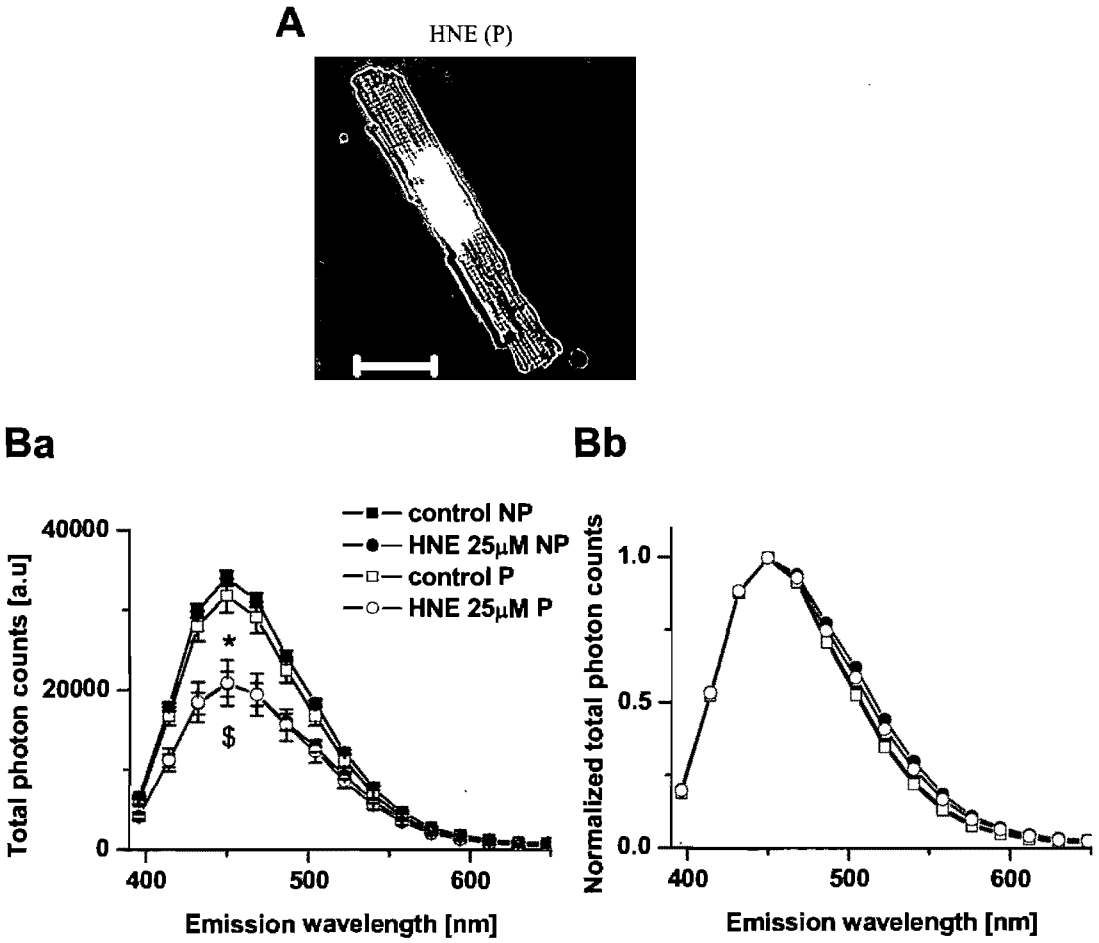

Figure 23: Comparison of cardiomyocyte AF responses to HNE in P vs. NP. A: transmission images of living cardiomyocytes (number of cells/ number of animals) isolated from P, treated with HNE (25 μM, 25/5) scale = 33 μm. Ba: steady state and Bb: normalized NAD(P)H fluorescence spectra in NP or P in the absence or presence of HNE. *$p< 0.05$ vs. NP control; \$ $p< 0.05$ vs. P control.

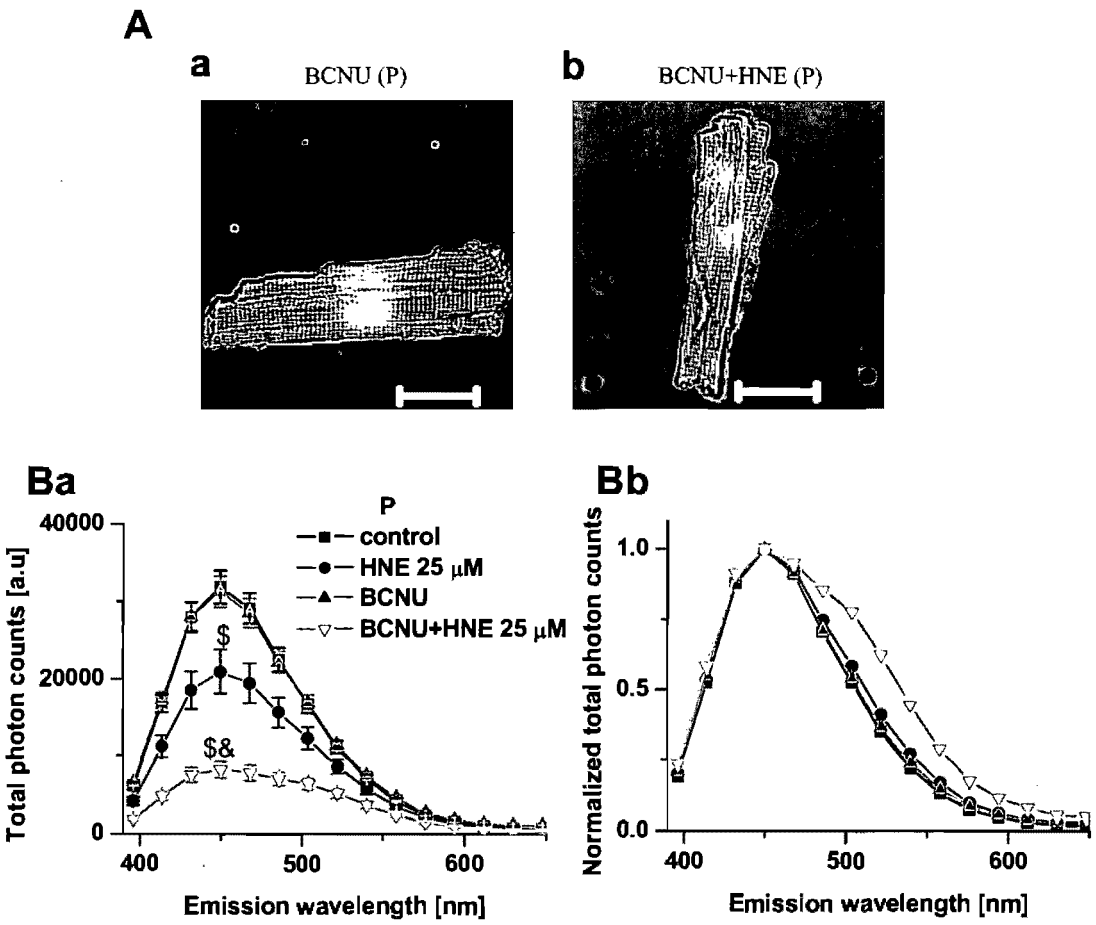

Figure 24: Comparison of the response of cardiomyocyte AF to HNE in the absence or presence of GR inhibition in P. A: transmission images of living cardiomyocytes (number of cells/ number of animals) isolated from P; a: BCNU alone (100 μM, 25/5), b: pre-treated with BCNU and then HNE (25 μM) (25/5) scale = 33 μm. Ba: steady state and Bb: normalized NAD(P)H fluorescence spectra in P in the absence or presence of HNE and/or BCNU. $ $p < 0.05$ vs. P control; & $p < 0.05$ vs. P HNE.

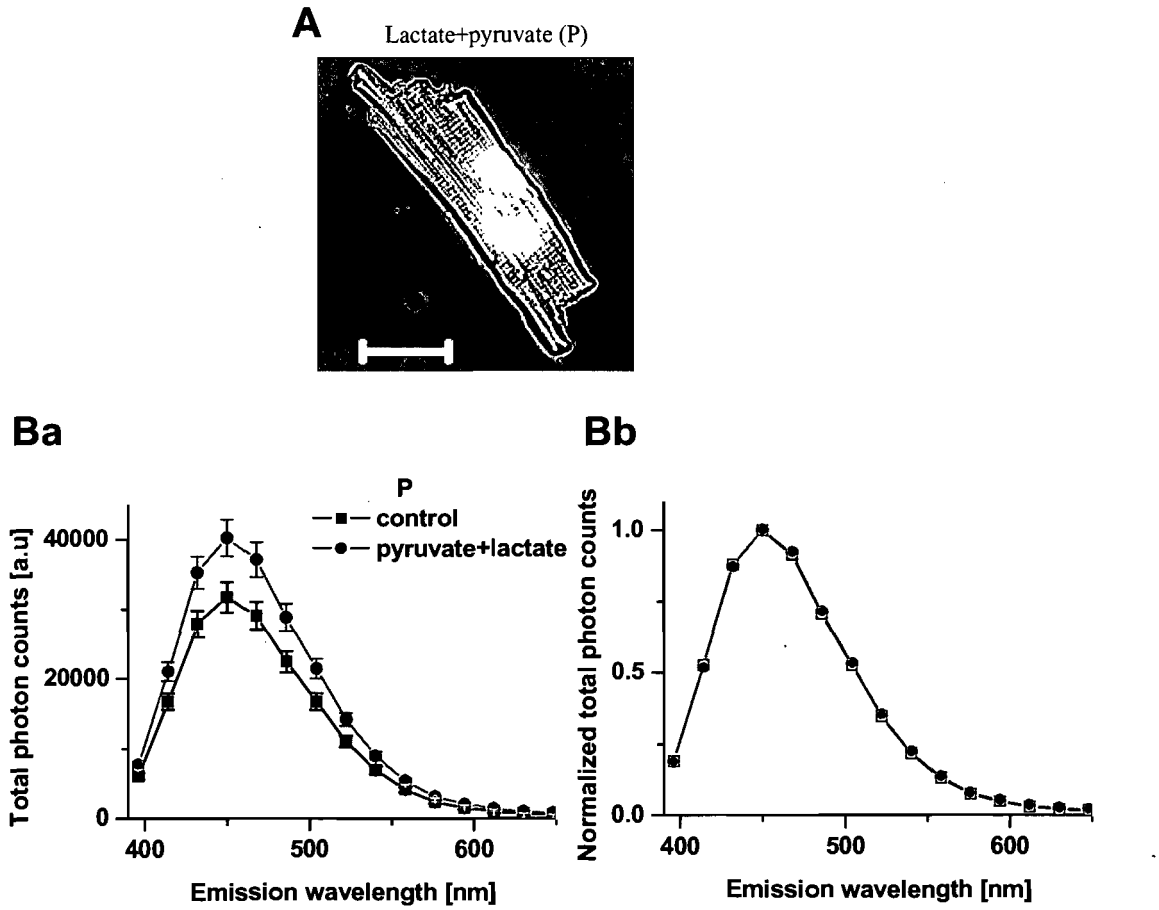

Figure 25: The effect of lactate/ pyruvate ratio in P. A: transmission image of living cardiomyocytes (number of cells/ number of animals) isolated from P, supplemented with pyruvate (100 μM) and lactate (1 mM) (15/3) scale = 33 μm. Ba: steady state and Bb: normalized NAD(P)H fluorescence spectra in P in the absence or presence of lactate/pyruvate.

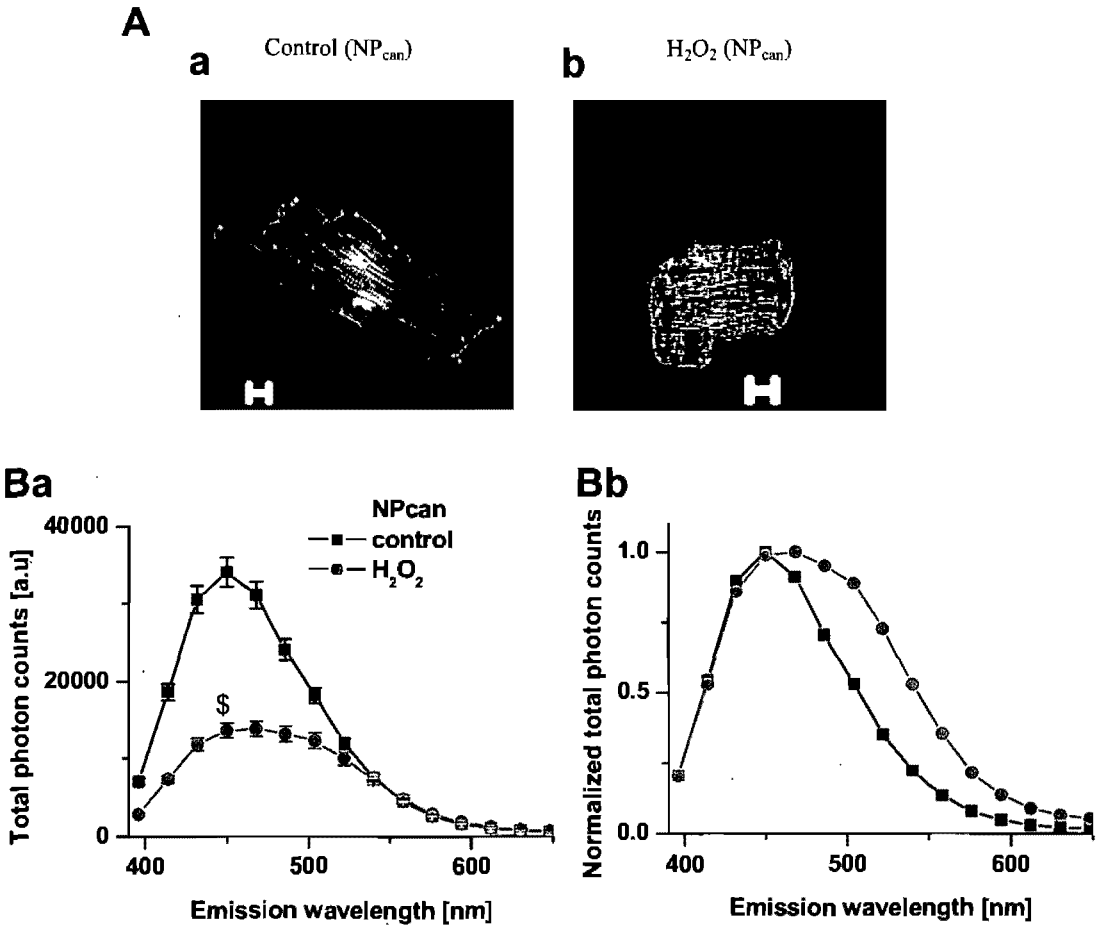

Figure 26: The response to oxidative stress induced by H_2O_2 in NP_{can}. A: transmission images of living cardiac cells (number of cells/ number of animals) obtained from NP_{can} rats; a: control (20/4), b: treated with H_2O_2 (1 μM, 15/3) scale = 10 μm. Ba: steady state and Bb: normalized NAD(P)H fluorescence spectra in the absence or presence of H_2O_2. \$ $p< 0.05$ vs. NP_{can} control.

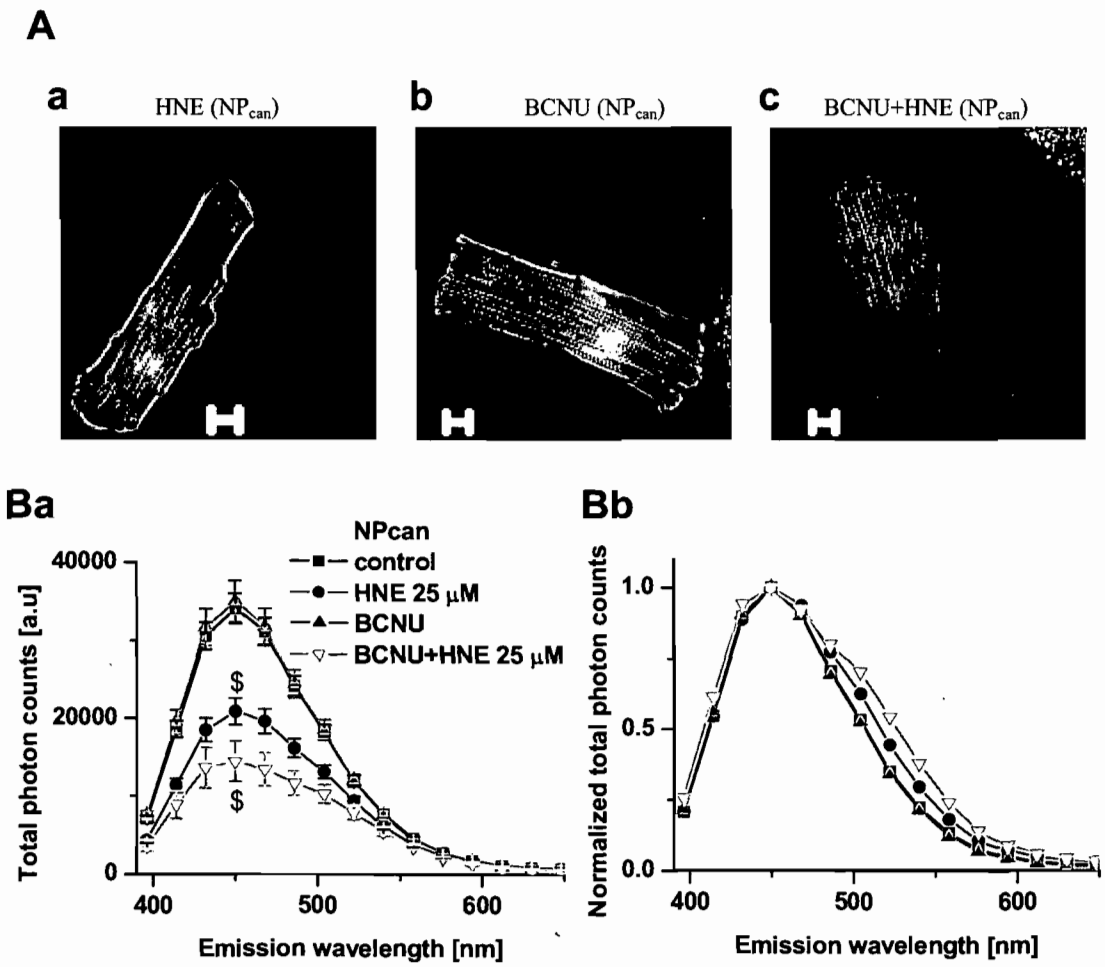

Figure 27: The response to HNE in the absence or presence of GR inhibition in NP_{can}. A: transmission images of living cardiomyocytes (number of cells/ number of animals) isolated from NP_{can} ; a: HNE alone (25 μM, 15/3), b: BCNU alone (100 μM, 15/3), c: pre-treated with BCNU (15/3) scale = 10 μm. Ba: steady state and D: normalized NAD(P)H fluorescence spectra in NP_{can} in the absence or presence of HNE and/or BCNU. *$p< 0.05$ vs. NP control; \$ $p< 0.05$ vs. NP_{can} control.

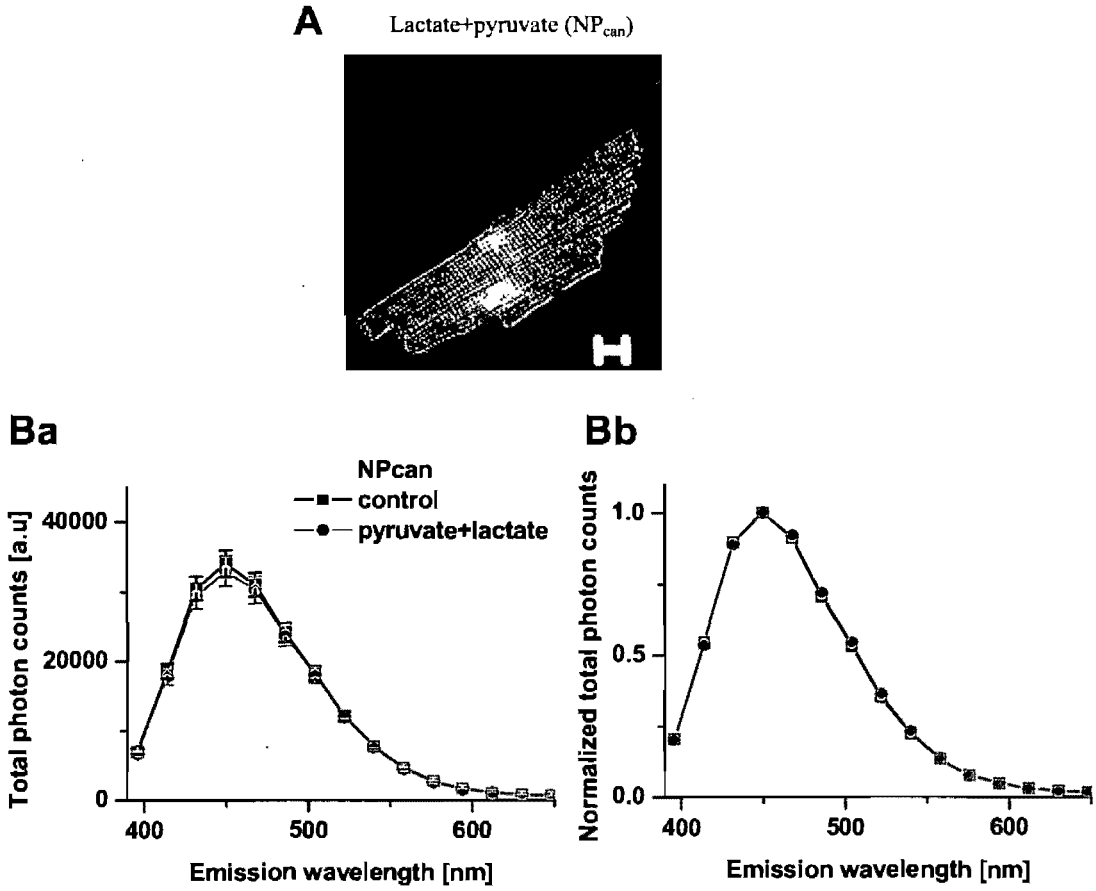

Figure 28: The effect of lactate/ pyruvate ratio in NP_{can}. A: transmission image of living cardiomyocyte (number of cells/ number of animals) isolated from NP_{can} supplemented with pyruvate (100 μM) and lactate (1 mM) (15/3) scale = 10 μm. Ba: steady state and Bb: normalized NAD(P)H fluorescence spectra in the absence or presence of lactate/pyruvate.

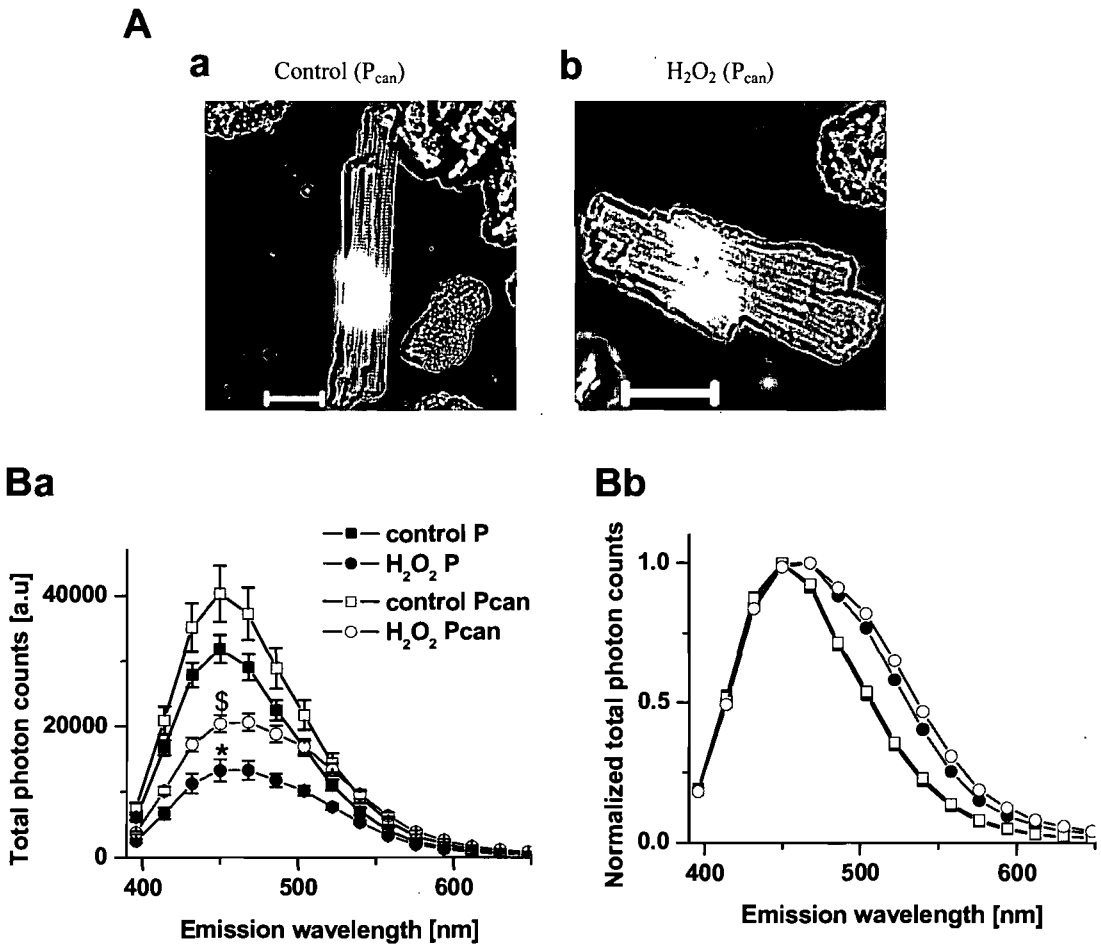

Figure 29: Comparison of the response of cardiomyocyte AF to oxidative stress triggered by H_2O_2 in P_{can} vs. P. A: transmission images of living cardiac cells (number of cells/ number of animals) obtained from P_{can} rats; a: control (20/4), b: treated with H_2O_2 (1 μM, 20/4) scale = 33 μm. (Ba and Bb): steady state and normalized NAD(P)H fluorescence spectra in P or P_{can} in the absence or presence of H_2O_2. *$p< 0.05$ vs. P control; \$ $p< 0.05$ vs. P_{can} control.

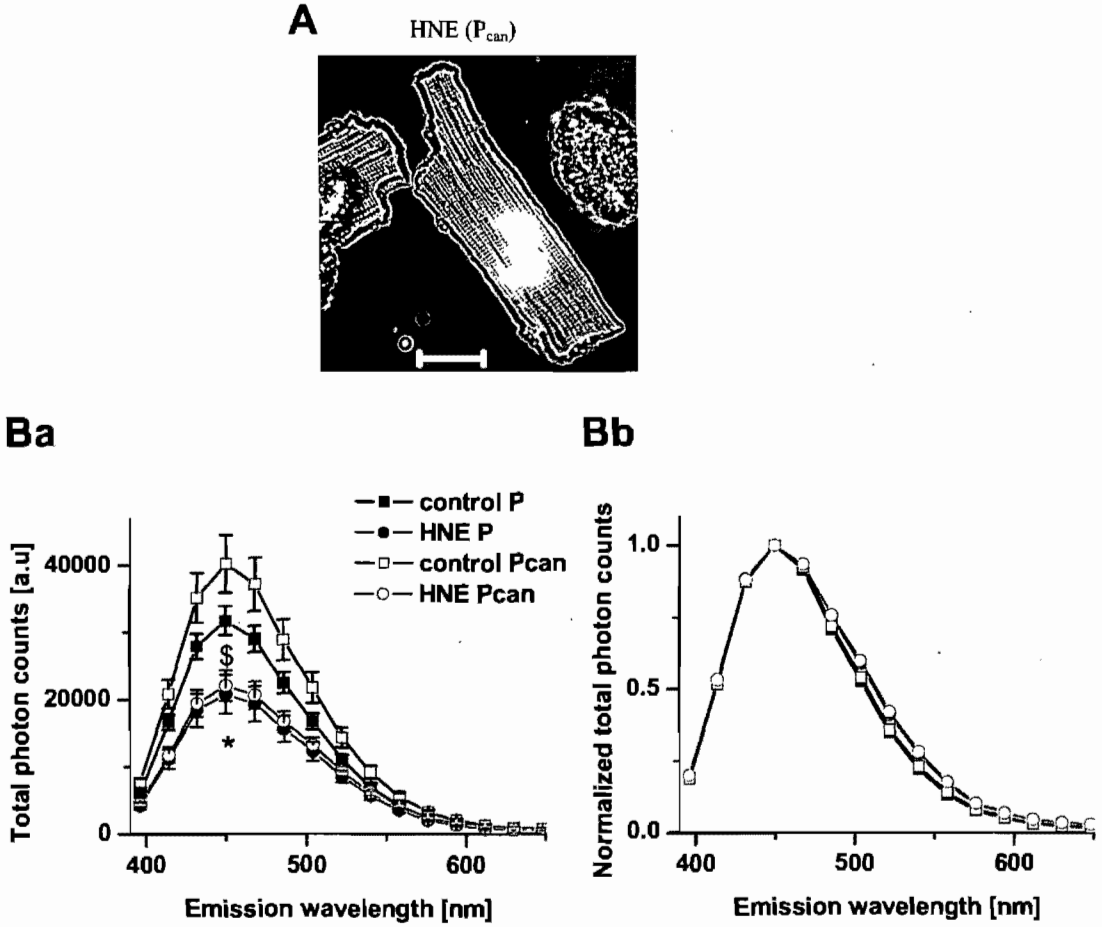

Figure 30: Comparison of the response of cardiomyocyte AF to HNE in P_{can} vs. P. A: transmission image of living cardiomyocyte (number of cells/ number of animals) isolated from P_{can} treated with HNE (25 μM, 20/4) scale = 33 μm. Ba: steady state and Bb: normalized NAD(P)H fluorescence spectra in P_{can} or P in the absence or presence of HNE. *$p< 0.05$ vs. P control; \$ $p< 0.05$ vs. P_{can} control

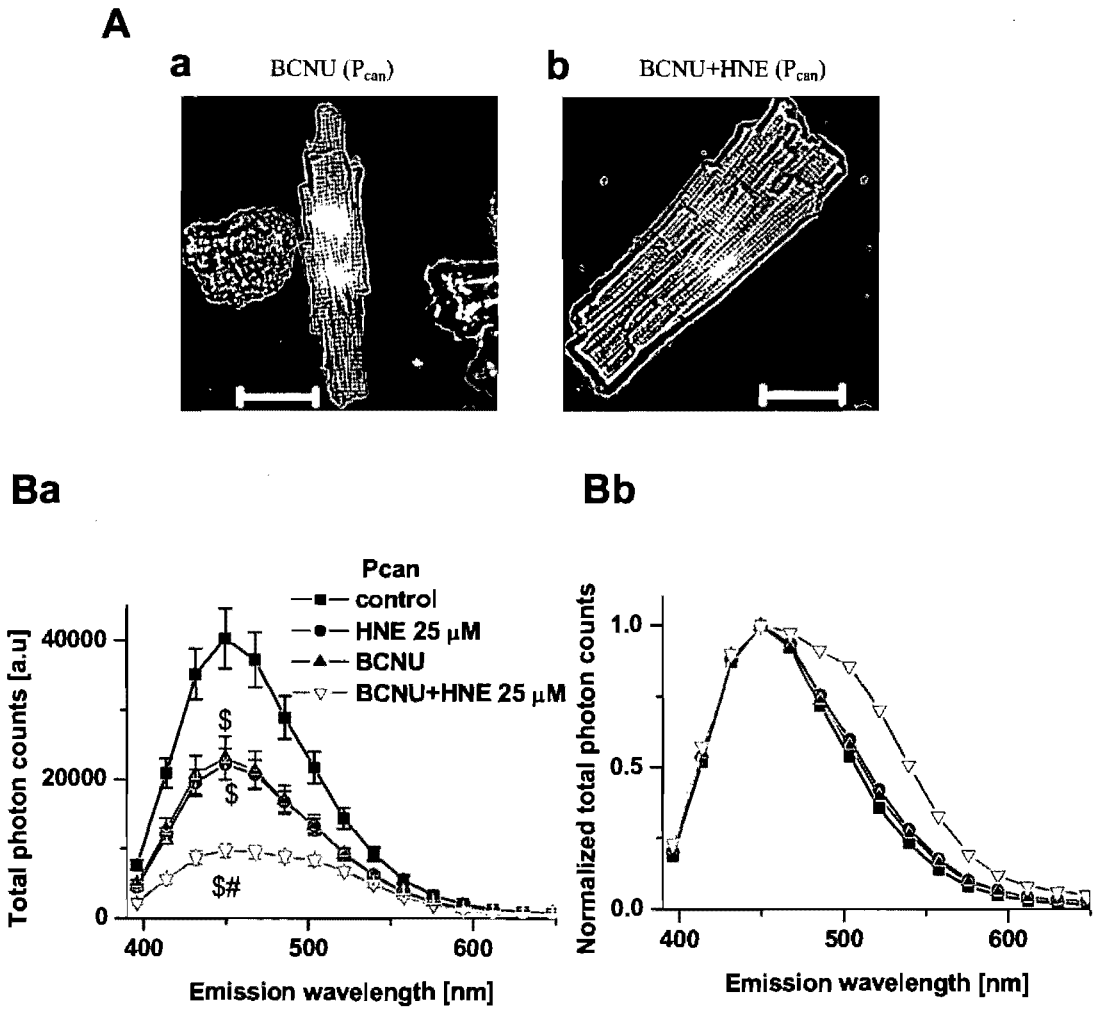

Figure 31: The response of cardiomyocyte AF to HNE in the absence or presence of GR inhibition in P_{can}. A: transmission images of living cardiomyocytes (number of cells/ number of animals) isolated from P_{can}; a: BCNU alone (100 μM, 20/4), b: pre-treated with BCNU and then HNE (25 μM) (20/4) scale = 33 μm. Ba: steady state and Bb: normalized NAD(P)H fluorescence spectra in P_{can} in the absence or presence of HNE and/or BCNU. $p< 0.05 vs. P_{can} control; #p< 0.05 vs. P_{can} HNE.

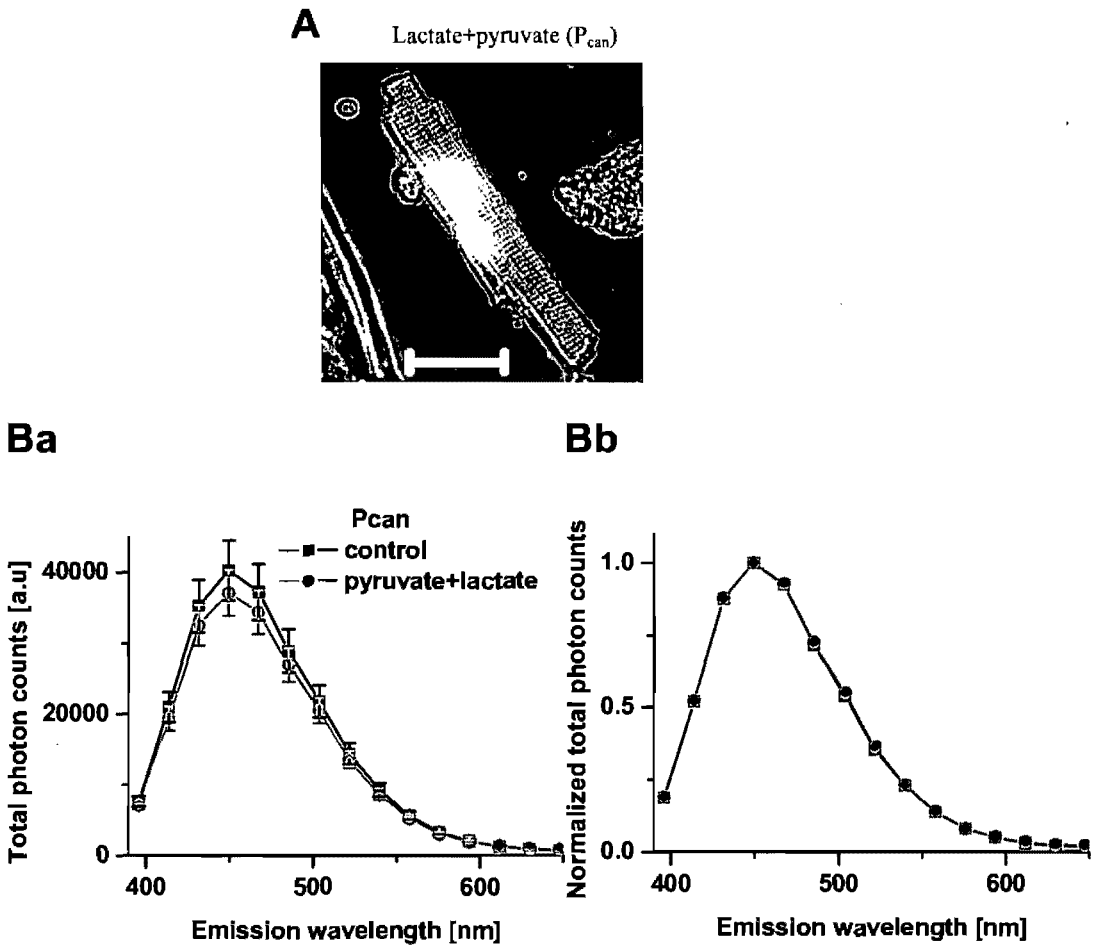

Figure 32: The effect of lactate/ pyruvate ratio in P_{can}. A: transmission image of living cardiomyocyte (number of cells/ number of animals) isolated from P_{can} supplemented with pyruvate (100 μM) and lactate (1 mM) (20/4) scale = 33 μm. Ba: steady state and Bb: normalized NAD(P)H fluorescence spectra in P_{can} in the absence or presence of lactate/pyruvate

Parameters	Unit	NP	NP_{can}	P	P_{can}
Pyruvate	µM	104.8±16.2 (9)	92±13.8 (6)	124.2±13.1 (8)	118.3±15.4 (10)
Lactate	mM	1.6±0.2 (9)	1±0.2 (6)*	2.8±0.2 (8)*	2.2±0.2 (12) &,#
Lactate/Pyruvate	-	16.4±1.5 (9)	11.9±2.3 (6)	23.8±1.8 (8)*	20.3±1.2 (8) &
Glucose	mM	14.3±0.8 (9)	14.8±0.7 (6)	8.3±0.9 (8)*	6.9±0.4 (8) &
Triglycerides	mM	1.5±0.2 (9)	1.6±0.3 (6)	3.5±0.5 (8)*	3.5±0.4 (8) &

Table 3: Blood analyses of different metabolic substrates. Blood metabolites obtained from total blood collected in fed state from NP, NP_{can}, P, and P_{can} rats. Data are presented as mean ± S.E.M. (number of samples), * $p < 0.005$ vs. NP, & $p < 0.05$ vs. NP_{can}, # $p < 0.05$ vs. P.

4. DISCUSSION

4.1. NAD(P)H fluorescence as a non-invasive tool for study of oxidative metabolic changes in living cardiac myocytes

Autofluorescence is one of the most versatile non-invasive tool for mapping the metabolic state in living tissues, such as eye[124] and skin[125, 126]. Today, AF spectroscopy is widely used in the early detection of different types of cancers[127, 128]. In the heart, despite attempts to use AF in investigation of rejection of transplanted hearts[129, 130] and in valve engineering[131, 132], we still lack tools for its convenient use. Recent developments in fluorescence technologies, especially combination of microscopy and time-resolved methods (e.g. fluorescence lifetime imaging microscopy) brought new and unprecedented insight into understanding of cell metabolic state. The non-invasive optical detection techniques combined with digital data analysis, when applied to intrinsic cellular fluorescence, can therefore greatly improve our understanding of changes in cell metabolism, and thus the cell functioning, particularly in metabolically highly active organs such as the heart.

Increasing interest in imaging and diagnostics of living cells and tissues based on their intrinsic fluorescence rather than fluorescence labeling is closely connected to latest developments in high-performance spectroscopic and microscopic techniques[125, 133]. Enzymes involved in the mitochondrial metabolic chain are often sources of intrinsic cell fluorescence, thus possessing a potential for being suitable endogenous indicators of cellular metabolic state. Blue AF of cardiac myocytes was demonstrated to correlate with metabolic changes and was ascribed to mitochondrial NAD(P)H[94, 134], while the yellow/green fluorescence was rather assigned to oxidized flavoproteins in the respiratory complexes, following excitation by UV or visible light, respectively[95, 115].

In the present study we have investigated fluorescence characteristics of NADPH. We have demonstrated that NADPH fluorescence intensity is concentration and pH-dependent, and that its fluorescence decays can be characterized by at least two exponential

decay. Our data also confirmed that fluorescence of NADPH and NADH molecules have close spectral characteristics[135], which makes it difficult to distinguish between the two molecules, as previously reported[93]. Furthermore, quantum yield of NADPH fluorescence was found smaller than that of NADH[135], as described before[102]. Our original findings point out towards possible differences in NADH and NADPH fluorescence lifetimes[135]. However, this issue is still presently controversial and needs to be further investigated, as the observed differences can be reflection of different kinetics of the two molecules, but also the presence of impurities in the recorded samples. Therefore we suggest that the fluorescence characteristics need to be compared after further purification of the tested molecules in the future.

In agreement with previous findings[103], the results of our *in vitro* experiments showed sensitivity of NADPH fluorescence intensity to changes in its microenvironment (concentration, pH or viscosity). However, as each molecular species and/or its conformational state having specific spectral and lifetime characteristics[90], spectral profile gathered from the total photon counts recorded in complex systems, such as in cells, results from a mixture of theses conformations. One should also take into consideration that the fluorescence intensity depends not only on the relative amplitudes, but also on their fluorescence lifetimes, as defined by equation (2) (Section 2.2.2.). Indeed, as each molecular species and/or its conformational state is having specific spectral and lifetime characteristics[91], spectral profile gathered from the total photon counts recorded in complex systems, such as in cells, results from a mixture of specific conformations. Total photon counts therefore cannot, by itself, give full information about the fluorescing molecule, especially when several parameters are changing simultaneously e.g. pH, viscosity, binding of molecules to specific enzymatic proteins and/or oxidation-reduction reactions which is an often situation in living cellular responses. Under such conditions, simple analysis of fluorescence intensity can thus result in misleading interpretations. Therefore, more profound analysis of fluorescence, such as recording time-resolved fluorescence spectra,

give more precise insight into the true behavior of the fluorescing molecule in the real environment.

It is also noteworthy to precise that the photochemical destruction of a fluorophore, which is referred to as photobleaching, may complicate the observation of fluorescent molecules, since they will eventually be destroyed by the light exposure necessary to stimulate them into fluorescing species. We did not specifically study the changes of NAD(P)H fluorescence characteristics induced by photobleaching. However, the loss of activity caused by photobleaching can be controlled by several ways and in our experiments: this was achieved by reducing the time-span of light exposure and by each recording being taken from a separate cell.

To date, AF of NAD(P)H has been particularly long used for non-invasive fluorescent probing of metabolic state[134] and has been an extremely useful and powerful tool for monitoring energy metabolism[99]. In previous work done in the laboratory, steady-state fluorescence spectra of NAD(P)H[135, 136] were characterized in living rat cardiomyocytes. Lifetime pools of NAD(P)H have been previously identified, corresponding to free and protein-bound NAD(P)H in the heart mitochondria[102], as well as neuronal tissues[85]. Nevertheless, their separation is often complicated by strongly overlapping absorption, as well as fluorescence spectra. In this context, the fluorescence lifetimes are considered to provide additional tool for separation of different molecular conformations and/or complexes contributing to AF of biological samples. Monitoring NAD(P)H by multi-parametric AF assays could therefore provide rapid and non destructive measurement of metabolic state directly in living cells. Such insight can become fundamental for understanding the dynamic changes of the cellular energy metabolism. Recent advances in fluorescence techniques, namely introduction of multispectral imaging and fluorescence lifetime detection brought the possibility to simultaneously measure and synchronously identify dynamic changes of several AF molecules in biological samples[137]. Recently, a significant progress was achieved in the separation of different chromophores

combining spectral unmixing and lifetime analysis[91]. Therefore, we applied a new technique and analyzed multi-dimensional time-resolved spectra in living cardiac cells by multi-wavelength TCSPC[109]. Our lab was inspired by these methods and developed new algorithms for spectral analysis and linear unmixing[118], which were tested for their ability to efficiently separate also contributions of individual components of flavin AF from the TCSPC data[138]. We investigated its possible application to quantitatively assess changes of individually resolved NAD(P)H components to provide highly sensitive fundamental tool for optical fingerprinting of metabolic oxidative state directly in living cells.

To resolve principal fluorescence components in the time-resolved NAD(P)H signals, an original PCA approach was used, already successfully attempted for free and bound flavin AF in cardiomyocytes[118, 138] accompanied by spectral unmixing[137, 139]. First, to consolidate analysis of spectral and temporal distribution of AF intensity, we undertook a complementary approach to exponential decay analysis by applying semi-quantitative TRES representation[140]. This approach allowed us to resolve time-dependent changes in NAD(P)H spectra, see section 2.2.2, (equation 8). TRES analysis revealed 2 peaks at 456 nm and 496 nm in control conditions. In contrast to the 2nd peak, the 1st peak (456 nm) rapidly faded in the first couple of ns, suggesting the presence of the process with the corresponding lifetime of 1-2 ns or less. Next, we examined the reference fluorescence spectra and lifetimes of principal NAD(P)H components. In contrast to externally-applied fluorescence probes, the reference spectra of AF components are dependent on the cell environment and its physiological state, and, thus, cannot be simply estimated from isolated fluorophores measured in solutions. As biochemical isolation of individual proteins from biological samples and subsequent determination of their spectral properties are both difficult and carry the risk of altering the kinetic spectral properties of specific protein conformations after protein isolation in solution (*vs.* its membrane-bound state), a more appropriate method is necessary for reference spectra estimation in cells. We adopted an approach developed previously by our group for the spectral separation of flavin components in multispectral microscopy images[118], and reference spectra were identified

by analyzing cell responses to modulators of the cellular metabolic state. To separate the individual spectral components, PCA was performed (see section 3.4.3. and Chorvat and Chorvatova 2006[109] for details). With this approach, we resolved 3 major components with distinct fluorescence spectra and fluorescence lifetimes: the 1st component with 450 nm spectral maximum and 1.7 ns lifetime, the 2nd component with 470 nm spectral maximum and 1 ns lifetime, and the 3rd component with 510 nm spectral maximum and 1.2 ns lifetime.

To assign molecular origins to the resolved components, their regulation by metabolic modulators was examined by spectral unmixing of the recorded data. Time-resolved data for each component were used to reconstitute the fluorescence decay of each component. Monoexponential fit was applied to gather information on the fluorescence lifetime and amplitude of each resolved component. In these conditions, as expected, the amplitudes of the 1st and 2nd components were heightened by inhibition of the respiratory chain with rotenone and cyanide. The fluorescence lifetime of the 1st component remained unchanged in the presence of applied regulators of mitochondrial metabolism, with the exception of response to LPO by-product HNE. In contrast, the lifetime of the 2nd component was sensitive to metabolic oxidative modulation: a number of the applied chemicals shortened the fluorescence lifetime of the 2nd component, with the most noticeable effect being induced by the application of modulators of the respiratory chain, changes in the cytosolic NAD(P)H redox status (addition of lactate and pyruvate), or mimicking intense oxidative stress by addition of HNE and/or GR inhibitor BCNU .

Multiple efforts were made to distinguish the free *vs.* bound states of NAD(P)H molecules in living tissues. Free NADH in water was proposed to exist in 2 conformations: a folded (NADH with stacked dinucleotide and adenine moieties) with a lifetime of 350 ps and an extended (opened form) with a lifetime of 760 ps. When existing as a mix in water solution, the average lifetime of free NADH was described to be in the range of 400-500 ps[85, 100], which was in agreement with the lifetime resolved for the 2nd component in our

experimental conditions in the presence of lactate/pyruvate, or BCNU suggesting that it can be attributable to such free forms. On the other hand, the long lifetime pool covering the lifetimes of 2-5 ns was attributed to the bound state of NAD(P)H[85]. NAD(P)H binding to enzymes mostly involves non-covalent electrostatic interactions between the protein and NAD(P)H, adopting rotationally immobile (at the ns scale), "opened" conformation[85]. Thus, one could expect that the fluorescence kinetics of such a state would be similar to NAD(P)H in very viscous environments. Indeed, we found rise in the fluorescence lifetime of this component with increased viscosity (data not shown). Also, the sensitivity of the component lifetime to HNE may suggest possible alteration of bound conformational states. We therefore propose that the 1st lifetime component with 1.7 ns lifetime and 450 nm spectral maximum most likely corresponds to such an enzyme-bound (unfolded) NAD(P)H conformation, whereas the 2nd lifetime component with 0.4-1 ns lifetime and 470 nm spectral maximum correlates with free (likely folded and extended) conformation(s). Furthermore, significantly shorter lifetime of the 2nd component after the addition of lactate/pyruvate, inducing cytosolic NAD(P)H redox changes, points to the faster kinetics of molecules in the cytoplasmic, *vs.* mitochondrial compartments. Thus, this result also explains the apparent lack of cytosolic NAD(P)H fluorescence in confocal images[95], and the observed preferential mitochondrial AF distribution. On the other hand, the absence of changes in the 1st fluorescence lifetime by the metabolic regulators supports its origin in the bound form of the molecules. We also resolved 3rd component; however the amplitude of this component was rather small and the component responded poorly to metabolic modulation (data not shown). Further studies are therefore needed to better understand this issue in the future.

Our results are in agreement with existing models that have proposed a 2-stage kinetics scheme for the excited-state reaction of NAD(P)H[103, 104], consisting of free and bound-state conformations of the molecules. At low temperatures, NADH fluorescence decay in most solutions has been reported to be 2-exponential[103], dependent on solvent polarity and viscosity. Decay behavior has been proposed to have its origins in a reversible

excited-state reaction transforming fluorescent, reduced NADH, possibly to a non-fluorescent NAD^+ product. Our findings are therefore in agreement with the use of NAD(P)H fluorescence as a sensitive non-invasive tools for monitoring metabolic oxidative state changes in living cardiac cells.

In the heart, ATP, produced in the process of mitochondrial oxidative phosphorylation, is the primary molecular energy source for the contraction of cardiac myocytes. This process is coupled to oxidation of reduced NADH, the principal electron donor for the electrochemical gradient indispensable for oxidative energy metabolism. The first step in this process, which accounts for 95% of ATP generation needed for cardiomyocyte contraction, is the dehydrogenation of NADH by the flavoproteins of the Complex I of the mitochondrial respiratory chain. Simultaneously, NADPH is an important cofactor for enzymes involved in antioxidant processes put in place to counteract the generation of ROS by oxidative respiration and/or oxidative stress[50]. As only bound forms of these molecules can have functional responses, it is crucial to be able to distinguish the bound from the free form; which is exactly the feature of fluorescence lifetime analysis. During normal cellular metabolism, mitochondrial electron transport results in the formation of superoxide anion O_2^- and subsequently H_2O_2. At low concentrations, ROS are important cellular signalling molecules, while at higher levels of oxidative stress the same molecules contribute to oxidative damage[77]. Because H_2O_2 concentration increases under certain (patho)physiological conditions and can oxidatively modify cellular components, it is critical to understand the response of mitochondria to H_2O_2[141]. H_2O_2 is degraded into water via the GR pathway powered by NADPH.

Our data gathered in *vitro* demonstrated that NADPH fluorescence intensity is sensitive to dehydrogenation by GR. This result, accompanied with no change in the NADPH lifetime kinetic properties, demonstrated the sensitivity of NADPH fluorescence to changes in the NADPH dehydrogenation. On the other hand, when NADPH dehydrogenation by GR was tested in single cells, BCNU, an inhibitor of GR induced no

visible change in the total counts of NAD(P)H fluorescence intensity. BCNU, an agent that is widely used in the chemotherapy for cancer brain tumours, has been shown to inhibit GR, the enzyme that catalyzes recycling of GSH from oxidized glutathione disulfide (GSSG)[142]. This action was proposed to contribute to both the therapeutic and toxic effects of BCNU. Inhibition of GR results in the depletion of GSH and the accumulation of GSSG[143, 144], which is likely to compromise cellular oxidative defences which highly rely on antioxidant actions of glutathione[145]. Indeed, BCNU-treated cells have been reported to be more vulnerable to oxidative stress[144]. Decreased levels of cellular GSH have been linked to the increased production of ROS, calcium dysregulation and cell death[146-148]. We expected an increase in the fluorescence due to an accumulation of NADPH molecules after GR inhibition by the drug, but we rather noted no change or a decreasing tendency of the signal. This finding is in agreement with observations of the BCNU effect on NAD(P)H fluorescence in synaptosomes[117]. These authors proposed that such result can be due to non-specificity of BCNU, possibly affecting other cellular enzymes. At the same time, the component analysis revealed that while characteristics of the first component were unchanged in the presence of BCNU, the amplitude of the second component was increased, and this effect was accompanied by shorter fluorescence lifetime. This observation suggests possible accumulation of NADPH molecules after GR inhibition, but associated with the change in the fluorescence kinetics, possibly due to change in its environment. Such result can explain no modification, or even decrease in the overall photon counts, despite the fact that NADPH accumulation is taking place.

Application of H_2O_2 in living cells induced a decrease in the total photon counts of NAD(P)H fluorescence. This result is also in agreement with observations in synaptosomes[117], that showed a significantly lower NAD(P)H fluorescence and was explained, at least partially, by H_2O_2-induced effect via BCNU-sensitive GR pathway. Previous observations[23] showed a correlation between a rise in the ROS generation and the decrease in the NAD(P)H fluorescence under physiological conditions, namely cell contraction. The decrease in the fluorescence amplitude was correlated with higher

consumption of NADPH via GR cycle[149]. This is also in agreement with our observation of partial recovery of the H_2O_2-induced decrease by BCNU. Our result therefore confirms that H_2O_2 effect implicates a stimulation of GR-related consumption of NADPH. In the future, higher concentration of BCNU should be tested to improve the observed recovery. Component analysis performed on NAD(P)H fluorescence signal in the presence of H_2O_2 revealed that observed decrease in the fluorescence is primarily due to change in the amplitudes of NAD(P)H fluorescence, pointing to change in the amount of these molecules. Surprisingly, at the concentration of 1μM of H_2O_2, and despite visible modifications in the cell membrane quality, this analysis revealed no significant change in the fluorescence lifetime characteristics that can be attributable to modification in the molecular environment. Our data demonstrated that H_2O_2 decreased the amount of NADH accumulated after inhibition of the respiratory chain by rotenone. The results present in this thesis concur with those previously reported by Tretter and Adam-Visi [117] in the presence of this inhibitor, which indicated that when NAD(P)H levels are diminished and maximal inhibition of respiration was observed, specific Krebs cycle enzymes exhibit decline in activity in response to treatment with H_2O_2. Upon consumption of H_2O_2, NAD(P)H levels and the enzyme activities return to control levels, suggesting that this inactivation is reversible and is not via direct interaction of H_2O_2 with α-ketoglutarate dehydrogenase and succinate dehydrogenase[141].

Next we investigated change in oxidative metabolic state by a different approach, using HNE, a lipid peroxidation by-product capable of protein modification[49]. Our observations showed a significant decrease in the fluorescence intensity in the presence of HNE accompanied by slight red spectral shift. This result was not correlated with changes in the amplitudes of the component 1 or 2, but with decreased fluorescence lifetimes of the component 1, as well as the component 2. Surprisingly, amplitudes of resolved components were not modified. Our *in vitro* data point to an increase in the fluorescence lifetimes together with blue spectral shift in the environment with higher viscosity. In this regard the effects of HNE can be interpreted as a possible lowering of the viscosity in cardiac cells by

the compound. Taking into consideration our findings of the sensitivity of NAD(P)H lifetimes to change in the environment viscosity by glycerol (Section 3.1.3.), these results suggest that HNE can affect NAD(P)H environment, possibly the viscosity of the compartments where the molecules are present, rather than the amount of the present molecules. We can speculate that as HNE can bind to various biomolecules (phospholipids, proteins and DNA), a modification of the phospholipid structure induced by addition of HNE can affect the viscosity of the medium. However that important issue remains to be investigated.

HNE was showed to activate NADPH-oxidase and thus increasing ROS production in left ventricular myocytes[150]. Being situated on the cell membrane, this action should induce a decrease in the cytosolic NAD(P)H concentration. Our data using lactate and pyruvate to clamp the cytosolic NAD/NADH redox ratio, point to a significant modulation of the 2nd component characteristics: a rise in the amplitude and a decrease in the lifetime of the component. This result indicates that the effect of HNE on cytosolic NAD(P)H via this pathway can account, at least in part, for the observed HNE action on the 2nd component. However it cannot explain the whole effect and it can not explain the lack of amplitude change in this condition.

Previous studies[49], based on the measurement of the enzyme protein expression, demonstrated that HNE is capable of decreasing NADP-ICDH activity in mitochondria via an enzyme inactivation. In this work, HNE was suggested to lead a decrease in the amount of available NADPH molecules. Furthermore, in isolated cardiac mitochondria, it has been reported that HNE inhibited α-ketoglutarate dehydrogenase and reduced the production of NADH[151]. However, component analysis failed to demonstrate modification in the amplitude of NAD(P)H fluorescence that could indicate change in the amount of NAD(P)H molecules at the studied HNE concentration (25 μM) and exposition time of (30-45) min. In the future, different concentrations and exposure time of HNE should be studied[49] to

properly answer the question whether HNE can affect the production of the NAD(P)H molecules at higher concentrations.

It has also been proposed that HNE can activate cellular uncoupling through an effect on endogenous uncoupling proteins (UCPs)[44, 152]. A possible role of the UCPs is to cause mild uncoupling in response to matrix superoxide and other oxidants, leading to lowered proton motive force and decreased superoxide production. This simple feedback loop would constitute a self-limiting cycle to protect against excessive superoxide production[63, 153-156]. Indeed, in our conditions, we have observed a particular relationship between the effects of HNE and the uncoupler DNP. Other students in our laboratory demonstrated a decrease in the first, as well as in the second component amplitude by DNP. This is in contrast with the action of HNE, which is rather pointing to a decrease in the fluorescence lifetimes. At the same time, application of DNP in the presence of HNE had a surprising additive effect, suggesting possible cooperation between the two actions. However, neither of the effects described above can explain lack of change in the component amplitudes. Our results therefore indicate that in addition to already described effect of HNE, it also seems to induce other processes in the cells, resulting in a maintenance of the amount of NAD(P)H molecules, in cells, as evidenced by no change in the amplitudes of the fluorescing component.

Gathered data demonstrate that NAD(P)H fluorescence is a sensitive tool that can be applied to uncover the behaviour of living cardiac cells with oxidative metabolic changes. It is therefore interesting to determine whether this is also the case of oxidative metabolic changes in (patho)physiological conditions.

4.2. Application of NAD(P)H fluorescence for study of pathophysiological conditions

Several heart pathologies in particular, ischemic conditions, but also adaptations to enhanced workload under physiological situations such as exercise or pregnancy, are usually accompanied by changes in myocardial metabolic state[68, 157]. Its monitoring is therefore crucial for understanding of cardiac functioning. The heart is a pump converting chemical energy into mechanical work and the power for this work is gathered almost entirely from oxidation of carbon fuels, and to a great extent these fuels are provided by coronary (myocardial) blood flow[158]. Such oxidative metabolism is primarily the function of mitochondria in the process of oxidative phosphorylation. When deprived of oxygen (anoxia), cardiac cells can maintain ATP levels by glycolytic ATP production, and can then revert smoothly to oxidative metabolism on reperfusion[159]. However, if blood flow is restricted, as in the case of myocardial infarct, or when cardiac work demand is increased and not fulfilled, the cells accumulate glycolytic by-products (lactate, H^+) in addition to suffering from oxygen deprivation[160]. This condition known as ischemia and depending on the degree of the insult can damage cardiac cells irreversibly. Paradoxically, however, the major damage to ischemic cells comes on the re-introduction of oxygen (reperfusion). During reperfusion, the cells typically undergo further contraction (hypercontracture) and membrane damage, followed by cell death[161, 162]. It is widely acknowledged that ischemia and reperfusion lead to mitochondrial, as well as cellular damage in cardiac cells[163-165]. Because of the high oxidative metabolism, heart cells have a high oxidative capacity, demonstrated by their ultrastructure: 25–35% of total cardiomyocyte volume is occupied by mitochondria[68, 166]. During hypoxia or ischemia, O_2 supply to the respiratory chain fails, leading to blocking of the TCA cycle and no energy being available from oxidative phosphorylation. This results in an increase of cytoplasmic NADH, which is accompanied, in ischemia, by accumulation of lactate and a decrease in cytoplasmic pH (5.5–6)[167, 168]. Many researchers have identified Complex I as a major site of damage to the respiratory

chain in ischemia[169, 170]. They observed reduction in oxidation rate for NADH-linked substrates by up to 60%. Typically, oxidation rates with succinate as a substrate were unchanged, suggesting that damage was restricted to the Complex I.

Metabolic state also changes in certain physiological conditions such as heart adaptation to new workload in pregnancy[68] or physical exercise[157]. This was our reason behind choosing a pregnant rat model to test the sensitivity of the newly developed fluorescence method to metabolic oxidative changes *in vivo*. As described in our Introduction (Section 1.3.), pregnancy is a particular physiological condition, which induces major haemodynamic adaptations necessary for foetal homeostasis and well-being[64]. This is associated with significant changes in carbohydrate metabolism[70] to allow continuous nutrients availability to the developing foetus, depending primarily on glucose. This leads to a rapid conversion from predominantly carbohydrate to predominantly fat utilization by the mother, correlating with increased lactate and pyruvate levels. Metabolic remodeling during pregnancy therefore also affects the heart function. Accordingly to previous studies performed in our laboratory by other students[68], our results confirmed a significant decrease in glycemia during normal pregnancy, in agreement with glucose being used by the foetus. There was also a significant increase in the levels of blood triglycerides and lactate with a similar trend on pyruvate, which leads to a significant change in the lactate/pyruvate ratio, indicating an important modification of the redox status. It was suggested that the increase in lactate levels, correlating with increased workload, is consistent with elevated glycolysis[2].

In pregnancy, oxidative stress was proposed to rise, culminating in the last trimester, in parallel with increase in total antioxidant capacity[171]. Nevertheless, in normal pregnancy, our results showed no significant change in the blood levels of HNE-protein adducts, indicating a lack of significant change in oxidative stress conditions evaluated with this marker. If confirmed by other oxidative stress indicators, this result is interesting, as pregnancy was proposed to be an "oxidative condition"[78, 83]. Consistent with this

observation, our fluorescence measurement data also showed no significant change in the responsiveness of cells isolated from pregnant rats to the oxidative stressors HNE or H_2O_2, suggesting that in pregnancy cardiac cells maintain full capacity to adapt to this physiological condition. It is also noteworthy that cells were more sensitive to the application of lactate in the presence of pyruvate in P *vs.* NP, in agreement with the expected increased use of those substrates in this condition.

As mentioned previously in the Introduction (Section 1.3.), pregnancy is also associated with pronounced changes in the endocrine system, which are linked to increased blood volume and cardiac output during the course of gestation. Aldosterone is one of the hormones that rise during pregnancy, which acts on epithelium through the RAAS[172], to promote sodium and water retention as well as potassium excretion and thus contributing to blood volume and blood pressure homeostasis. This has been observed in humans[173] as well as in rats[174]. Lack of hormonal changes during complicated pregnancy[174] points to the importance of these hormonal adaptations during gestation. Aldosterone is known to act via its MR on non-epithelial tissues, including the heart. MR antagonists, such as spironolactone, have been demonstrated to significantly reduce mortality and morbidity among patients with severe congestive heart failure [175]. Despite the fact that MR inhibition was described to be beneficial in certain pathological conditions such as in hypertensive kidney or cardiovascular diseases, their inhibition in physiological conditions, such as pregnancy, can be harmful. The RAAS is significantly increased in normal pregnancy, but blunted in pathological pregnancies, such as pregnancy induced hypertension[174] suggesting that RAAS is one of the hormonal systems that help cardiovascular adaptations put in place during pregnancy. A decrease in blood pressure in normal pregnancy, accompanied by elevated RAAS is paradoxical to other known conditions. RAAS pathway is also known to induce oxidative changes under pathological conditions[77], namely by altering aldosterone regulation via its MR, we have therefore opted for inhibition of RAAS pathways by canrenoate, the metabolite of spironolactone[176] to induce the conditions of oxidative stress *in vivo* conditions.

One of the most important pathways by which aldosterone exerts its negative effects on cardiovascular system is through production of ROS[77]. In a normal cell, mitochondria act as net scavengers of ROS[177], but in situations with cellular stress, mitochondrial cytochromes become significant sources of ROS[77]. Two major systems that are acting as scavengers of oxygen radicals are glutathione and the thioredoxin system, but when larger amounts of superoxide or other oxidative by-products are formed, oxidative damage predominate[72]. Paradoxically, our results in non-pregnant as well as in pregnant conditions indicated that treatment with canrenoate induced changes in the blood that can be correlated with increased oxidative stress markers. Interestingly, this rise in oxidative stress markers correlated with a decrease in lactate concentration in both conditions, an observation that was not reported so far. This result can suggest a possible relationship between metabolic switch in the use of energy substrates in pregnancy and oxidative stress changes and need to be further studied in the future. We therefore propose the hypothesis that MR can assist the heart in its adaptations to pregnancy by acting on the cell availability of metabolic substrates such as lactate, as well as by helping to protect it from oxidative stress.

In NP rats treated with canrenoate, we observed similar modifications in the fluorescence levels in response to oxidative stressors as in non-treated ones. These results allow us to conclude that the heart of these animals is capable of adapting to the MR inhibition by canrenoate. However, in P_{can} rats, we noted differences in the responsiveness of the cells to H_2O_2 but not HNE. We also observed the differential effect of BCNU. These results point to possible lack of adaptation of the cells in these conditions. At the same time, it is important to take into consideration that in canrenoate-treated animals, cardiac cells would be exposed to both the presence of higher HNE and lower lactate levels, which may result in altered NAD(P)H levels. This is one of the limitations of our study which was only done using equal concentrations of substrates when different conditions were studied, which is not the case *in vivo*. In the future, it would be interesting to compare NAD(P)H fluorescence in media specific to normal *vs.* canrenoate-treated pregnancy to comprehend

the changes in metabolic oxidative state. Also, it would have been interesting to quantify HNE-protein adducts in the cardiac tissue in addition to the blood, as well as to test the effect of HNE concentrations similar to those observed *in vivo*, which are likely to be close to the nanomolar rather than micromolar range.

Our data provide the first information on the use of spectrally-resolved TCSPC technique as a powerful new tool that can be applied to investigate metabolic changes directly in freshly-isolated living cardiomyocytes. We project that future development of application of this technique can eventually lead to new diagnostic approaches for early detection of mitochondrial dysfunction associated with pathological conditions.

5. CONCLUSIONS AND PERSPECTIVES

The presented work is unique and valuable, focusing on investigation of NAD(P)H fingerprinting by advanced spectrally-resolved lifetime spectrometry technique as a useful tool to study dynamic mitochondrial oxidative metabolism in living cardiomyocytes and its modifications by oxidative stressors. We demonstrate that spectrally-resolved TCSPC recordings of cardiomyocyte AF allow fast and reproducible measurements of NAD(P)H-based fluorescence spectra and fluorescence decays, with sufficient sensitivity to detect oxidative metabolic changes in living cardiac cells in response to oxidative stress challenge. We also analyzed in details fluorescence parameters of AF to gather more profound understanding of the effects of metabolic modulators. Component analysis, performed for the first time in our experimental conditions, proved to be highly beneficial in bringing more profound insight into parameters underlying changes in fluorescent characteristics of NAD(P)H molecules, including not only their amounts, but also modifications in their microenvironment.

Our data of preliminary experiments showed that this technique can also be used to study changes in metabolic oxidative status and its responses to oxidative stressors under (patho)physiological conditions. We have chosen pregnancy as an example of major physiological changes in cardiac metabolism associated with changes in global energy balance reflected by modifications of blood energy substrate concentrations. We have found that during normal pregnancy, cardiomyocyte response to oxidative insult, evaluated with NAD(P)H fluorescence, was not significantly different from that observed in non-pregnant condition. This result indicates that the heart has the full capacity to adapt to conditions of normal gestation without affecting its response to oxidative stressors at the cellular level. On the other hand, we have also examined the sensitivity of NAD(P)H fluorescence in living cardiomyocytes isolated from rats treated with MR inhibitor canrenoate. In canrenoate-treated pregnant rats, in addition to blood oxidative metabolic changes, we have noted some significant differences in cardiomyocyte responses to

NAD(P)H fluorescence modulators when compared to normally pregnant ones, strongly suggesting a role of the RAAS in the heart response to oxidative stressors in this condition. However, due to complexity of the studied conditions, further experiments are necessary in the future to confirm and fully understand this finding.

Our results have shown that employed technique combined with applied analytical approaches is very powerful in understanding rapid cellular adaptations to changes in energy and/or metabolic conditions. However, this work requests intense data processing and use of advanced analytical methods. In fact, due to an unanticipated and overwhelming amount of data to process, we were unable to perform component analysis in (patho) physiological conditions, and this constitutes the limitation of the presented preliminary study. We therefore intend to perform the component analysis under all studied pathophysiological conditions in the future to properly understand changes related to individual components. Also, we propose to investigate NAD(P)H fluorescence using distinct concentrations of substrates such as lactate and pyruvate in external media, but also fatty acids, as determined by the blood analyses, to mimic differential changes in the substrate availability during pregnancy. Utilization of specific modulators of respective cytosolic and mitochondrial redox state could also shed more light on the regulatory and crosstalk processes involved between cytosol and mitochondria for energy metabolism and response to oxidative stress.

We are convinced that information gathered on the regulation of NAD(P)H in cardiomyocytes will be useful for subsequent studies. Combined with data obtained from complementary approaches i.e. using electrophysiology or working heart perfusions could also be essential for better understanding of relations between cardiac NAD(P)H and contractile function. This method will expand our knowledge about the sensitivity of oxidative metabolic state to pathophysiological conditions such as complicated (hypertensive or diabetic) pregnancy, at different stages of gestation. It will also bring a

completely new insight into investigation of the effects of pharmaceutical drugs on mitochondrial metabolism and oxidative stress in numerous pathological conditions.

REFERENCES

1. **Saks V, Favier R, Guzun R, Schlattner U, Wallimann T.** Molecular system bioenergetics: regulation of substrate supply in response to heart energy demands. *J Physiol* 2006 Dec 15; 577(Pt 3): 769-77.

2. **O'Donnell JM, Kudej RK, LaNoue KF, Vatner SF, Lewandowski ED.** Limited transfer of cytosolic NADH into mitochondria at high cardiac workload. *Am J Physiol Heart Circ Physiol* 2004 Jun; 286(6): H2237-H2242.

3. **Stanley WC, Recchia FA, Lopaschuk GD.** Myocardial substrate metabolism in the normal and failing heart. *Physiol Rev* 2005 Jul; 85(3): 1093-129.

4. **Ventura-Clapier R, Garnier A, Veksler V.** Energy metabolism in heart failure. *J Physiol* 2004 Feb 15; 555(Pt 1): 1-13.

5. **Budd SL, Nicholls DG.** A reevaluation of the role of mitochondria in neuronal Ca2+ homeostasis. *J Neurochem* 1996 Jan; 66(1): 403-11.

6. **Wang X.** The expanding role of mitochondria in apoptosis. *Genes Dev* 2001; 15: 2922-33.

7. **Rich PR.** The molecular machinery of Keilin's respiratory chain. *Biochem Soc Trans* 2003 Dec; 31(Pt 6): 1095-105.

8. **Alberts B, Bray D, Lewis J, Raff M, Roberts K, Watson JD.** *Molecular Biology of The Cell.* 3rd ed. New York: Garland Publishing, Inc.; 1994.

9. **Berg JM.** Biochemistry. 5 ed. New York: Freeman and Co, U.S.A.; 2002.

10. **Randle PJ, England PJ, Denton RM.** Control of the tricarboxylate cycle and its interactions with glycolysis during acetate utilization in rat heart. *Biochem J* 1970 May; 117(4): 677-95.

11. **Zhou L, Stanley WC, Saidel GM, Yu X, Cabrera ME.** Regulation of lactate production at the onset of ischaemia is independent of mitochondrial NADH/NAD^+: insights from *in silico* studies. *J Physiol* 2005; 569(3): 925-37.

12. **Liu Y, Fiskum G, Schubert D.** Generation of reactive oxygen species by the mitochondrial electron transport chain. *J Neurochem* 2002 Mar; 80(5): 780-7.

13. **Kussmaul L, Hirst J.** The mechanism of superoxide production by NADH:ubiquinone oxidoreductase (complex I) from bovine heart mitochondria. *Proc Natl Acad Sci U S A* 2006 May 16; 103(20): 7607-12.

14. **Chen Q, Vazquez EJ, Moghaddas S, Hoppel CL, Lesnefsky EJ.** Production of reactive oxygen species by mitochondria: central role of complex III. *J Biol Chem* 2003 Sep 19; 278(38): 36027-31.

15. **Li N, Ragheb K, Lawler G, Sturgis J, Rajwa B, Melendez JA, et al.** Mitochondrial complex I inhibitor rotenone induces apoptosis through enhancing

mitochondrial reactive oxygen species production. *J Biol Chem* 2003 Mar 7; 278(10): 8516-25.

16. **Kushnareva Y, Murphy AN, Andreyev A.** Complex I-mediated reactive oxygen species generation: modulation by cytochrome c and NAD(P)+ oxidation-reduction state. *Biochem J* 2002 Dec 1; 368(Pt 2): 545-53.

17. **Kunz WS, Gellerich FN.** Quantification of the content of fluorescent flavoproteins in mitochondria from liver, kidney cortex, skeletal muscle, and brain. *Biochem Med Metab Biol* 1993 Aug; 50(1): 103-10.

18. **Rocheleau JV, Head WS, Piston DW.** Quantitative NAD(P)H/flavoprotein autofluorescence imaging reveals metabolic mechanisms of pancreatic islet pyruvate response. *J Biol Chem* 2004 Jul 23; 279(30): 31780-7.

19. **Bielawski J, Thompson TE, Lehninger AL.** The effect of 2,4-dinitrophenol on the electrical resistance of phospholipid bilayer membranes. *Biochem Biophys Res Commun* 1966 Sep 22; 24(6): 948-54.

20. **Skulachev VP.** Uncoupling: new approaches to an old problem of bioenergetics. *Biochim Biophys Acta* 1998 Feb 25; 1363(2): 100-24.

21. **Balaban RS.** Regulation of oxidative phosphorylation in the mammalian cell. *Am J Physiol* 1990 Mar; 258(3 Pt 1): C377-C389.

22. **Hout-Gonzalez C, Nury H, Trezeguet V, Lauquin GJ, Pebay-Peyroula E, Brandolin G.** Molecular, functional, and pathological aspects of the mitochondrial ADP/ATP carrier. *Physiology (Bethesda)* 2006 Aug; 21: 242-9.

23. **Heinzel FR, Luo Y, Dodoni G, Boengler K, Petrat F, Di LF, et al.** Formation of reactive oxygen species at increased contraction frequency in rat cardiomyocytes. *Cardiovasc Res* 2006 Jul 15; 71(2): 374-82.

24. **Zacks MA, Wen JJ, Vyatkina G, Bhatia V, Garg N.** An overview of chagasic cardiomyopathy: pathogenic importance of oxidative stress. *An Acad Bras Cienc* 2005 Dec; 77(4): 695-715.

25. **Kirkinezos IG, Moraes CT.** Reactive oxygen species and mitochondrial diseases. *Semin Cell Dev Biol* 2001 Dec; 12(6): 449-57.

26. **Cadenas E.** Mitochondrial free radical production and cell signaling. *Mol Aspects Med* 2004 Feb; 25(1-2): 17-26.

27. **Valko M, Leibfritz D, Moncol J, Cronin MT, Mazur M, Telser J.** Free radicals and antioxidants in normal physiological functions and human disease. Int J *Biochem Cell Biol* 2007; 39(1): 44-84.

28. **Loschen G, Flohe L, Chance B.** Respiratory chain linked H(2)O(2) production in pigeon heart mitochondria. *FEBS Lett* 1971 Nov 1; 18(2): 261-4.

29. **Turrens JF.** Mitochondrial formation of reactive oxygen species. *J Physiol* 2003 Oct 15; 552(Pt 2): 335-44.

30. **Antunes F, Han D, Cadenas E.** Relative contributions of heart mitochondria glutathione peroxidase and catalase to H(2)O(2) detoxification in in vivo conditions. *Free Radic Biol Med* 2002 Nov 1; 33(9): 1260-7.

31. **Han D, Canali R, Rettori D, Kaplowitz N.** Effect of glutathione depletion on sites and topology of superoxide and hydrogen peroxide production in mitochondria. *Mol Pharmacol* 2003 Nov; 64(5): 1136-44.

32. **Chen Q, Camara AK, Stowe DF, Hoppel CL, Lesnefsky EJ.** Modulation of electron transport protects cardiac mitochondria and decreases myocardial injury during ischemia and reperfusion. *Am J Physiol Cell Physiol* 2007 Jan; 292(1): C137-C147.

33. **Brioukhanov AL, Netrusov AI, Eggen RI.** The catalase and superoxide dismutase genes are transcriptionally up-regulated upon oxidative stress in the strictly anaerobic archaeon Methanosarcina barkeri. *Microbiology* 2006 Jun; 152(Pt 6): 1671-7.

34. **Nordberg J, Arner ES.** Reactive oxygen species, antioxidants, and the mammalian thioredoxin system. *Free Radic Biol Med* 2001 Dec 1; 31(11): 1287-312.

35. **Curello S, Ceconi C, Bigoli C, Ferrari R, Albertini A, Guarnieri C.** Changes in the cardiac glutathione status after ischemia and reperfusion. *Experientia* 1985 Jan 15; 41(1): 42-3.

36. **Maker HS, Weiss C, Brannan TS.** The effects of BCNU (1,3-bis(2-chloroethyl)-1-nitrosourea) and CCNU (1-(2-chloroethyl)-3-cyclohexyl-1-nitrosourea) on

glutathione reductase and other enzymes in mouse tissue. *Res Commun Chem Pathol Pharmacol* 1983 Jun; 40(3): 355-66.

37. **Rigobello MP, Folda A, Scutari G, Bindoli A.** The modulation of thiol redox state affects the production and metabolism of hydrogen peroxide by heart mitochondria. *Arch Biochem Biophys* 2005 Sep 15; 441(2): 112-22.

38. **Doroshenko N, Doroshenko P.** The glutathione reductase inhibitor carmustine induces an influx of Ca2+ in PC12 cells. *Eur J Pharmacol* 2004 Aug 16; 497(1): 17-24.

39. **Butterfield DA, Koppal T, Howard B, Subramaniam R, Hall N, Hensley K, et al.** Structural and functional changes in proteins induced by free radical-mediated oxidative stress and protective action of the antioxidants N-tert-butyl-alpha-phenylnitrone and vitamin E. *Ann N Y Acad Sci* 1998 Nov 20; 854: 448-62.

40. **Marnett LJ.** Oxyradicals and DNA damage. *Carcinogenesis* 2000 Mar; 21(3): 361-70.

41. **Abuja PM, Albertini R.** Methods for monitoring oxidative stress, lipid peroxidation and oxidation resistance of lipoproteins. *Clin Chim Acta* 2001 Apr; 306(1-2): 1-17.

42. **le-Donne I, Rossi R, Giustarini D, Milzani A, Colombo R.** Protein carbonyl groups as biomarkers of oxidative stress. *Clin Chim Acta* 2003 Mar; 329(1-2): 23-38.

43. **Gedik CM, Boyle SP, Wood SG, Vaughan NJ, Collins AR.** Oxidative stress in humans: validation of biomarkers of DNA damage. *Carcinogenesis* 2002 Sep; 23(9): 1441-6.

44. **Echtay KS, Esteves TC, Pakay JL, Jekabsons MB, Lambert AJ, Portero-Otin M, et al.** A signalling role for 4-hydroxy-2-nonenal in regulation of mitochondrial uncoupling. *EMBO J* 2003 Aug 15; 22(16): 4103-10.

45. **Ceconi C, Boraso A, Cargnoni A, Ferrari R.** Oxidative stress in cardiovascular disease: myth or fact? *Arch Biochem Biophys* 2003 Dec 15; 420(2): 217-21.

46. **Zarkovic N.** 4-hydroxynonenal as a bioactive marker of pathophysiological processes. *Mol Aspects Med* 2003 Aug; 24(4-5): 281-91.

47. **Awasthi YC, Yang Y, Tiwari NK, Patrick B, Sharma A, Li J, et al.** Regulation of 4-hydroxynonenal-mediated signaling by glutathione S-transferases. *Free Radic Biol Med* 2004 Sep 1; 37(5): 607-19.

48. **Dwivedi S, Sharma A, Patrick B, Sharma R, Awasthi YC.** Role of 4-hydroxynonenal and its metabolites in signaling. *Redox Rep* 2007; 12(1): 4-10.

49. **Benderdour M, Charron G, Deblois D, Comte B, Des RC.** Cardiac mitochondrial NADP+-isocitrate dehydrogenase is inactivated through 4-hydroxynonenal adduct formation: an event that precedes hypertrophy development. *J Biol Chem* 2003 Nov 14; 278(46): 45154-9.

50. **Benderdour M, Charron G, Comte B, Ayoub R, Beaudry D, Foisy S, et al.** Decreased cardiac mitochondrial NADP+-isocitrate dehydrogenase activity and expression: a marker of oxidative stress in hypertrophy development. *Am J Physiol Heart Circ Physiol* 2004 Nov; 287(5): H2122-H2131.

51. **Yang JH, Yang ES, Park JW.** Inactivation of NADP+-dependent isocitrate dehydrogenase by lipid peroxidation products. *Free Radic Res* 2004 Mar; 38(3): 241-9.

52. **Humphries KM, Yoo Y, Szweda LI.** Inhibition of NADH-linked mitochondrial respiration by 4-hydroxy-2-nonenal. *Biochemistry* 1998 Jan 13; 37(2): 552-7.

53. **Reiss PD, Zuurendonk PF, Veech RL.** Measurement of tissue purine, pyrimidine, and other nucleotides by radial compression high-performance liquid chromatography. *Anal Biochem* 1984 Jul; 140(1): 162-71.

54. **Williamson DH, Lund P, Krebs HA.** The redox state of free nicotinamide-adenine dinucleotide in the cytoplasm and mitochondria of rat liver. *Biochem J* 1967 May; 103(2): 514-27.

55. **Lin SJ, Guarente L.** Nicotinamide adenine dinucleotide, a metabolic regulator of transcription, longevity and disease. *Curr Opin Cell Biol* 2003 Apr; 15(2): 241-6.

56. **Veech RL, Eggleston LV, Krebs HA.** The redox state of free nicotinamide-adenine dinucleotide phosphate in the cytoplasm of rat liver. *Biochem J* 1969 Dec; 115(4): 609-19.

57. **Magni G, Orsomando G, Raffaelli N.** Structural and functional properties of NAD kinase, a key enzyme in NADP biosynthesis. *Mini Rev Med Chem* 2006 Jul; 6(7): 739-46.

58. **Singh R, Mailloux RJ, Puiseux-Dao S, Appanna VD.** Oxidative stress evokes a metabolic adaptation that favors increased NADPH synthesis and decreased NADH production in Pseudomonas fluorescens. *J Bacteriol* 2007 Sep; 189(18): 6665-75.

59. **Comte B, Vincent G, Bouchard B, Benderdour M, Des RC.** Reverse flux through cardiac NADP(+)-isocitrate dehydrogenase under normoxia and ischemia. *Am J Physiol Heart Circ Physiol* 2002 Oct; 283(4): H1505-H1514.

60. **Brioukhanov AL, Netrusov AI.** Catalase and superoxide dismutase: distribution, properties, and physiological role in cells of strict anaerobes. *Biochemistry (Mosc)* 2004 Sep; 69(9): 949-62.

61. **Jo SH, Son MK, Koh HJ, Lee SM, Song IH, Kim YO, et al.** Control of mitochondrial redox balance and cellular defense against oxidative damage by mitochondrial NADP+-dependent isocitrate dehydrogenase. *J Biol Chem* 2001 May 11; 276(19): 16168-76.

62. **Koh HJ, Lee SM, Son BG, Lee SH, Ryoo ZY, Chang KT, et al.** Cytosolic NADP+-dependent isocitrate dehydrogenase plays a key role in lipid metabolism. *J Biol Chem* 2004 Sep 17; 279(38): 39968-74.

63. **Jezek P, Hlavata L.** Mitochondria in homeostasis of reactive oxygen species in cell, tissues, and organism. *Int J Biochem Cell Biol* 2005 Dec; 37(12): 2478-503.

64. **Jensen E, Wood C, Keller-Wood M.** The normal increase in adrenal secretion during pregnancy contributes to maternal volume expansion and fetal homeostasis. *J Soc Gynecol Investig* 2002 Nov; 9(6): 362-71.

65. **Schannwell CM, Zimmermann T, Schneppenheim M, Plehn G, Marx R, Strauer BE.** Left ventricular hypertrophy and diastolic dysfunction in healthy pregnant women. *Cardiology* 2002; 97(2): 73-8.

66. **Robson SC, Hunter S, Boys RJ, Dunlop W.** Serial study of factors influencing changes in cardiac output during human pregnancy. *Am J Physiol* 1989 Apr; 256(4 Pt 2): H1060-H1065.

67. **Katz R, Karliner JS, Resnik R.** Effects of a natural volume overload state (pregnancy) on left ventricular performance in normal human subjects. *Circulation* 1978 Sep; 58(3): 434-41.

68. **Bassien-Capsa V, Fouron JC, Comte B, Chorvatova A.** Structural, functional and metabolic remodeling of rat left ventricular myocytes in normal and in sodium-supplemented pregnancy. *Cardiovasc Res* 2006 Feb 1; 69(2): 423-31.

69. **Hunter S, Robson SC.** Adaptation of the maternal heart in pregnancy. *Br Heart J* 1992 Dec; 68(6): 540-3.

70. **Leturque A, Hauguel S, Revelli JP, Burnol AF, Kande J, Girard J.** Fetal glucose utilization in response to maternal starvation and acute hyperketonemia. *Am J Physiol* 1989 Jun; 256(6 Pt 1): E699-E703.

71. **Randle PJ, Garland PB, HALES CN, Newsholme EA.** The glucose fatty-acid cycle. Its role in insulin sensitivity and the metabolic disturbances of diabetes mellitus. *Lancet* 1963 Apr 13; 1: 785-9.

72. **Chatham JC, Des RC, Forder JR.** Evidence of separate pathways for lactate uptake and release by the perfused rat heart. *Am J Physiol Endocrinol Metab* 2001 Oct; 281(4): E794-E802.

73. **Longo LD.** Maternal blood volume and cardiac output during pregnancy: a hypothesis of endocrinologic control. *Am J Physiol* 1983 Nov; 245(5 Pt 1): R720-R729.

74. **Virdis A, Neves MF, Amiri F, Viel E, Touyz RM, Schiffrin EL.** Spironolactone improves angiotensin-induced vascular changes and oxidative stress. *Hypertension* 2002 Oct; 40(4): 504-10.

75. **Nishiyama A, Abe Y.** Aldosterone and renal injury. *Nippon Yakurigaku Zasshi* 2004 Aug; 124(2): 101-9.

76. **Callera GE, Touyz RM, Tostes RC, Yogi A, He Y, Malkinson S, et al.** Aldosterone activates vascular p38MAP kinase and NADPH oxidase via c-Src. *Hypertension* 2005 Apr; 45(4): 773-9.

77. **Skott O, Uhrenholt TR, Schjerning J, Hansen PB, Rasmussen LE, Jensen BL.** Rapid actions of aldosterone in vascular health and disease--friend or foe? *Pharmacol Ther* 2006 Aug; 111(2): 495-507.

78. **Little RE, Gladen BC.** Levels of lipid peroxides in uncomplicated pregnancy: a review of the literature. *Reprod Toxicol* 1999 Sep; 13(5): 347-52.

79. **Diamant S, Kissilevitz R, Diamant Y.** Lipid peroxidation system in human placental tissue: general properties and the influence of gestational age. *Biol Reprod* 1980 Nov; 23(4): 776-81.

80. **Wickens D, Wilkins MH, Lunec J, Ball G, Dormandy TL.** Free radical oxidation (peroxidation)products in plasma in normal and abnormal pregnancy. *Ann Clin Biochem* 1981 May; 18(Pt 3): 158-62.

81. **Uotila J, Tuimala R, Aarnio T, Pyykko K, Ahotupa M.** Lipid peroxidation products, selenium-dependent glutathione peroxidase and vitamin E in normal pregnancy. *Eur J Obstet Gynecol Reprod Biol* 1991 Nov 26; 42(2): 95-100.

82. **Toescu V, Nuttall SL, Martin U, Kendall MJ, Dunne F.** Oxidative stress and normal pregnancy. *Clin Endocrinol (Oxf)* 2002 Nov; 57(5): 609-13.

83. **Patil SB, Kodliwadmath MV, Kodliwadmath SM.** Correlation between lipid peroxidation and non-enzymatic antioxidants in pregnancy induced hypertension. *Indian Journal of Clinical Biochemistry*, 2008; 23(1): 45-8.

84. **Patil SB, Kodliwadmath MV, Kodliwadmath SM.** Role of lipid peroxidation and enzymatic antioxidants in pregnancy-induced hypertension. *Clin Exp Obstet Gynecol* 2007; 34(4): 239-41.

85. **Vishwasrao HD, Heikal AA, Kasischke KA, Webb WW.** Conformational dependence of intracellular NADH on metabolic state revealed by associated fluorescence anisotropy. *J Biol Chem* 2005 Jul 1; 280(26): 25119-26.

86. **Pogue BW, Pitts JD, Mycek MA, Sloboda RD, Wilmot CM, Brandsema JF, et al.** In vivo NADH fluorescence monitoring as an assay for cellular damage in photodynamic therapy. *Photochem Photobiol* 2001 Dec; 74(6): 817-24.

87. **Chance B, Williams GR.** A method for the localization of sites for oxidative phosphorylation. *Nature* 1955 Aug 6; 176(4475): 250-4.

88. **Chance B, Williams GR.** Respiratory enzymes in oxidative phosphorylation. III. The steady state. *J Biol Chem* 1955 Nov; 217(1): 409-27.

89. **Monici M.** Cell and tissue autofluorescence research and diagnostic applications. *Biotechnol Annu Rev* 2005; 11: 227-56.

90. **Bottiroli G, Croce AC.** Autofluorescence spectroscopy of cells and tissues as a tool for biomedical diagnosis. *Photochem Photobiol Sci* 2004 Nov; 3(11-12): 189-210.

91. **Becker W.** Advanced Time-Correlated Single Photon Counting techniques. 1 ed. New York: Springer; 2005.

92. **Niesner R, Peker B, Schlusche P, Gericke KH.** Noniterative biexponential fluorescence lifetime imaging in the investigation of cellular metabolism by means of NAD(P)H autofluorescence. *Chemphyschem* 2004 Aug 20; 5(8): 1141-9.

93. **Schuchmann S, Kovacs R, Kann O, Heinemann U, Buchheim K.** Monitoring NAD(P)H autofluorescence to assess mitochondrial metabolic functions in rat hippocampal-entorhinal cortex slices. *Brain Res Brain Res Protoc* 2001 Jul; 7(3): 267-76.

94. **Nuutinen EM.** Subcellular origin of the surface fluorescence of reduced nicotinamide nucleotides in the isolated perfused rat heart. *Basic Res Cardiol* 1984 Jan; 79(1): 49-58.

95. **Eng J, Lynch RM, Balaban RS.** Nicotinamide adenine dinucleotide fluorescence spectroscopy and imaging of isolated cardiac myocytes. *Biophys J* 1989 Apr; 55(4): 621-30.

96. **Coremans JM, Ince C, Bruining HA, Puppels GJ.** (Semi-)quantitative analysis of reduced nicotinamide adenine dinucleotide fluorescence images of blood-perfused rat heart. *Biophys J* 1997 Apr; 72(4): 1849-60.

97. **Estabrook RW.** Fluorometric measurement of reduced pyridine nucleotide in cellular and subcellular particles. *Anal Biochem* 1962 Sep; 4: 231-45.

98. **Avi-Dor Y, Olson JM, Doherty MD, Kaplan NO.** Fluorescence of pyridine nucleotides in mitochovdria. *J Biol Chem* 1962; 237: 2377-83.

99. **Chance B, Schoener B, Oshino R, Itshak F, Nakase Y.** Oxidation-reduction ratio studies of mitochondria in freeze-trapped samples. NADH and flavoprotein fluorescence signals. *J Biol Chem* 1979 Jun 10; 254(11): 4764-71.

100. Wakita M, Nishimura G, Tamura M. Some characteristics of the fluorescence lifetime of reduced pyridine nucleotides in isolated mitochondria, isolated hepatocytes, and perfused rat liver in situ. *J Biochem (Tokyo)* 1995 Dec; 118(6): 1151-60.

101. Joubert F, Fales HM, Wen H, Combs CA, Balaban RS. NADH enzyme-dependent fluorescence recovery after photobleaching (ED-FRAP): applications to enzyme and mitochondrial reaction kinetics, in vitro. *Biophys J* 2004 Jan; 86(1 Pt 1): 629-45.

102. Blinova K, Carroll S, Bose S, Smirnov AV, Harvey JJ, Knutson JR, et al. Distribution of mitochondrial NADH fluorescence lifetimes: steady-state kinetics of matrix NADH interactions. *Biochemistry* 2005 Feb 22; 44(7): 2585-94.

103. Gafni A, Brand L. Fluorescence decay studies of reduced nicotinamide adenine dinucleotide in solution and bound to liver alcohol dehydrogenase. *Biochemistry* 1976 Jul 27; 15(15): 3165-71.

104. Gruber BA, Leonard NJ. Dynamic and static quenching of 1,N6-ethenoadenine fluorescence in nicotinamide 1,N6-ethenoadenine dinucleotide and in 1,N6-etheno-9-(3-(indol-3-yl) propyl) adenine. *Proc Natl Acad Sci U S A* 1975 Oct; 72(10): 3966-9.

105. Chorvatova A, Hussain M. Effects of caffeine on potassium currents in isolated rat ventricular myocytes. *Pflugers Arch* 2003 Jul; 446(4): 422-8.

106. **Battista MC, Calvo E, Chorvatova A, Comte B, Corbeil J, Brochu M.** Intra-uterine growth restriction and the programming of left ventricular remodelling in female rats. *J Physiol* 2005 May 15; 565(Pt 1): 197-205.

107. **Williamson DH, Mellanby J.** Methods in Enzymatic Analysis. Academic Press, NY; 1974.

108. **Asselin C, Bouchard B, Tardif JC, Des RC.** Circulating 4-hydroxynonenal-protein thioether adducts assessed by gas chromatography-mass spectrometry are increased with disease progression and aging in spontaneously hypertensive rats. *Free Radic Biol Med* 2006 Jul 1; 41(1): 97-105.

109. **Chorvat D, Jr., Chorvatova A.** Spectrally resolved time-correlated single photon counting: a novel approach for characterization of endogenous fluorescence in isolated cardiac myocytes. *Eur Biophys J* 2006 Oct 11.

110. **Marino D, Gonzalez EM, Frendo P, Puppo A, rrese-Igor C.** NADPH recycling systems in oxidative stressed pea nodules: a key role for the NADP+ -dependent isocitrate dehydrogenase. *Planta* 2007 Jan; 225(2): 413-21.

111. **Davies KJ, Doroshow JH.** Redox cycling of anthracyclines by cardiac mitochondria. I. Anthracycline radical formation by NADH dehydrogenase. *J Biol Chem* 1986 Mar 5; 261(7): 3060-7.

112. **Lambert AJ, Brand MD.** Inhibitors of the quinone-binding site allow rapid superoxide production from mitochondrial NADH:ubiquinone oxidoreductase (complex I). *J Biol Chem* 2004 Sep 17; 279(38): 39414-20.

113. **Tsubaki M.** Fourier-transform infrared study of cyanide binding to the Fea3-CuB binuclear site of bovine heart cytochrome c oxidase: implication of the redox-linked conformational change at the binuclear site. *Biochemistry* 1993 Jan 12; 32(1): 164-73.

114. **Heytler PG.** Uncouplers of oxidative phosphorylation. *Methods Enzymol* 1979; 55: 462-42.

115. **Romashko DN, Marban E, O'Rourke B.** Subcellular metabolic transients and mitochondrial redox waves in heart cells. *Proc Natl Acad Sci U S A* 1998 Feb 17; 95(4): 1618-23.

116. **Opie LH, Owen P.** Effects of increased mechanical work by isolated perfused rat heart during production or uptake of ketone bodies. Assessment of mitochondrial oxidized to reduced free nicotinamide-adenine dinucleotide ratios and oxaloacetate concentrations. *Biochem J* 1975 Jun; 148(3): 403-15.

117. **Tretter L, dam-Vizi V.** Inhibition of Krebs cycle enzymes by hydrogen peroxide: A key role of [alpha]-ketoglutarate dehydrogenase in limiting NADH production under oxidative stress. *J Neurosci* 2000 Dec 15; 20(24): 8972-9.

118. **Chorvat D, Jr., Kirchnerova J, Cagalinec M, Smolka J, Mateasik A, Chorvatova A.** Spectral unmixing of flavin autofluorescence components in cardiac myocytes. *Biophys J* 2005 Dec; 89(6): L55-L57.

119. **Roy-Clavel E, Picard S, St Louis J, Brochu M.** Induction of intrauterine growth restriction with a low-sodium diet fed to pregnant rats. *Am J Obstet Gynecol* 1999 Mar; 180(3 Pt 1): 608-13.

120. **Barron WM.** Volume homeostasis during pregnancy in the rat. *Am J Kidney Dis* 1987 Apr; 9(4): 296-302.

121. **Duvekot JJ, Peeters LL.** Renal hemodynamics and volume homeostasis in pregnancy. *Obstet Gynecol Surv* 1994 Dec; 49(12): 830-9.

122. **Morris JM, Gopaul NK, Endresen MJ, Knight M, Linton EA, Dhir S, et al.** Circulating markers of oxidative stress are raised in normal pregnancy and pre-eclampsia. *Br J Obstet Gynaecol* 1998 Nov; 105(11): 1195-9.

123. **Patrick TE, Hubel CA, Roberts JM.** Evidence of increased oxidative stress, unexplained by lipid changes, is present in nulliparous black women from early gestation. *Hypertens Pregnancy* 2004; 23(1): 91-100.

124. **Schweitzer D, Schenke S, Hammer M, Schweitzer F, Jentsch S, Birckner E, et al.** Towards metabolic mapping of the human retina. *Microsc Res Tech* 2007 May; 70(5): 410-9.

125. **Konig K, Ehlers A, Stracke F, Riemann I.** In vivo drug screening in human skin using femtosecond laser multiphoton tomography. *Skin Pharmacol Physiol* 2006; 19(2): 78-88.

126. **Schenke-Layland K, Riemann I, Damour O, Stock UA, Konig K.** Two-photon microscopes and in vivo multiphoton tomographs--powerful diagnostic tools for tissue engineering and drug delivery. *Adv Drug Deliv Rev* 2006 Sep 15; 58(7): 878-96.

127. **Yang Y, Katz A, Celmer EJ, Zurawska-Szczepaniak M, Alfano RR.** Fundamental differences of excitation spectrum between malignant and benign breast tissues. *Photochem Photobiol* 1997 Oct; 66(4): 518-22.

128. **Katz A, Savage HE, Schantz SP, McCormick SA, Alfano RR.** Noninvasive native fluorescence imaging of head and neck tumors. *Technol Cancer Res Treat* 2002 Feb; 1(1): 9-15.

129. **Morgan DC, Wilson JE, MacAulay CE, MacKinnon NB, Kenyon JA, Gerla PS, et al.** New method for detection of heart allograft rejection: validation of sensitivity and reliability in a rat heterotopic allograft model. *Circulation* 1999 Sep 14; 100(11): 1236-41.

130. **Yamani MH, van de Poll SW, Ratliff NB, Kuban BE, Starling RC, McCarthy PM, et al.** Fluorescence spectroscopy of endomyocardial tissue post-human heart transplantation: does it correlate with histopathology? *J Heart Lung Transplant* 2000 Nov; 19(11): 1077-80.

131. **Schenke-Layland K, Opitz F, Gross M, Doring C, Halbhuber KJ, Schirrmeister F, et al.** Complete dynamic repopulation of decellularized heart valves by application of defined physical signals-an in vitro study. *Cardiovasc Res* 2003 Dec 1; 60(3): 497-509.

132. **Schenke-Layland K, Riemann I, Opitz F, Konig K, Halbhuber KJ, Stock UA.** Comparative study of cellular and extracellular matrix composition of native and tissue engineered heart valves. *Matrix Biol* 2004 May; 23(2): 113-25.

133. **Huang S, Heikal AA, Webb WW.** Two-photon fluorescence spectroscopy and microscopy of NAD(P)H and flavoprotein. *Biophys J* 2002 May; 82(5): 2811-25.

134. **Chance B.** Pyridine nucleotide as an indicator of the oxygen requirements for energy-linked functions of mitochondria. *Circ Res* 1976 May; 38(5 Suppl 1): I31-I38.

135. **Aneba S., Cheng Y, Mateasik A, Comte B, Chorvat D, Chorvatova A.** Probing of Cardiomyocyte Metabolism by Spectrally Resolved Lifetime Detection of NAD(P)H Fluorescence. *Computers in Cardiology* 2007. 34:349–352.

136. **Cheng Y, Dahdah N., Porier N., Miro J., Chorvat D, Chorvatova A.** Spectrally and time-resolved study of NADH autofluorescence in cardiac myocytes from human biopsies. *Proceedings of SPIE: the International Society for Optical Engineering* 2007; 6771(Advanced Photon Counting Techniques II): 677104-1-677104-13.

137. **Dickinson ME, Bearman G, Tilie S, Lansford R, Fraser SE.** Multi-spectral imaging and linear unmixing add a whole new dimension to laser scanning fluorescence microscopy. *Biotechniques* 2001 Dec; 31(6): 1272, 1274-6, 1278.

138. **Chorvat D, Mateasik A, Kirchnerova J, Chorvatova A.** Application of spectral unmixing in multi-wavelength time-resolved spectroscopy. *Proceedings of SPIE:*

the International Society for Optical Engineering 2007; 6771(Advanced Photon Counting Techniques II): 677105-1-677105-12.

139. **Zimmermann T, Rietdorf J, Pepperkok R.** Spectral imaging and its applications in live cell microscopy. *FEBS Lett* 2003 Jul 3; 546(1): 87-92.

140. **O'Connor DV, Phillips D.** Time-Correlated Single Photon Counting. 1 ed. London: Academic Press; 1984.

141. **Nulton-Persson AC, Szweda LI.** Modulation of mitochondrial function by hydrogen peroxide. *J Biol Chem* 2001 Jun 29; 276(26): 23357-61.

142. **Frischer H, Ahmad T.** Severe generalized glutathione reductase deficiency after antitumor chemotherapy with BCNU" [1,3-bis(chloroethyl)-1-nitrosourea]. *J Lab Clin Med* 1977 May; 89(5): 1080-91.

143. **Smith AC, Boyd MR.** Preferential effects of 1,3-bis(2-chloroethyl)-1-nitrosourea (BCNU) on pulmonary glutathione reductase and glutathione/glutathione disulfide ratios: possible implications for lung toxicity. *J Pharmacol Exp Ther* 1984 Jun; 229(3): 658-63.

144. **Ma W, Kleiman NJ, Sun F, Li D,** Spector A. Peroxide toxicity in conditioned lens epithelial cells--evaluation of multi-defense systems. *Exp Eye Res* 2003 Dec; 77(6): 711-20.

145. **Meister A.** Glutathione-ascorbic acid antioxidant system in animals. *J Biol Chem* 1994 Apr 1; 269(13): 9397-400.

146. **Jurma OP, Hom DG, Andersen JK.** Decreased glutathione results in calcium-mediated cell death in PC12. *Free Radic Biol Med* 1997; 23(7): 1055-66.

147. **Pereira CM, Oliveira CR.** Glutamate toxicity on a PC12 cell line involves glutathione (GSH) depletion and oxidative stress. *Free Radic Biol Med* 1997; 23(4): 637-47.

148. **Froissard P, Monrocq H, Duval D.** Role of glutathione metabolism in the glutamate-induced programmed cell death of neuronal-like PC12 cells. *Eur J Pharmacol* 1997 May 12; 326(1): 93-9.

149. **Pai EF, Karplus PA, Schulz GE.** Crystallographic analysis of the binding of NADPH, NADPH fragments, and NADPH analogues to glutathione reductase. *Biochemistry* 1988 Jun 14; 27(12): 4465-74.

150. **Nakamura K., Miura D., Matsubara H., Sumita W., Nagase S., Sakuragi S., et al.** 4-Hydroxy-2-nonenal induces calcium overload via NADPH oxidase-derived reactive oxygen species in isolated rat cardiac myocytes. *J Mol Cell Cardiol* 2006; 41(6): 1050.

151. **Humphries KM, Szweda LI.** Selective inactivation of alpha-ketoglutarate dehydrogenase and pyruvate dehydrogenase: reaction of lipoic acid with 4-hydroxy-2-nonenal. *Biochemistry* 1998 Nov 10; 37(45): 15835-41.

152. **Echtay KS, Roussel D, St-Pierre J, Jekabsons MB, Cadenas S, Stuart JA, et al.** Superoxide activates mitochondrial uncoupling proteins. *Nature* 2002 Jan 3; 415(6867): 96-9.

153. **Brand MD, Buckingham JA, Esteves TC, Green K, Lambert AJ, Miwa S, et al.** Mitochondrial superoxide and aging: uncoupling-protein activity and superoxide production. *Biochem Soc Symp* 2004;(71): 203-13.

154. **Echtay KS, Pakay JL, Esteves TC, Brand MD.** Hydroxynonenal and uncoupling proteins: a model for protection against oxidative damage. *Biofactors* 2005; 24(1-4): 119-30.

155. **Echtay KS, Brand MD.** 4-hydroxy-2-nonenal and uncoupling proteins: an approach for regulation of mitochondrial ROS production. *Redox Rep* 2007; 12(1): 26-9.

156. **Murphy MP, Echtay KS, Blaikie FH, sin-Cayuela J, Cocheme HM, Green K, et al.** Superoxide activates uncoupling proteins by generating carbon-centered radicals and initiating lipid peroxidation: studies using a mitochondria-targeted spin trap derived from alpha-phenyl-N-tert-butylnitrone. *J Biol Chem* 2003 Dec 5; 278(49): 48534-45.

157. **Goodwin GW, Taegtmeyer H.** Improved energy homeostasis of the heart in the metabolic state of exercise. *Am J Physiol Heart Circ Physiol* 2000 Oct; 279(4): H1490-H1501.

158. **Mudge GH, Jr., Mills RM, Jr., Taegtmeyer H, Gorlin R, Lesch M.** Alterations of myocardial amino acid metabolism in chronic ischemic heart disease. *J Clin Invest* 1976 Nov; 58(5): 1185-92.

159. **Das AM, Harris DA.** Regulation of the mitochondrial ATP synthase in intact rat cardiomyocytes. *Biochem J* 1990 Mar 1; 266(2): 355-61.

160. **Dennis SC, Gevers W, Opie LH.** Protons in ischemia: where do they come from; where do they go to? *J Mol Cell Cardiol* 1991 Sep; 23(9): 1077-86.

161. **Schluter KD, Jakob G, Ruiz-Meana M, Garcia-Dorado D, Piper HM.** Protection of reoxygenated cardiomyocytes against osmotic fragility by nitric oxide donors. *Am J Physiol* 1996 Aug; 271(2 Pt 2): H428-H434.

162. **Piper HM, Abdallah Y, Schafer C.** The first minutes of reperfusion: a window of opportunity for cardioprotection. *Cardiovasc Res* 2004 Feb 15; 61(3): 365-71.

163. **Piper HM, Noll T, Siegmund B.** Mitochondrial function in the oxygen depleted and reoxygenated myocardial cell. *Cardiovasc Res* 1994 Jan; 28(1): 1-15.

164. **Piper HM, Siegmund B, Ladilov Y, Schluter KD.** Calcium and sodium control in hypoxic-reoxygenated cardiomyocytes. *Basic Res Cardiol* 1993 Sep; 88(5): 471-82.

165. **Lesnefsky EJ, Moghaddas S, Tandler B, Kerner J, Hoppel CL.** Mitochondrial dysfunction in cardiac disease: ischemia--reperfusion, aging, and heart failure. J *Mol Cell Cardiol* 2001 Jun; 33(6): 1065-89.

166. **James TN, Sherf L.** Ultrastructure of myocardial cells. *Am J Cardiol* 1968 Sep; 22(3): 389-416.

167. **Smith DR, Stone D, Darley-Usmar VM.** Stimulation of mitochondrial oxygen consumption in isolated cardiomyocytes after hypoxia-reoxygenation. *Free Radic Res* 1996 Mar; 24(3): 159-66.

168. **Vuorinen K, Ylitalo K, Peuhkurinen K, Raatikainen P, Ala-Rami A, Hassinen IE.** Mechanisms of ischemic preconditioning in rat myocardium. Roles of adenosine, cellular energy state, and mitochondrial F1F0-ATPase. *Circulation* 1995 Jun 1; 91(11): 2810-8.

169. **Cairns CB, Ferroggiaro AA, Walther JM, Harken AH, Banerjee A.** Postischemic administration of succinate reverses the impairment of oxidative phosphorylation after cardiac ischemia and reperfusion injury. *Circulation* 1997 Nov 4; 96(9 Suppl): II-5.

170. **Hardy L, Clark JB, Darley-Usmar VM, Smith DR, Stone D.** Reoxygenation-dependent decrease in mitochondrial NADH:CoQ reductase (Complex I) activity in the hypoxic/reoxygenated rat heart. *Biochem J* 1991 Feb 15; 274 (Pt 1): 133-7.

171. **Toescu V, Nuttall SL, Martin U, Nightingale P, Kendall MJ, Brydon P, et al.** Changes in plasma lipids and markers of oxidative stress in normal pregnancy and pregnancies complicated by diabetes. *Clin Sci (Lond)* 2004 Jan; 106(1): 93-8.

172. **Booth RE, Johnson JP, Stockand JD.** Aldosterone. *Adv Physiol Educ* 2002 Dec; 26(1-4): 8-20.

173. **Elsheikh A, Creatsas G, Mastorakos G, Milingos S, Loutradis D, Michalas S.** The renin-aldosterone system during normal and hypertensive pregnancy. *Arch Gynecol Obstet* 2001 Jan; 264(4): 182-5.

174. **Beausejour A, Auger K, St Louis J, Brochu M.** High-sodium intake prevents pregnancy-induced decrease of blood pressure in the rat. *Am J Physiol Heart Circ Physiol* 2003 Jul; 285(1): H375-H383.

175. **Pitt B, Zannad F, Remme WJ, Cody R, Castaigne A, Perez A, et al.** The effect of spironolactone on morbidity and mortality in patients with severe heart failure. Randomized Aldactone Evaluation Study Investigators. *N Engl J Med* 1999 Sep 2; 341(10): 709-17.

176. **Sadee W, Abshagen U, Finn C, Rietbrock N.** Conversion of spironolactone to canrenone and disposition kinetics of spironolactone and canrenoate-potassium in rats. *Naunyn Schmiedebergs Arch Pharmacol* 1974 Jul 3; 283(3): 303-18.

177. **Andreyev AY, Kushnareva YE, Starkov AA.** Mitochondrial metabolism of reactive oxygen species. *Biochemistry (Mosc)* 2005 Feb; 70(2): 200-14.

APPENDIX I

Aneba S., Cheng Y., Mateasik A., Comte B., Chorvat D. Jr, Chorvatova A., 2007: Probing of Cardiomyocyte Metabolism by Spectrally Resolved Lifetime Detection of NAD(P)H Fluorescence. *The Computers in Cardiology*. 39:349-352.

Probing of Cardiomyocyte Metabolism by Spectrally Resolved Lifetime Detection of NAD(P)H Fluorescence

S Aneba[1], Y Cheng[1], A Mateasik[2], B Comte[1,3], D Chorvat Jr[2], A Chorvatova[1,4]

[1]Research Centre, CHU Sainte-Justine, Montreal, Canada
[2]International Laser Centre, Bratislava, Slovakia
[3]Department of Nutrition, University of Montreal, Montreal, Canada
[4]Department of Pediatrics, University of Montreal, Montreal, Canada

Abstract

NAD(P)H, crucial in effective management of cellular oxidative metabolism and the principal electron donors for enzymatic reactions, is a major source of autofluorescence induced in cardiac cells following excitation by UV light. Spectrally-resolved time-correlated single photon counting was used to simultaneously measure the fluorescence spectra and fluorescence lifetimes of NAD(P)H, following excitation by a pulsed picosecond 375 nm laser diode. Spectra, as well as fluorescence lifetimes of NADH and NADPH molecules were investigated in solution at different concentrations Effects of their respective dehydrogenation by lipoamide dehydrogenase (LipDH) or glutathione reductase (GR) were also questioned. NAD(P)H autofluorescence recorded in vitro was compared to the one measured in freshly isolated cardiac cells. We observed a good comparability between NAD(P)H parameters recorded in solution and in cells.

1. Introduction

Endogenous fluorescence of NAD(P)H, induced following excitation with the UV light, is long used for non-invasive fluorescent probing of metabolic state. Blue autofluorescence of rat cardiac myocytes was demonstrated to correlate with metabolic changes and was mostly ascribed to mitochondrial NADH and NADPH [2]. Adenosine trisphosphate (ATP), produced in the process of mitochondrial oxidative phosphorylation, is the primary molecular energy source for the contraction of cardiac myocytes. This process is coupled to oxidation of reduced NADH, the principal electron donor for the electrochemical gradient indispensable for oxidative energy metabolism. The first step in this process, which accounts for 95% of ATP generation needed for cardiomyocyte contraction, is the dehydrogenation of NADH by Complex I of the mitochondrial respiratory chain. NADH consumption rate is long investigated using fluorescence techniques in tissues and isolated mitochondria. On the other hand, NADPH is an important cofactor for several enzymes involved in different metabolic pathways (i.e. pentose phosphate pathway, Krebs cycle) and is essential for antioxidant processes in the glutathione reductase (GR) reaction. This enzyme allows the recycling of glutathione by converting its oxidized form (GSSG) into reduced glutathione. Oxidative stress can modulate the cellular NADPH content through the release of peroxides and various by-products that has been shown to decrease the activity of several enzymes, such as the NADP-isocitrate dehydrogenase (NADP-ICDH) [1]. Here, we investigate NAD(P)H fingerprinting by spectrally-resolved lifetime spectroscopy. More precisely, we characterize fluorescence spectra and fluorescence lifetimes of NADH and NADPH in intracellular-like solutions and compare resolved data with spectral and temporal characteristics of endogenous NAD(P)H fluorescence, directly in living cardiomyocytes.

2. Methods

2.1. Cardiomyocyte isolation

Left ventricular myocytes were isolated from Sprague-Dawley rats (13-14 weeks old, Charles River, Canada) following retrograde perfusion of the heart with proteolytic enzymes [4]. All procedures were performed in accordance with Institutional Committee accredited by the Canadian Council for the Protection of Animals (CCPA). Myocytes were maintained in a storage solution at 4°C until used. Only cells that showed clearly defined striations were used in up to 10 hrs following isolation.

2.2. TCSPC

We have used time correlated single photon counting (TCSPC) setup based on inverted microscope (Axiovert 200M, Zeiss, Canada) [4]. In brief, a picosecond diode laser with emission line at 375 nm (BHL-375, Becker-Hickl, Boston Electronics, USA) was used as an excitation source (output power ~1 mW, repetition rate 20 MHz, pulse widths typically < 100 ps). The laser beams were combined by dichroic filters and reflected to the sample through epifluorescence path of Axiovert 200 inverted microscope to create slightly defocused elliptical spot (10-20 μm). The emitted fluorescence was spectrally decomposed by 16-channel photomultiplier array (PML-16, Becker-Hickl, Boston Electronics, USA), running in the photon-counting regime and feeding the time-correlated single photon counting interface card SPC 830 using SPCM software (both Becker-Hickl, Boston Electronics, USA), attached to the imaging spectrograph (Solar 100, Proscan, Germany). Fluorescence decays were measured for 30 s with 25 ns TAC time-base sampled by 1024 points. Cells were studied at room temperatures in 4-well chambers with UV-proof coverslip-based slides (LabTech).

2.3. Solutions, drugs and data analysis

The basic external solution contained (in mM): NaCl, 140; KCl, 5.4; $CaCl_2$, 2; $MgCl_2$, 1; glucose, 10; HEPES, 10; adjusted to pH 7.35 with NaOH. Basic intracellular solution contained (in mM): KCl, 140; NaCl, 10; glucose, 10; HEPES, 10; adjusted to pH 7.25 with NaOH. LipDH (porcine; 2 U/μL), NADH or NADPH in concentrations ranging from 1 to 20 μM were added to basic internal solution. NADPH was also produced from NADP-ICDH (3.9 U/mL) by reaction of Isocitrate (89 mM) and NADP (0.5 mM) with or without GSSG (50 nM) and GR (0.5 U/mL or 1 U/mL). Chemicals were from Sigma-Aldrich (Canada). Data were analyzed using SPCImage software (Becker-Hickl, Boston Electronics, USA), Origin 7.0 (OriginLab, USA) and custom-written procedures for data correction and analysis written in C++. Home-made database was used for appropriate data management. Data are shown as means ± standard errors (SEM).

3. Results

3.1. NADH and NADPH in vitro

Fluorescence spectra and fluorescence lifetimes of intrinsic NADH and NADPH fluorescence were recorded in vitro in intracellular media-mimicking solutions. Steady-state emission spectra measured simultaneously at 16 acquisition channels were determined as the total photon counts on each spectral channel. Concentrations ranging from 1 to 20 μM were used to question the dose dependence of spectral and lifetime properties of the NADH and NADPH fluorescence. Spectral intensity of NADH fluorescence followed linear concentration-dependence (Fig. 1A), as described previously [2].

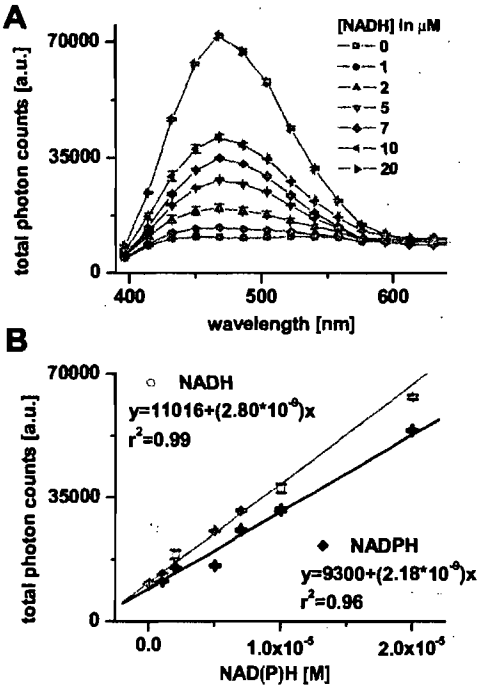

Figure 1. Emission spectra of NADH *in vitro* in intracellular solutions at concentrations ranging from 1 to 20 μM (n=5 samples each) (**A**). Concentration-dependence of the NADH and NADPH autofluorescence at spectral peak of 450 nm (**B**).

Normalized spectra superimposed perfectly for NADH concentrations between 1 to 20 μM (data not shown), confirming the same molecular origin. Free NADPH and NADH had autofluorescence with spectral maximum at 450 and 470 nm respectively in intracellular solution (Fig. 4). The spectral intensity of NADPH/NADH was linearly dependent on their concentration, as illustrated in Fig. 1B at 450 nm. Quantum yield of NADPH was smaller than that of NADH, as previously reported [2]. Normalized fluorescence intensity recorded in intra cellular medium showed slight shift of about 20 nm between NADPH and NADH (Fig. 4). At the fluorescence maximum wavelength of 450 nm we have resolved three fluorescence lifetimes for NADH (20 μM, n=10 samples): $\tau 1$ = 0.39±0.01 ns (with relative amplitude of 69.9±1.0%), $\tau 2$ = 1.46±0.05 ns (20.5±0.8%) and $\tau 3$ = 8.12±0.07 ns (9.8±0.2%), but only 2 significant ones for

NADPH (20 μM, n=5 samples): τ1 = 0.31±0.01 ns (74.6 ±2.4%) and τ2 = 0.75±0.02 ns (25.3±2.9%). Resolved lifetime parameters were independent on the studied emission wavelength, or concentrations (data not shown).

3.2. NADPH regulation by GR and NADH regulation by LipDH

NADPH produced *in vitro* from NADP-ICDH had same spectral and lifetime characteristics as NADPH in intracellular solution (data not shown). In the presence of GSSG, GR lowered (0.5 U/mL) or nearly completely abolished (1 U/mL) NADPH autofluorescence produced by NADP-ICDH (Fig. 2A), in agreement with dehydrogenation of NADPH by GR. Normalized and blank-corrected spectra showed no difference of NADPH spectral properties in the presence or absence of GR with GSSG and our data revealed no modifications of NADPH lifetime kinetic properties by GR (data not shown).

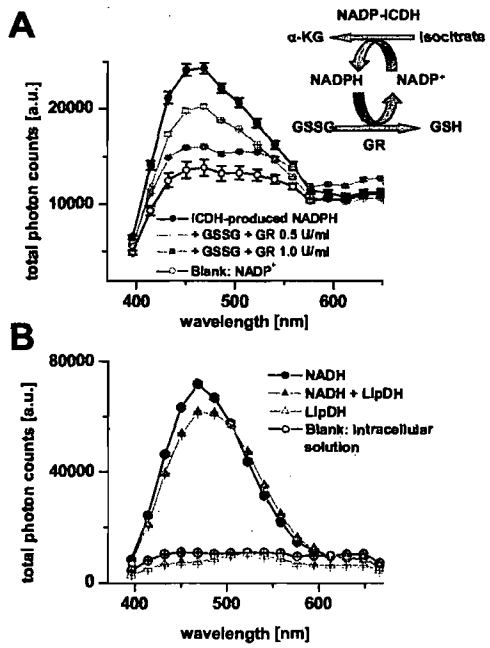

Figure 2. Normalized, background-corrected steady-state emission spectra of ICDH-produced NADPH in the absence and presence of GR (0.5 or 1 U/mL, n=5 samples each) (**A**) and of 20 μM NADH (n=10) in the absence and presence of 2 U/μL LipDH in intracellular solution (n=5) (**B**).

On the other hand, dehydrogenation of NADH (20 μM) to NAD^+ by LipDH (at 2 U/μL) - a disulfide oxidoreductase which is a part of the multienzyme Complex I - decreased fluorescence intensity (Fig. 2B). The effect was accompanied by a spectral broadening of about 10 nm towards red spectral region, as demonstrated by normalized emission spectra (Fig. 3A). NADH fluorescence decays were prolonged by LipDH (Fig. 3B) due to a significantly increased lifetime of the component 2 (at 504 nm, τ2 was prolonged from 1.84±0.12 ns to 2.74±0.18 ns, $p<0.05$).

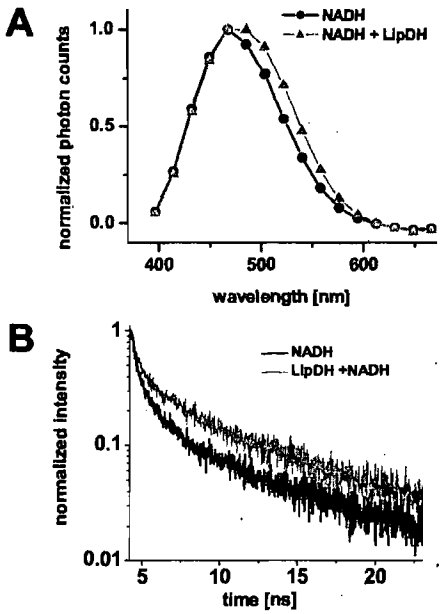

Figure 3. Comparison of normalized, background-corrected steady-state emission spectra of NADH (20 μM; n=10 samples) in the absence or presence LipDH (2 U/μL) in intracellular solution (n=5) (**A**). NADH normalized fluorescence lifetimes (20 μM) at 504 nm with or without LipDH (2 U/μL) (**B**).

3.3. Endogenous NAD(P)H in cardiac cells

To investigate the endogenous fluorescence of NAD(P)H in living cardiomyocytes, spectrally and time-resolved autofluorescence decays were recorded in cells bathed in basic external solutions. Normalized steady-state emission spectra of the cardiomyocyte auto fluorescence had spectral maximum at 450 nm (Fig. 4) and showed a slight blue-spectral shift when compared to NADH *in vitro*, while being closer to those of NADPH. Analysis of exponential decay of cardiomyocyte autofluorescence showed acceptable chi-square values ($\chi^2<1.2$; n=70/13 animals) and flat plot of weighted residuals when using at least a 3-exponential model, namely τ1 = 0.69±0.01 ns (69.3±1.0%), τ2 = 2.03±0.05 ns (27.6±0.9%) and τ3 = 12.68±0.08 ns (3.1±0.2%).

4. Discussion and conclusions

Although spectra of intrinsically fluorescing substances are now well characterized in cardiac tissue, the fluorescence lifetimes, considered to provide better quantitative measurement of different NAD(P)H conformations and/or molecular complexes contributing to the UV-excited autofluorescence of biological samples, are much less clearly identified in living cells. Here we demonstrate that NAD(P)H autofluorescence can be measured in living cardiomyocytes by time-resolved emission spectroscopy approach with good reproducibility. Recorded autofluorescence kinetics were comparable to already published data in cardiac mitochondria [2]. As expected, comparison with NADH and NADPH kinetics in vitro pointed to the NAD(P)H origins of the autofluorescence. While our data confirmed close spectral characteristics of NADH and NADPH molecules, curiously, we have identified differences in their lifetimes. This can be due to distinct kinetics of the two molecules, or the presence of impurities; kinetics of further purified molecules need to be done in the future.

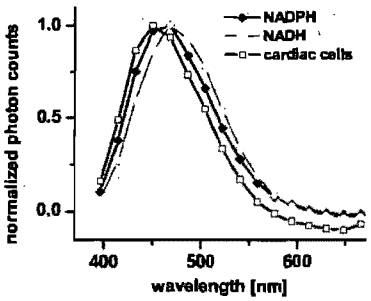

Figure 4. Normalized, background-corrected emission spectra, determined as total photon counts of NAD(P)H autofluorescence of single cardiac cells, compared to NADH and NADPH (both 20 μM) in basic extracellular solution.

The LipDH flavoprotein served as example to investigate NADH dehydrogenation. Observed increase in the lifetime kinetics can be related to conformational changes of NADH induced by the enzyme. Indeed, upon dehydrogenation, the oxidized form of the protein promotes the binding of the neutral dihydro-nicotinamide moiety of NADH [3], in addition to the formation of negatively charged charge-transfer complexes between transiently bound NAD^+ and covalently bound flavin adenine dinucleotide (FAD) cofactor. In this reduced form, nicotinamide moiety is in a different conformation from uniformly ordered structure of NADH juxtaposing nicotinamide and isoalloxazine flavin ring systems and is not proximal to FAD [3], which can be reflected in the change of fluorescence kinetics. On the other hand, appearance of the red-spectral shoulder points to possible presence of Förster resonant energy transfer (FRET). Being a flavoprotein, excitation of LipDH by visible light (420-460 nm) results in green FAD-autofluorescence with emission maximum around 500 nm [4]. As the LipDH-binding domain for NADH is in close proximity to FAD^+-binding one [3] and the 450 nm emission maximum of NADH corresponds exactly to an absorption peak of the FAD^+ moiety, this fulfils the prerequisites for the FRET between the two molecules. Nevertheless, since no decrease in NADH lifetime(s) was observed, further study is needed to fully understand significance of changes in NADH fluorescence following its binding to enzymes in living cells. Failure to observe lifetime kinetic changes following NADPH dehydrogenation by GR can be due to much faster kinetics of the NADPH molecule and/or much lower signal recorded in these experiments. Gathered data demonstrate the robustness of the TCSPC approach for NAD(P)H autofluorescence study directly in living cells. This approach brings an important insight into the understanding of metabolic state(s) of the heart in pathophysiological conditions.

Acknowledgements

Supported by CIHR (MOP 84450) grant to AC.

References

[1] Benderdour M, Charron G, Comte B, et al. Decreased cardiac mitochondrial $NADP^+$-isocitrate dehydrogenase activity and expression: a marker of oxidative stress in hypertrophy development. Am J Physiol Heart Circ Physiol 2004;287:H2122-H2131.

[2] Blinova K, Carroll S, Bose S et al. Distribution of mitochondrial NADH fluorescence lifetimes: steady-state kinetics of matrix NADH interactions. Biochemistry 2005;44:2585-2594.

[3] Brautigam CA, Chuang JL, Tomchick DR, Machius M, Chuang DT. Crystal structure of human dihydrolipoamide dehydrogenase: NAD^+/NADH binding and the structural basis of disease-causing mutations. J Mol Biol 2005;350:543-552.

[4] Chorvat D Jr, Chorvatova A. Spectrally resolved time-correlated single photon counting: a novel approach for characterization of endogenous fluorescence in isolated cardiac myocytes. Eur Biophys J 2006;36:73-83.

Address for correspondence

Dr. Chorvatova Alzbeta
Research Center of CHU Sainte Justine, University of Montreal
3175 Cote Sainte Catherine, H3T 1C5 Montreal, Canada
Email. [information retirée / information withdrawn]